


APPROVAL SHEET

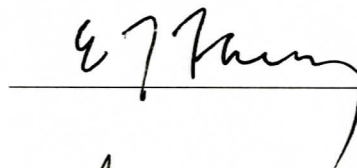
The thesis is submitted in partial fulfillment of the
requirements for the degree of

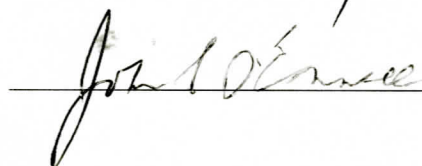
Master of Science (Chemical Engineering)


AUTHOR


This thesis has been read and approved by the examining Committee:


Thesis advisor





Accepted for the School of Engineering and Applied Science:


Dean, School of Engineering and
Applied Science

May 2012

Discovering Small-molecule Modulators of Amyloid-beta Aggregation and Neurotoxicity: Potential Therapies for Alzheimer's Disease

A Thesis

Presented to

the faculty of the School of Engineering and Applied Science

University of Virginia

In Partial Fulfillment

of the requirements for the Degree

Masters of Science (Chemical Engineering)

by

Hann-Chung E. Wong

May 2012

Abstract

An important pathological hallmark of AD is the formation of extracellular plaques and lesions composed primarily of a protein called amyloid-beta ($A\beta$). While $A\beta$ forms amyloid fibrils which are toxic, growing evidence has shown that soluble $A\beta$ oligomers are highly neurotoxic and cause a cascade of events that lead to cell death and disease onset. Our research focuses on discovering safe, biocompatible, BBB-permeable compounds that can effectively modulate $A\beta$ -associated neurotoxicity. To this end, we have investigated two groups of molecules, Brilliant Blue G (BBG) and its family of triphenylmethane dyes, and erythrosine B (ER) and its family of halogenated xanthene benzoate derivatives. BBG is a close structural analogue of Brilliant Blue FCF, which is a Food and Drug Administration (FDA)-approved food dye. More importantly, BBG is BBB-permeable and neuroprotective. ER is an FDA-approved food dye and has been shown to penetrate the BBB in *in vitro* uptake studies. We found that a number of molecules from each group modulated aggregation and aggressively inhibited $A\beta$ -associated toxicity.

Of the triphenylmethane dyes, Brilliant Blue G (BBG) and Brilliant blue R (BBR) were both capable of completely eliminating $A\beta$ -associated cytotoxicity at 3x concentration (ratio of dye to $A\beta$). BBG half-maximally inhibited $A\beta$ cytotoxicity at 0.55x. Both BBG and BBR inhibited fibril formation and reduced cytotoxicity by promoting the formation of non-toxic $A\beta$ oligomers. Alternatively, Brilliant Blue FCF and Fast Green FCF were less effective in modulating both aggregation and toxicity. Based on the comparison between the efficacy and structure of the molecules, we also identified two additional methyl groups on BBG and BBR that may be responsible for their unique modulating activity.

Of the halogenated xanthene benzoate derivatives, erythrosine B and eosin Y eliminated A β -associated toxicity by promoting the formation of non-toxic A β aggregates and inhibiting fibrillogenesis. Alternatively, eosin B (EB) and phloxine B were less effective, and Rose Bengal and ethyl eosin were not significantly effective at modulating A β cytotoxicity at 1x concentration. Despite close structural similarity, all of the molecules possessed unique A β aggregation modulating activity, and all were able to inhibit fibril formation. Comparison between structure and modulating activity showed that a benzoate attached to the xanthene was more effective at modulating A β cytotoxicity than a tetrachlorobenzoate or an ethyl benzoate attached to xanthene.

Our work has uncovered a number of potent A β neurotoxicity modulators and demonstrated that triphenylmethane and halogenated xanthene benzoate derivatives are novel families of molecules that show remarkable promise in the search for AD therapies.

Acknowledgements

I would like to thank the following people:

My research advisor Professor Inchan Kwon for his continuing guidance and insight.

Professors Erik Fernandez and John O'Connell for serving on my committee.

Members from the Kwon group for their assistance, guidance and insight, particularly

Simpson Gregoire, Jacob Irwin, and Shun Zheng

Undergraduate student Russell Baird for his work on this project.

My friends and family, especially my mom, Chi Chen, and my aunt, Lin Chen, for their unconditional love and support.

And finally, I would like to dedicate this thesis in loving memory of my grandfather who even in his absence pushes me to do my best.

Table of Contents

Abstract	i
Acknowledgements	iii
Table of Contents	iv
List of Figures	vi
List of Tables	xiv
 Chapter 1. Introduction	 1
<i>1.1 Scope</i>	<i>2</i>
<i>1.2 Objectives</i>	<i>3</i>
 Chapter 2. A Safe, Blood-Brain Barrier Permeable Triphenylmethane Dye Inhibits Amyloid-β Neurotoxicity by Generating Nontoxic Aggregates	 5
<i>2.1 Abstract</i>	<i>6</i>
<i>2.2 Introduction</i>	<i>11</i>
<i>2.3 Materials and Methods</i>	<i>11</i>
<i>2.4 Results and Discussion</i>	<i>14</i>
<i>2.5 Conclusions</i>	<i>39</i>
<i>2.6 Literature Cited</i>	<i>40</i>
<i>2.7 Appendix</i>	<i>49</i>
 Chapter 3. Xanthene Food Dye, a Modulator of Amyloid-beta-associated Neuronal Cell Function Impairment and Aggregation	 52
<i>3.1 Abstract</i>	<i>53</i>
<i>3.2 Introduction</i>	<i>54</i>
<i>3.3 Materials and Methods</i>	<i>56</i>
<i>3.4 Results and Discussion</i>	<i>59</i>
<i>3.5 Conclusions</i>	<i>72</i>
<i>3.6 Literature Cited</i>	<i>76</i>
 Chapter 4. Halogenated Xanthene Benzoate Dyes Can Potently Modulate Amyloid-beta Aggregation and Neurotoxicity	 77
<i>4.1 Abstract</i>	<i>78</i>
<i>4.2 Introduction</i>	<i>79</i>
<i>4.3 Materials and Methods</i>	<i>81</i>
<i>4.4 Results and Discussion</i>	<i>84</i>
<i>4.5 Conclusions</i>	<i>100</i>
<i>4.6 Literature Cited</i>	<i>101</i>

Chapter 5. Conclusions and Recommendations for Future Work.....	106
<i>5.1 Abstract</i>	<i>107</i>
<i>5.2 Introduction.....</i>	<i>110</i>

List of Figures

Figure 2.1. Chemical structures of Brilliant Blue G (BBG), Brilliant Blue FCF (BBF), Brilliant Blue R (BBR), and Fast Green FCF (FGF) at neutral pH.

Figure 2.2. Monitoring A β aggregation by dot blotting. Oligomer-specific A11 antibody and A β -sequence specific antibodies, 4G8 and 6E10, were used. 50 μ M A β was incubated in the absence (-) (top panels) or presence of 3x BBG (+) (bottom panels) for 1 to 3 days at 37 °C. Samples were taken on the indicated day and spotted onto a nitrocellulose membrane. Each membrane was immunostained with the A11 (*A*), 4G8 (*B*), or 6E10 (*C*) antibody. The blot images were taken by a UVP BioSpectrum imaging system.

Figure 2.3. Monitoring A β aggregate and fibril formation by TEM. 50 μ M A β was incubated in the absence (-) (top panels) or presence of 3x BBG (+) (bottom panels) for 1 to 3 days at 37 °C. Presence of oligomers and protofibrils (Top-left); protofibrils and isolated fibrils (Top-middle); fibril mesh network (Top-right); oligomers and protofibrils (Bottom-left); protofibrils (Bottom-middle); protofibrils (Bottom-right). Scale bar is 100 nm.

Figure 2.4. TEM images of 50 μ M of A β incubated for two days at 37 °C in the absence of any dye (*A*), or in the presence of 10x BBG (*B*), 10x BBR (*C*), 10x BBF (*D*), or 10x FGF (*E*). Scale bar is 100 nm.

Figure 2.5. Time course of ThT fluorescence of A β samples with varying concentrations of BBG. 50 μ M of A β monomer was incubated at 37 °C in the absence (no BBG) or presence of the indicated concentrations of BBG (from 0.001x to 10x) for up to 80 hours. 5 μ L of A β sample was taken at 0, 6, 24, 32, 48, 54, 72 and 80 hours for ThT fluorescence analysis. ThT fluorescence was measured in arbitrary units (a.u.). Values represent means \pm standard deviation (n = 3).

Figure 2.6. Dose-dependence of A β aggregation modulation by BBG. 50 μ M of A β monomer was incubated at 37 °C in the absence (No BBG) or presence of the indicated concentrations of BBG (from 0.001x to 10x) for up to 3 days. Samples were taken on the indicated day and spotted onto a nitrocellulose membrane. Each membrane was immunostained with the A11 (A), 4G8 (B), or 6E10 (C) antibody. The blot images were taken by a UVP BioSpectrum imaging system. The blot image of A11-reactive signal of A β samples incubated with varying concentrations of BBG for two days was processed by ImageJ (NIH). The data were fitted to a sigmoid curve ($R^2 = 0.99$) (D).

Figure 2.7. A saturation binding curve of BBG into A β peptide. 49 μ M BBG was incubated with the varying concentrations of A β peptide (0 to 300 μ M) until they reached an equilibrium and the absorbance of the BBG bound to the A β peptide was measured at 595 nm.

Figure 2.8. Viability of neuroblastoma SH-SY5Y cells incubated with preformed A β samples in the absence or presence of BBG. Preformed A β aggregates were prepared by incubating 50 μ M of A β monomer in the absence or presence of BBG at 37 °C for 0 to 3 days, as indicated in the graph. Aggregates were then administered to SH-SY5Y cells at a final concentration of 5 μ M.

After 48 hours, mitochondrial metabolic activity was measured using MTT reduction. Cells administered with PBS as a control (*Black*), 3x BBG (15 μ M) dye only (*White with pattern*), A β incubated without BBG (*White*), A β incubated with 3x BBG (*Grey*). Values represent means \pm standard deviation ($n \geq 3$). Values are normalized to the viability of cells administered with PBS only. Two-sided Student's t-tests were applied to the data. * $P < 0.001$, ** $P < 0.005$.

Figure 2.9. Dose-dependence of inhibition of A β -associated cytotoxicity by BBG. Preformed A β aggregates were prepared by incubating 50 μ M of A β monomer in the presence of varying concentrations of BBG (0.001x, 0.01x, 0.1x, 0.5x, 1x, 3x, 5x, and 10x) at 37 °C for 2 days. A β aggregates were then administered to SH-SY5Y cells at a final concentration of 5 μ M. After incubation, mitochondrial metabolic activity was measured after 48 hours using MTT reduction. Values represent means \pm standard deviation ($n \geq 3$). Values are normalized to the viability of cells administered with PBS only. The data were fitted to a sigmoid curve ($R^2 = 0.99$).

Figure 2.10. Modulation of A β aggregation by BBG analogs, BBR, BBF and FGF. 50 μ M of A β monomer was incubated at 37 °C in the absence (No Dye) or presence of the indicated concentrations of BBR, BBF or FGF (1x, 3x, and 10x) for up to three days. Samples were taken on the indicated day and spotted onto a nitrocellulose membrane. Each membrane was immunostained with the A11 (*A*), 4G8 (*B*), or 6E10 (*C*) antibody.

Figure 2.11. Viability of neuroblastoma SH-SY5Y cells incubated with preformed A β samples in the presence of BBG or BBG analogs (BBR, BBF, and FGF). Preformed A β aggregates were prepared by incubating 50 μ M of A β monomer in the presence of BBG or BBG analogs at 37 °C

for two days, as indicated in the graph. Aggregates were then administered to SH-SY5Y cells at a final concentration of 5 μ M. After 48 hours, mitochondrial metabolic activity was measured using MTT reduction. Cells administered with PBS as a control (*Black*), A β samples incubated without BBG (*White with pattern*), A β samples incubated with 1x dye (*White*) or 3x dye (*Grey*). Values represent means \pm standard deviation ($n \geq 3$). Values are normalized to the viability of cells administered with PBS only. Two-sided Student's t-tests were applied to the data. * $P < 0.001$, ** $P < 0.01$.

Figure A2.1. The data on the BBG-A β binding saturation curve (Figure 2.7) were fitted into a straight-line according to the equation, $P_T/Y = 1/(nk) [1/(1 - Y)] + D_T/n$ derived from $Y = nk(D)(P_T/D_T)/(1 + k(D))$ where Y , n , k , D , D_T , and P_T mean the fractional saturation of ligand binding sites, the number of binding sites, the binding constant, the dye concentration in solution, the total dye concentration, and the total protein concentration, respectively (I). The BBG concentration (D_T) was fixed at 49 μ M. The A β concentration (P_T) was varied from 0 to 300 μ M. The data at four P_T values between 20 μ M and 120 μ M were used for the fitting to a straight-line ($R^2 = 0.98$). The values of n and k were 3.2 and 1.1×10^4 (M^{-1}), respectively.

Figure A2.2. Alamar blue reducing activities of neuroblastoma SH-SY5Y cells incubated with pre-formed A β samples in the absence or presence of 3x BBG. Preformed A β aggregates were prepared by incubating 50 μ M of A β monomer in the absence of BBG at 37 $^{\circ}$ C for 0 to 3 days or in the presence of 3x BBG for 2 days, as indicated in the graph. The A β aggregates were then administered to SH-SY5Y cells at a final concentration of 5 μ M. After 3 days, cell viability was measured using alamar blue reduction. Cells administered with PBS as a control (*Control*), A β

incubated without BBG for 0 (*Day 0*), 1 (*Day 1*), 2 (*Day 2*), or 3 days (*Day 3*), or A β incubated with 3x BBG for 2 days (*Day 2**). Values represent means \pm standard deviation ($n \geq 3$). Values are normalized to the viability of cells administered with PBS only. One-sided Student's t-tests were applied to the data. * $P < 0.05$.

Figure A2.3. Dose-dependence inhibition of ThT fluorescence of A β samples by BBG. 50 μ M of A β monomer was incubated at 37 °C in the absence (no BBG) or presence of the indicated concentrations of BBG (from 10^{-5} x to 50x). 5 μ L of A β sample was taken at 72 hours of incubation. ThT fluorescence was measured in arbitrary units (a.u.). Values represent means \pm standard deviation ($n = 3$). The data were fitted to a sigmoid curve ($R^2 = 0.99$).

Figure 3.1. Chemical structure of erythrosine B (ER)

Figure 3.2. TEM images of A β aggregates. A β monomers were incubated for one to three days in the absence (no ER) (far-left panels) and the presence of 1x (middle-left panels), 5x (middle-right panels), or 10x ER (far-right panels) and visualized by TEM. Scale bars are 100 nm.

Figure 3.3. ThT fluorescence of A β samples. A β monomers were incubated for four days in the absence (no ER) or in the presence of 0.01x, 0.1x, 0.5x, 1x, 3x, 5x, or 10x of ER. Values represent means \pm standard deviation ($n = 3$).

Figure 3.4. Dot-blotting of A β samples using four A β -specific antibodies. A β monomers were incubated at 37 °C in the absence (no ER) or presence of the indicated concentrations of ER

(from 1x to 10x) for up to 3 days. Samples were spotted onto a nitrocellulose membrane and immunostained with the 4G8, 6E10, A11, or OC antibody.

Figure 3.5. TEM images of A β aggregates after three day incubation. A β monomers were incubated for three days in the absence (no ER) or in the presence of 1x, 5x, or 10x ER and visualized by TEM. Scale bars are 20 nm.

Figure 3.6. Viability of neuroblastoma SH-SY5Y cells treated with A β samples (5 μ M) formed in the absence or presence of 10x ER incubated at 37 °C for one to three days, measured by MTT reduction. Values represent means \pm standard deviation ($n \geq 3$). Values are normalized to the viability of cells administered with PBS only. Two-sided Student's t-tests were applied to the data (* $P < 0.001$; ** $P < 0.005$).

Figure 3.7. Viability of neuroblastoma SH-SY5Y cells treated with A β samples (5 μ M) incubated at 37 °C for one day in the absence of (no ER) or in the presence of 1x, 3x, 5x, or 10x ER, measured by MTT reduction. Values represent means \pm standard deviation ($n \geq 3$). Values are normalized to the viability of cells administered with PBS only. Two-sided Student's t-tests were applied to the data (* $P < 0.001$; NS: not significant).

Figure 4. 1. The structure of erythrosine B and its halogenated xanthene benzoate analogues at pH 7.

Figure 4.2. Confirmation of fibril formation by ThT fluorescence and CD. ThT (A) and CD (B) results were obtained by sampling A β incubated at 37°C in the absence of dye. CD was performed on day 5 and shows the characteristic β -sheet structure present in protofibrils and fibrils. The CD spectra is the average of five readings.

Figure 4.3. TEM images of A β aggregates formed after a three day incubation. A β monomer was incubated for 5 days at 37°C in the absence (A) or in the presence of 10x ER (B), EY (C), EB (D), RB (E), PH (F), and EE (F) and visualized by TEM. Scale bars are 100 nm.

Figure 4.4. Comparison of Aggregate Length Distributions. Aggregate lengths were measured manually using representative TEM images for each of the dyes (n = 200). Aggregate lengths were binned in 10 nm length interval.

Figure 4.5. Monitoring A β aggregation by dot blotting. Conformational-specific antibodies A11 and OC were used to detect prefibrillar oligomers and fibrillar species, respectively. A β -sequence specific antibodies, 4G8 and 6E10, were used. 50 μ M A β was incubated in the absence or presence of 1x, 3x or 10x dye for 6 days at 37 °C. Samples were obtained on the indicated day and spotted onto a nitrocellulose membrane. Each membrane were immunostained with the A11 (A), OC (B), 4G8 (B), or 6E10 (C) antibody.

Figure 4.6. Viability of neuroblastoma SH-SY5Y cells incubated with preformed A β samples in the absence or presence of 1x dyes. Mitochondrial metabolic activity was measured by MTT reduction. Preformed A β aggregates were prepared by incubating 50 μ M of A β monomer in the

absence or presence of ER, EY, EB, RB, PH or EE at 37 °C for 5 days. A β monomer was prepared using the sample preparation method outlined in Materials and Methods.

Figure 4.7. Comparison of dot blot intensities at 1x dye concentration from day 5. Dot blot intensities were obtained by integrating dots using ImageJ.

Figure 4.8. Secondary Structure of A β , and ER-, EY-, EB- and RB-induced aggregates on day 5. The secondary structure of A β aggregates formed in the absence or presence of dye were obtained by CD. Since the dyes absorb within the measured wavelengths, peptide spectra were obtained by subtracting the background spectra that were obtained separately. Each spectra is the average of five readings. A β and EB resemble the spectra for β -sheet structure. A β aggregates induced by ER, EY and RB resemble the spectra for random coil structure.

List of Tables

Table 3.1. Length distribution of A β aggregates incubated in the presence of 1x, 5x, and 10x for one, two, and three days. Two hundred A β aggregates observed in negative-stain TEM images at each concentration of ER were analyzed. Each bin has a 100 nm interval in the length of A β aggregates. The number indicates the maximum length of A β aggregates in each bin. ND denotes Not Detected.

Table 4.1. Comparison of long aggregate inhibition by each dye.

Chapter 1

Introduction

1.1 Scope

Alzheimer's disease (AD) is the most common form of senile dementia and has become a leading cause of death in the United States. Patients progressively lose cognitive capabilities as well as suffer changes to behavior. Gradually, bodily functions deteriorate which ultimately leads to death.

Pathological hallmarks of AD are extracellular plaques and brain lesions formed from the deposition and accumulation of a protein called amyloid-beta ($A\beta$). $A\beta$ is generated from the sequential cleavage of the amyloid precursor protein by a group of secretases. Depending on the cleavage site, multiple isoforms can be created. However, the two most physiologically abundant isoforms are $A\beta_{40}$ and $A\beta_{42}$. After generation, $A\beta$ undergoes a complex aggregation process to form amyloid fibrils.

While a number of aggregate conformers, including fibrils, are known to be toxic, growing evidence has shown that certain soluble $A\beta$ oligomers are highly neurotoxic. They cause a cascade of events, including oxidative stress that leads to cell death. Most importantly their presence strongly correlates with disease. Consequently, the reduction of toxic $A\beta$ oligomers and fibrils is a promising strategy to inhibit $A\beta$ -induced toxicity.

Numerous small-molecules have been investigated for their ability to modulate the formation of toxic $A\beta$ species and reduce $A\beta$ -associated toxicity. Despite certain successes, most molecules are limited by their practical application, due to their inherent toxicity or an inability to pass through the blood-brain barrier (BBB). Discovery of safe, effective, non-invasive therapies for Alzheimer's disease represents a significant challenge. The most precipitous obstacle is identifying molecules that are BBB permeable. 98% of small-molecules and nearly 100% of proteins cannot pass through the BBB. Due to the stringency of these requirements, the

pool of promising candidates remains relatively small compared to the growing need. But more importantly, a cure has yet to be found. Therefore, a strong driving force for new discovery remains.

1.2 Objective

Our research effort focuses on discovering small-molecule modulators of A β 40 aggregation and cytotoxicity. Our starting point is compounds with known safety profiles and potential BBB-permeability. Brilliant Blue G (BBG) and erythrosine B (ER) met all of these preliminary requirements. BBG is a close structural analogue of Brilliant Blue FCF a common food dye. In animal models, systemic administration of BBG reduced damage and expedited recovery after spinal cord injury. BBG was also found to confer neuroprotection to the brain by inhibiting adverse inflammatory reactions. Alternatively, ER is a Food and Drug Administration (FDA)-approved food dye and demonstrated high in *in vitro* BBB uptake studies. In order to potentially expand the pool of therapeutic candidates, we also investigated BBG analogues, a family of triphenylmethane dyes, which includes Brilliant Blue FCF (BBF), Brilliant Blue R (BBR), and Fast Green FCF (FGF). We also tested ER analogues, a family of halogenated xanthene benzoate derivatives, which includes eosin Y, eosin B, Rose Bengal, phloxine B and ethyl eosin. Of the analogues, BBF and FGF are also FDA-approved food dyes. Our research goals were as follows:

- 1) Evaluate the ability of BBG to modulate A β aggregation and cytotoxicity.
- 2) Evaluate the ability of BBG analogues to modulate A β aggregation and cytotoxicity.

- 3) Compare the efficacy of BBG and its analogues to determine structure-to-activity relationships.
- 4) Evaluate the ability of ER to modulate A β aggregation and cytotoxicity.
- 5) Evaluate the ability of ER analogues to modulate A β aggregation and cytotoxicity.
- 6) Compare the efficacy of ER and its analogues to determine structure-to-activity relationships.

3-(4,5-Dimethylthiazol-2-yl)-2,5-diphenyltetrazolium bromide (MTT) and Alamar blue were employed to evaluate the modulation of A β -associated toxicity. Both cell-based assays measure cellular metabolism and are used to monitor cell viability. To characterize aggregation modulation, TEM and dot blotting were employed. Aggregate morphology can be obtained by TEM and the information can be used to differentiate large aggregates, protofibrils and fibrils. Dot blotting with a panel of sequence-specific and conformation-specific A β -reactive antibodies was used to monitor the formation of immunologically relevant A β conformers. The A11 and OC antibodies can detect prefibrillar and fibrillar species, respectively. Additionally, assays such as Thioflavin T fluorescence and circular dichroism were employed to confirm fibril formation and peptide secondary structure, respectively. Collectively these results were used to discover effective molecules and to characterize their modulating activity.

Chapter 2

A Safe, Blood-Brain Barrier Permeable Triphenylmethane Dye Inhibits Amyloid- β
Neurotoxicity by Generating Nontoxic Aggregates

2.1 Abstract

Growing evidence suggests that on-pathway amyloid-beta ($A\beta$) oligomers are primary neurotoxic species and have a direct correlation with the onset of Alzheimer's disease (AD). One promising therapeutic strategy to block AD progression is to reduce the levels of these neurotoxic $A\beta$ species using small molecules. While several compounds have been shown to modulate $A\beta$ aggregation, compounds with such activity combined with safety and high blood-brain barrier (BBB) permeability have yet to be reported. Brilliant Blue G (BBG) is a close structural analog of a Food and Drug Administration (FDA)-approved food dye and has recently garnered prominent attention as a potential drug to treat spinal cord injury due to its neuroprotective effects along with BBB permeability and high degree of safety. In this work, we demonstrate that BBG is an effective $A\beta$ aggregation modulator, that it reduces $A\beta$ -associated cytotoxicity in a dose-dependent manner, and that it acts by promoting the formation of off-pathway, non-toxic aggregates. Comparative studies of BBG and three structural analogs, Brilliant Blue R (BBR), Brilliant Blue FCF (BBF) and Fast Green FCF (FGF), revealed that BBG is most effective, BBR is moderately effective, and BBF and FGF are least effective in modulating $A\beta$ aggregation and cytotoxicity. Therefore, the two additional methyl groups of BBG and other structural differences between the congeners are important in the interaction of BBG with $A\beta$ leading to formation of non-toxic $A\beta$ aggregates. Our findings support the hypothesis that generating non-toxic aggregates using small molecule modulators is an effective strategy for reducing $A\beta$ cytotoxicity. Furthermore, key structural features of BBG identified through structure-function studies can open new avenues into therapeutic design for combating AD.

2.2 Introduction

With an ever increasing number of new cases each year, Alzheimer's disease (AD) has become the most common form of senile dementia. The disease is primarily diagnosed in persons over the age of 65 (1). Symptoms manifest in a slow and progressive manner, but are ultimately debilitating and fatal. Currently, 5.3 million people in U.S. are affected by AD, with the number projected to rise to 13.5 million by 2050 (2). Although several U.S. Food and Drug Administration (FDA)-approved drugs temporarily reduce symptoms, no treatment exists that slows or stops the progression of AD.

A pathological hallmark of AD is the accumulation of insoluble protein aggregates, composed primarily of neurotoxic amyloid-beta ($A\beta$). $A\beta$ is created from sequential proteolytic cleavage of the amyloid precursor protein (APP) by the β - and γ -secretases (3). Although a number of $A\beta$ isoforms, with lengths from 39 to 43 residues are generated, $A\beta_{40}$ and $A\beta_{42}$ are the most physiologically relevant. In AD patients, $A\beta_{40}$ and $A\beta_{42}$ are found in an approximate 9:1 ratio, but $A\beta_{42}$ is more aggregation-prone (4).

According to the original amyloid-cascade hypothesis, conversion of soluble $A\beta$ monomers into insoluble fibrils causes AD onset (5). Recently, this hypothesis has been further refined. Growing evidence suggests that certain types of soluble $A\beta$ oligomers and protofibrils are more toxic than $A\beta$ fibrils, and their presence correlates strongly with dementia (6-9). Therefore, reduction of neurotoxic $A\beta$ oligomers and protofibrils represents a promising strategy to inhibit $A\beta$ -associated neurotoxicity.

Numerous small molecules have been studied for their ability to modulate $A\beta$ aggregation and reduce neurotoxicity (10-13). Congo red, an amyloid-structure specific dye, has the ability to modulate fibril formation and reduce $A\beta$ neurotoxicity (14-18). Besides amyloid-

specific dyes, several lipid-based modulators and polyphenols, such as scyllo-inocitol, nordihydroguaiaretic acid, curcumin, epigallocatechin gallate (EGCG) and resveratrol, have been reported to modulate A β aggregation and reduce A β -associated toxicity (10, 19-25). Although the results from these molecules are encouraging and validate A β aggregation modulation as a promising strategy, a practical and effective therapeutic has yet to be identified. Most A β aggregation small molecule modulators identified are not suitable for AD therapeutic leads because they lack low toxicity or blood-brain barrier (BBB) permeability. Crossing the blood-brain barrier is a big challenge in AD drug development; 98% of small molecule drugs and almost 100% of large molecule drugs cannot cross the BBB (26). For example, therapeutic application of Congo red has been hindered by poor blood-brain barrier (BBB) permeability as well as carcinogenicity (27). Although several polyphenol-based A β modulators including tannic acid and EGCG are very effective in reducing A β neurotoxicity in cell-based assays (21, 28), tannic acid or EGCG do not cross the animal BBB or the human BBB, respectively (29-31). As a result, there remains a strong driving force to identify new small molecule AD therapeutic candidates that modulate A β aggregation and are also safe and BBB-permeable.

Here we identify a new A β modulator with all of these properties. To our knowledge, A β modulating capacities of triphenylmethane dyes have not yet been reported. Here we show that Brilliant Blue G (BBG), a triphenylmethane dye (Figure 2.1) with a demonstrated safety profile (32) and BBB-permeability (33), also substantially removes A β cytotoxicity even at below stoichiometric concentration. Brilliant Blue FCF (BBF), a close structural analog of BBG, is approved by the U.S. Food and Drug Administration (FDA) as a blue food dye (Figure 2.1) and has one of the highest safety profiles amongst the seven currently approved synthetic food dyes. In tests, it exhibits no observable toxicity up to a daily consumption of 600 mg/kg body mass in

healthy animals (34). In the United States, more than six thousand pounds of BBF is produced annually, and daily intake of up to 12.5 mg/kg is tolerable in humans (35). BBG has recently garnered prominent attention in neuroscience regarding its therapeutic potential to treat acute spinal cord injury. In animal models, systemic administration of BBG reduced damage and expedited recovery after spinal cord injury (33). BBG also confers neuroprotection to the brain by inhibiting adverse inflammatory reactions and mitigating multiple sclerosis symptoms (36, 37). With the possibility for systemic administration into the nervous system with no known adverse side effects, BBG is an attractive candidate A β aggregation modulator.

Here we explore BBG's ability to modulate A β aggregation and reduce neurotoxicity with biochemical, biophysical, and cell-based assays. In particular, we monitored A β oligomer formation via immunoblotting using the A β -conformation specific antibody, A11. Polyclonal A11 antibody reacts with soluble A β oligomers and protofibrils, including neurotoxic conformers, but not with A β monomers and fibrils (8, 38, 39). We report that BBG promotes A β monomer conversions into non-toxic aggregates. To begin identifying the BBG structural features responsible for this activity, we also evaluated the modulating capacities of three close structural analogs, Brilliant Blue R (BBR), BBF, and Fast Green FCF (FGF) on A β aggregation and cytotoxicity. Our findings suggest that the structural differences of BBG and BBR from BBF and FGF along with the two additional methyl groups attached to the triphenylmethane structure of BBG are important for effective modulation of A β aggregation and cytotoxicity. Unique interaction modes on A β of BBG and BBR are expected to provide a new insight on molecular mechanism of A β aggregation and cytotoxicity. Our findings validate a relatively new hypothesis that generating non-toxic A β aggregates by small molecules is an effective way to reduce A β -associated neurotoxicity even without preventing A β oligomer formation (21, 28). Thus, our

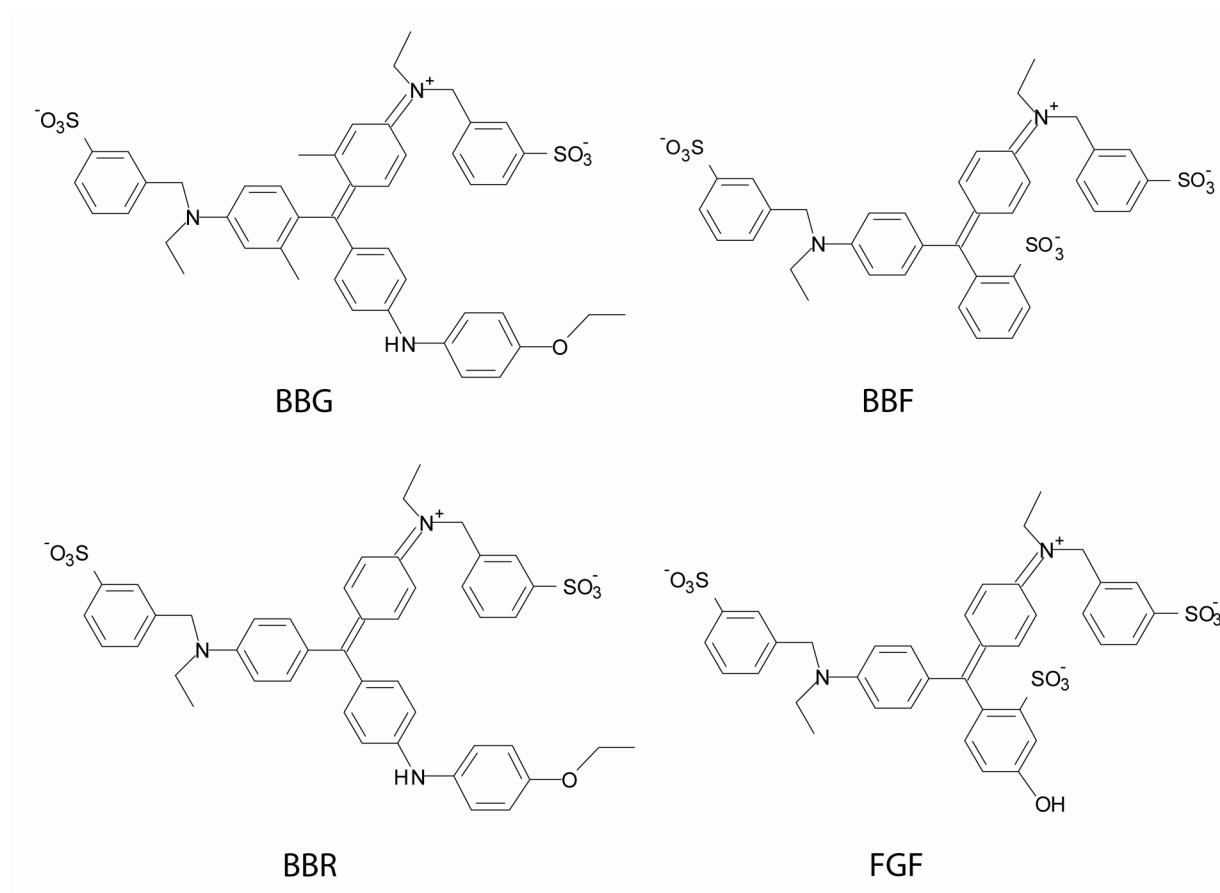


Figure 2.1. Chemical structures of Brilliant Blue G (BBG), Brilliant Blue FCF (BBF), Brilliant Blue R (BBR), and Fast Green FCF (FGF) at neutral pH.

work provides evidence of and mechanistic details of reduced A β -associated neurotoxicity for a novel type of A β aggregation inhibitor that also has encouraging attributes as a therapeutic lead compound.

2.3 Materials and Methods

A β 40 was purchased from Anaspec, Inc. (Fremont, CA). Human neuroblastoma SH-SY5Y cells were obtained from ATCC (Manassas, VA). Polyclonal A11 anti-oligomer and horseradish peroxidase (HRP)-conjugated anti-rabbit IgG antibodies were obtained from Invitrogen (Carlsbad, CA). 4G8 antibody was obtained from Abcam (Cambridge, MA). Monoclonal 6E10 was obtained from Millipore (Billerica, MA). ECL advance chemiluminescence kit was obtained from GE Healthcare Life Sciences. 10x Alamar Blue dye stock solution was obtained from Invitrogen (Calsbad, CA). All other chemicals were obtained from Sigma-Aldrich (St. Louis, MO) unless otherwise noted.

A β Sample Preparation. A β 40 samples were prepared as described earlier (59-61). A β 40 was dissolved in 0.1 % trifluoroacetic acid (TFA) to obtain a 1.0 mM stock solution, which was then incubated for 1 hour at room temperature without agitation. The freshly prepared 1.0 mM stock A β 40 solution was diluted with phosphate buffered saline (PBS) solution (10 mM NaH₂PO₄ and 150 mM NaCl at pH 7.4) to obtain a 50 μ M A β solution. 50 μ M A β samples were then incubated at 37 °C for the desired time.

Dot blotting. 2 μ L A β 40 samples were spotted onto a nitrocellulose membrane and were allowed to dry at room temperature. The nitrocellulose membrane was incubated in 5% skim

milk dissolved in 0.1 % Tween 20, Tris-buffered saline (TBS-T) solution for one hour. The 5% milk TBS-T solution was removed and the membrane was washed three times for 5 minutes each with TBS-T solution. The membrane was then incubated in antibody solution for 1 hour. The 4G8, A11 and 6E10 antibodies were diluted in 0.5% milk TBS-T solution according to the manufacturer's recommendation. After incubation the membrane was washed three times for 5 minutes using TBS-T solution. When a peroxidase (HRP)-conjugated antibody (4G8) was used as the primary antibody, membranes were coated with 2 mL of detection agent from the ECL Advance Detection Kit (GE Healthcare, Waukesha, WI) and the fluorescence was visualized. Otherwise, the membrane was incubated in (1:5000 dilution in 0.5% milk TBS-T) HRP-conjugated IgG for one hour. Then the membrane was washed three times for 5 minutes each with TBS-T solution and the same detection method as previously described was used. The blot images were captured using a BioSpectrum imaging system (UVP, Upland, CA).

Thioflavin T (ThT) Fluorescence Assay. 5 μ L of 50 μ M A β 40 sample solution was diluted in 250 μ L of 10 μ M ThT (dissolved in PBS) in 96-well plates. The resulting ThT fluorescence of A β sample was measured at an emission wavelength of 485 nm using an excitation wavelength of 450 nm using a Synergy 4 UV-Vis/fluorescence multi-mode microplate reader (Biotek, Winooski, VT).

Transmission Electron Microscopy (TEM). 10 μ L A β sample was adsorbed onto a formvar mesh grid for 1 min. The grids were then negatively stained with 2% uranyl acetate for 45 sec., blotted dry and viewed on a Jeol JEM1230 Transmission Electron Microscope at the Advanced Microscopy Laboratory at the University of Virginia operated at 80 kV.

A β -BBG Binding Assay. A saturation curve of BBG binding to A β was obtained according to the Bradford assay protocols described previously (63, 85, 86). 0.05 mg/mL stock solution of BBG was prepared by dissolving BBG powder in water. An acidified alcohol solution was prepared by combining 95% ethanol and 85% phosphoric acid in a 1:2 volumetric ratio. Then the modified Bradford reagent was created by adding 167 μ L of the BBG stock solution to 250 μ L of the acidified alcohol and the final volume was adjusted to 1 mL. For each sample, 50 μ L of the modified Bradford reagent was added to each well in a 96-well microplate. Next, 0 to 30 μ L of 1 mM A β monomer was added to each well, and the final volume was adjusted to 100 μ L with double distilled water. Absorbance of the samples was measured at 595 nm using a Synergy 4 UV-Vis/fluorescence multi-mode microplate reader (Biotek, Winooski, VT). The number of BBG binding sites and the intrinsic binding constant were derived from the saturation binding curve. The detailed procedures are described in the Supporting Information.

MTT and Alamar Blue Reduction Assays. 50 mg of 3-(4,5-Dimethylthiazol-2-yl)-2,5-diphenyltetrazolium bromide (MTT) obtained from Millipore (Billerica, MA) was dissolved overnight at 4 °C in 10 mL of PBS. The MTT solution was then sterile filtered. Human neuroblastoma SH-SY5Y cells were cultured in a humidified 5% CO₂/air incubator at 37 °C in DMEM 12:1:1 modified media with 10% fetal bovine serum and 1% penicillin-streptomycin (Thermofisher, Waltham, MA). 25,000 SH-SY5Y cells were seeded into 96-well plates and incubated for 48 hours. After incubation, the culture medium was replaced with 100 μ L of fresh media, and 10 μ L of the A β sample was added to each well to obtain a final A β concentration of 5 μ M. Cells were incubated for an additional 48 hours. The media was then aspirated and

replaced with 50 μ L of fresh media. 10 μ L of the sterile MTT solution was added, and cells were incubated for 6 hours at 37 °C in the dark. After incubation, 200 μ L of dimethylsulfoxide (DMSO) was added to each well to dissolve the reduced MTT, and the absorbance was measured at 506 nm using a Synergy 4 UV-Vis/fluorescence multi-mode microplate reader.

Alamar Blue reduction assay was performed according to the protocol in the literature (79-81) and the manufacturer's protocol (Invitrogen) with some modifications. 10,000 SH-SY5Y cells were seeded at each well in a 96-well plate. The cells were incubated for up to 1 week. After incubation, old media was replaced with 100 μ L of fresh media, and 10 μ L of the sample containing A β with or without BBG was added to each well. The cells were incubated for 3 days, and the media was then replaced with 100 μ L of fresh media followed by addition of 40 μ L of a 10x Alamar Blue stock solution. Next, the cells were incubated for 4 – 6 hours to allow the cells to metabolize the Alamar Blue. After incubation, fluorescence was measured using an emission wavelength of 555 nm using an excitation wavelength of 590 nm using a Synergy 4 UV-Vis/fluorescence microplate reader (Biotek, Winooski, VT).

2.4 Results and Discussion

Modulation of A β Aggregation by BBG. In order to evaluate the aggregation modulation capability of BBG, we employed dot-blotting, TEM and the ThT fluorescence assay. TEM and ThT fluorescence assays are widely used to monitor A β aggregation. TEM images provide morphological information of A β aggregates. ThT is a dye that fluoresces at 485 nm when it binds to amyloid fibrils (23, 40, 41). Therefore, ThT fluorescence measurement is an efficient tool to monitor the progression of fibril formation. However, the ThT assay is not very effective in detecting soluble oligomers that are known to be more neurotoxic than amyloid

fibrils (6-9). Furthermore, the diversity of A β aggregate morphologies and differing levels of neurotoxicity (42, 43) represent a challenge for correlating the aggregate morphology observed by TEM to A β -associated neurotoxicity. Recently, dot-blotting with A β -specific antibodies was successfully used to detect and distinguish the spectrum of A β conformer species (8, 38, 39, 44-46). In particular, A11 is useful for detecting neurotoxic A β intermediates (39, 45). Previously it was shown that A β -associated toxicity could be mitigated by reducing the presence of A11-reactive species (8, 21). Alternatively, 4G8 is an A β -sequence-specific monoclonal antibody (47-50) which has an epitope that lies within amino acids 17 to 24 of A β . The 4G8 epitope corresponds to a region of the A β peptide that is known to form β -sheet structures. During transition from monomers and low molecular weight oligomers to fibrils, β -sheet stacking buries the 4G8 epitope and ultimately limits 4G8 antibody binding. This leads to a dramatic loss of the 4G8 signal which can thereby be used to detect extensive fibril network structure formation (51). Lastly, 6E10 is a monoclonal antibody that recognizes residues 1-16 of A β , the N-terminus of A β (45, 51). Although the 6E10 antibody was originally thought to bind various A β species with equal strength, recent studies indicate that the 6E10 antibody binds to different A β species with different binding affinities (13, 45, 52). Similar to the 4G8 antibody, the 6E10 antibody binding affinity to fibrils is a few times lower than those of oligomers and monomers. According to the structural model of A β 40 fibril proposed by Grigorieff et. al., two pairs of A β protofibrils intertwine adjacently to form a fibril (53). In their model, the N-terminus of the each protofibril is interlocked to form a fibril, which can bury the 6E10 epitope upon fibril formation. We performed dot-blotting using a panel of A β -specific antibodies, together with traditional TEM and ThT fluorescence assay, to monitor the formation of neurotoxic A β oligomers, protofibrils, and fibrils.

Two pathologically important A β isoforms, A β 42 and A β 40, have been widely used to evaluate the modulating capacities of numerous small molecules on A β aggregation and cytotoxicity (54-58). We used the more abundant isoform, A β 40, in this study. A β samples were prepared by incubating 50 μ M of A β 40 monomer from 0 to 3 days at 37 °C without shaking either in the absence (control) or presence of BBG as described previously (59-61). In order to detect even a weak modulating effect of BBG on A β aggregation, we chose 150 μ M of BBG (3x BBG), which is three times higher than the concentration of A β (50 μ M). A β samples were taken periodically during incubation, and subjected to dot-blotting, ThT fluorescence assay, and TEM.

In the absence of BBG, dot-blotting results indicated that the majority of A11-reactive A β aggregates formed between day 1 and 2 (Figure 2.2). However, when the A β monomer was co-incubated with BBG, A11-reactive signals remained very low until day 3. However, reduction of the A11-reactive signals at day 1 and 2 did not result from a loss of A β moieties, as supported by the sustained 6E10 signal at days 1 and 2 compared to day 0 (Figure 2.2). In the absence of BBG, the 6E10 signal increased at days 1 and 2 from day 0 and then decreased at day 3 (Figure 2.2). This variation can be explained by the weaker binding affinity of 6E10 for A β monomers and fibrils compared to A β intermediates as described previously (52). In the presence of 3x BBG, the 6E10 signal at day 3 was very strong, suggesting the idea that A β intermediates rather than A β fibrils were predominant in the sample. In the A β control sample, the majority of 4G8 signal was lost between day 2 and 3 (Figure 2.2; Figure 2.8B), implying that the majority of 4G8 epitopes were buried due to compact stacking of β -sheet structures, a prototypical feature of amyloid fibrils (51). However, in the presence of 3x BBG, a significant 4G8 signal at day 3 was observed, which also supports the idea that A β fibril mesh networks were not formed. These

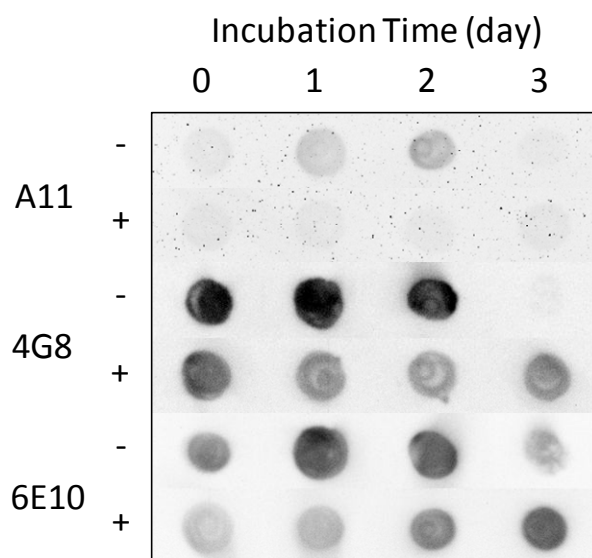


Figure 2.2. Monitoring A β aggregation by dot blotting. Oligomer-specific A11 antibody and A β -sequence specific antibodies, 4G8 and 6E10, were used. 50 μ M A β was incubated in the absence (-) (top panels) or presence of 3x BBG (+) (bottom panels) for 1 to 3 days at 37 °C. Samples were taken on the indicated day and spotted onto a nitrocellulose membrane. Each membrane was immunostained with the A11 (A), 4G8 (B), or 6E10 (C) antibody. The blot images were taken by a UVP BioSpectrum imaging system.

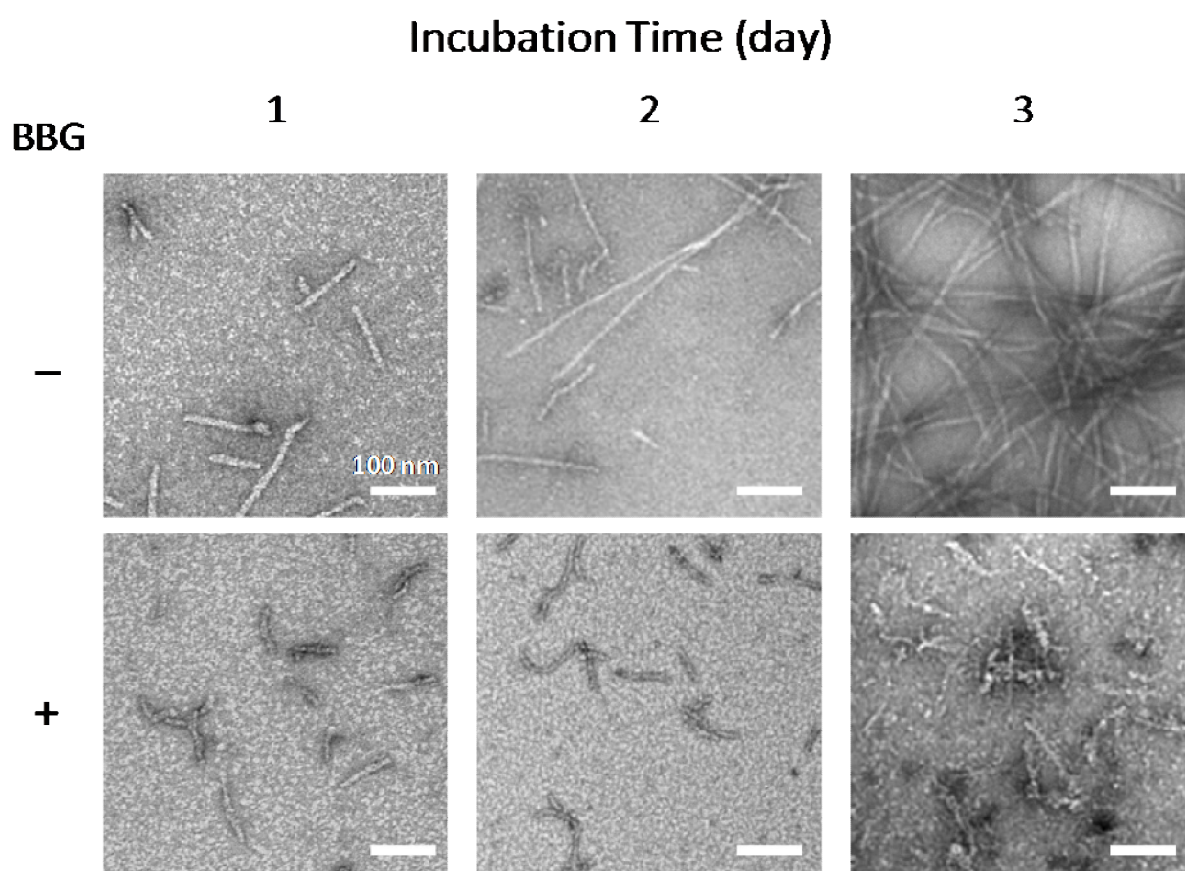


Figure 2.3. Monitoring A β aggregate and fibril formation by TEM. 50 μ M A β was incubated in the absence (-) (top panels) or presence of 3x BBG (+) (bottom panels) for 1 to 3 days at 37 °C. Presence of oligomers and protofibrils (Top-left); protofibrils and isolated fibrils (Top-middle); fibril mesh network (Top-right); oligomers and protofibrils (Bottom-left); protofibrils (Bottom-middle); protofibrils (Bottom-right). Scale bar is 100 nm.

findings imply that BBG effectively inhibits the formation of A11-reactive A β oligomers and A β fibrils, the most toxic A β species.

Next we characterized the morphology of the A β species formed with and without BBG using negative-stain TEM. TEM images clearly show a distinct morphological difference between A β samples incubated in the absence and those in the presence of 3x BBG (Figure 2.3). At day 1, in the absence of BBG, oligomers and protofibrils (~100 nm in length) were formed (Figure 2.3, top-left). Considering that high molecular weight A β protofibrils as well as oligomers were A11-reactive in the literature (21, 39, 62), there is the possibility that the protofibrils observed at day 1 were also A11-reactive. Interestingly, even in the presence of 3x BBG, protofibrils (~100 nm in length) were predominantly observed (Figure 2.3, bottom-left panel). Despite the morphological similarities, the A β aggregates prepared with 3x BBG possessed substantially lower immuno-reactivity to the A11 antibody than those prepared without BBG. These findings imply that at day 1, the low A11 reactivity of A β samples co-incubated with BBG resulted from promoted formation of A11-unreactive A β protofibrils.

At day 2, a mixture of protofibrils and fibrils was observed in the absence of BBG (Figure 2.3, top-middle; Figure 2.4A), which indicated that some A β oligomers and protofibrils were converted into longer protofibrils and fibrils. However, in the presence of 3x BBG, protofibrils (less than 100 nm) were still predominantly observed similar to day 1 (Figure 2.3, bottom-middle; Figure 2.4B).

At day 3, the A β sample prepared in the absence of BBG exhibited only long mature fibrils in a meshed network (Figure 2.3, top-right), which is consistent with dot-blotting and ThT fluorescence results. Here, ThT fluorescence sharply increased beginning at 48 hr (Figure 2.5), which was interpreted to be the onset of amyloid fibril formation. In dramatic contrast, in the

presence of 3x BBG, TEM showed that protofibrils (~100 nm) remained the predominant species (Figure 2.3, bottom-right), which supports the idea that co-incubation of 3x BBG stops or at least substantially slows down the A β aggregation process. Morphological similarities among the BBG-treated A β aggregates observed at days 1, 2 and 3 are consistent with very weak A11-reactivity of the BBG-treated samples at least until day 3.

These findings support that BBG is an efficient aggregation modulator and reduces the formation of A11-reactive A β aggregates. The results also show that BBG suppresses fibril formation for at least three days.

Dose-Dependent Modulation of A β Aggregation by BBG. To further characterize the aggregation modulation capabilities of BBG, we evaluated BBG dose-dependent aggregation using dot-blotting and ThT fluorescence assay. 50 μ M A β was co-incubated at 37 °C with various BBG concentrations ranging from 0.001x (50 nM) to 10x (500 μ M). Dot-blotting results of A β samples using three A β -specific antibodies (A11, 4G8, and 6E10) are shown in Figure 2.6. When A β was co-incubated with less than 0.1x BBG (5 μ M), no observable changes were found in the A11 immunoblotting patterns (Figure 2.6A). However, co-incubation with 0.5x BBG or greater resulted in a reduction in the concentration of A11-reactive species formed, over the course of the study, confirming previous results. Since A11-reactive A β species were most abundant at day 2, we wanted to quantify inhibition of A11-reactive A β species formation (Figure 2.6D). Therefore, for day 2, integrated A11 dot-blot signal intensities were plotted against BBG concentrations. A half-maximal value of inhibitory concentration (IC₅₀) of 0.72x BBG was derived from the data fitting to a sigmoid curve ($R^2=0.99$).

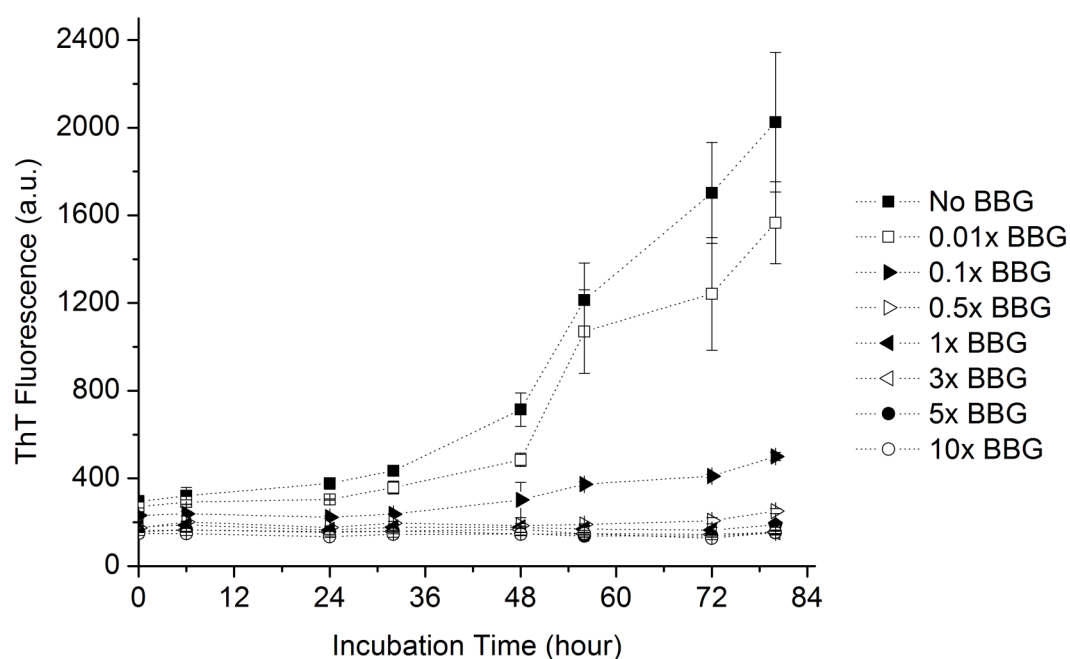


Figure 2.5. Time course of ThT fluorescence of A β samples with varying concentrations of BBG. 50 μ M of A β monomer was incubated at 37 °C in the absence (no BBG) or presence of the indicated concentrations of BBG (from 0.001x to 10x) for up to 80 hours. 5 μ L of A β sample was taken at 0, 6, 24, 32, 48, 54, 72 and 80 hours for ThT fluorescence analysis. ThT fluorescence was measured in arbitrary units (a.u.). Values represent means \pm standard deviation (n = 3).

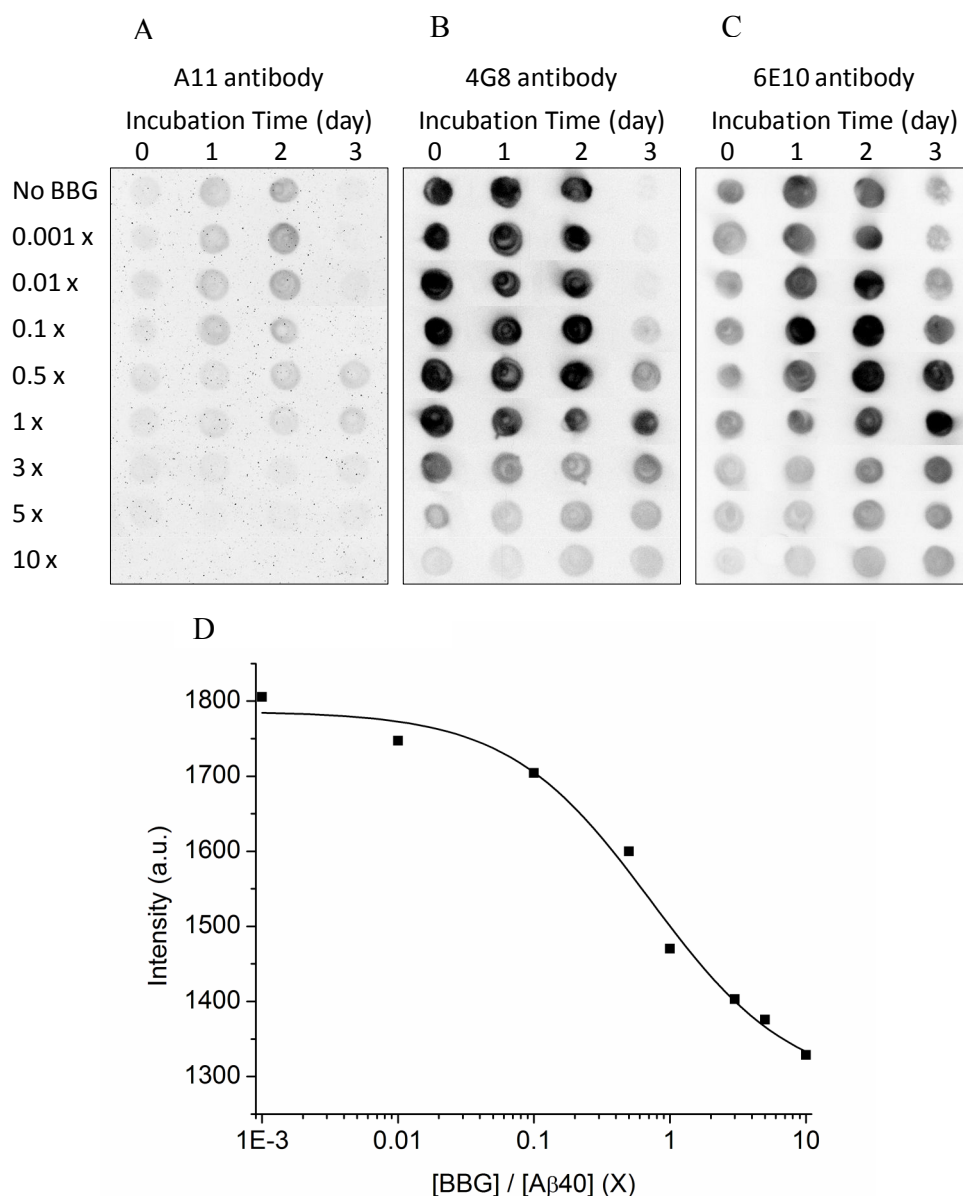


Figure 2.6. Dose-dependence of A β aggregation modulation by BBG. 50 μ M of A β monomer was incubated at 37 $^{\circ}$ C in the absence (No BBG) or presence of the indicated concentrations of BBG (from 0.001x to 10x) for up to 3 days. Samples were taken on the indicated day and spotted onto a nitrocellulose membrane. Each membrane was immunostained with the A11 (A), 4G8 (B), or 6E10 (C) antibody. The blot images were taken by a UVP BioSpectrum imaging system. The blot image of A11-reactive signal of A β samples incubated with varying concentrations of BBG for two days was processed by ImageJ (NIH). The data were fitted to a sigmoid curve ($R^2 = 0.99$) (D).

In the absence of BBG, the 6E10 antibody stained A β oligomers/protofibrils, monomers, and fibrils in decreasing order of intensity, which is consistent with a few fold weaker binding to A β fibrils by the 6E10 compared to oligomers/protofibrils as described previously (52). In Figure 2.6B and C, BBG at concentration below 1x increases 4G8 and 6E10 signals at day 3. These results are consistent with enhanced accessibility of the 4G8 and 6E10 epitopes due to BBG-induced conversion of A β aggregates from fibril mesh networks to oligomers and protofibrils. However, as the concentration of BBG increased above 1x, 4G8 and 6E10 reactive signals decreased. Finally, in the presence of 10x BBG, the 4G8- and 6E10-reactive signals are both very weak compared to those observed in the absence of BBG, suggesting that both 4G8 and 6E10 epitopes were substantially lost partially due to direct binding of BBG. The 4G8 epitope corresponds to a hydrophobic patch of the A β that is known to form β -sheet structures. The 6E10 epitope is the N-terminus of A β carrying both positive and negative charges. Therefore, we speculate that BBG preferentially binds to the hydrophobic patch of A β and weakly binds to the charged N-terminus of A β via electrostatic interaction.

BBG Binding to A β . Immunoblotting assays described in the previous section suggested that BBG binds to multiple sites on A β above 1x BBG concentration. In order to determine the number of BBG binding sites on A β , a binding curve (Figure 2.7) was obtained according to the method described previously (63). The number of binding sites (n) and the intrinsic association constant (k), 3.2 and 1.1×10^4 (M^{-1}), respectively, were determined by fitting the BBG-A β binding data to a straight line in the double reciprocal plot (Figure A2.1) in the Supplemental Information Section. More than one BBG binding site on A β can explain the reduced 4G8- and 6E10-reactivity of A β aggregates at high concentrations of BBG considering the reduced accessibility

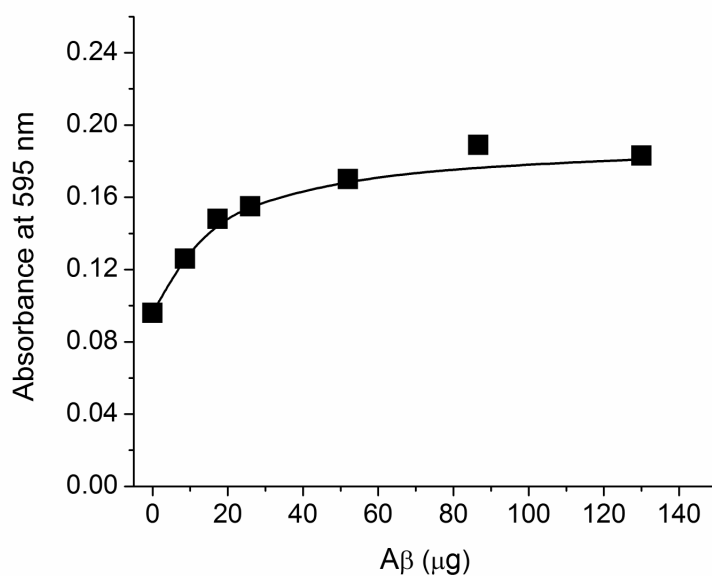


Figure 2.7. A saturation binding curve of BBG into A β peptide. 49 μ M BBG was incubated with the varying concentrations of A β peptide (0 to 300 μ M) until they reached an equilibrium and the absorbance of the BBG bound to the A β peptide was measured at 595 nm.

of the 4G8 and 6E10 antibodies to their epitopes caused by BBG binding. The dissociation constant, the reciprocal of the intrinsic association constant, is 92 μM .

Inhibition of A β -associated Cytotoxicity by BBG. Next, we sought to determine whether the conversion of A11-reactive aggregates into off-pathway aggregates reduces A β -associated neurotoxicity. In order to evaluate the cytotoxicity of A β species, we employed the MTT-reduction assay and neuroblastoma SH-SY5Y cells, widely used for this purpose (8, 22, 64-69). Although the MTT-reduction assay does not directly measure cell death, it detects any change in cellular redox activity that is considered an indication of cell viability (70). Therefore, inhibiting MTT reducing activity of cells has been often interpreted as cytotoxicity. Preformed A β aggregates were prepared by incubating A β monomers in the absence or presence of 3x BBG at 37 °C for the specified time duration. The preformed aggregates were then administered to neuroblastoma SH-SY5Y cells for 48 hours, and subsequent cell viability was measured by MTT reduction. Before testing the cytotoxicity of A β samples, we first determined whether BBG by itself is cytotoxic to neuroblastoma SH-SY5Y cells. In the presence of 3x BBG dye (15 μM), SH-SY5Y cell viability was 95% without any BBG, quite consistent with the good biocompatibility and low toxicity observed in animals (32, 33).

Next we evaluated A β -associated toxicity. At day 0, cells treated with A β monomers (5 μM) exhibited a mild reduction (15%) in the viability (Figure 2.4), which may be due to moderately toxic A β aggregates formed during the 48 hr incubation of A β monomers with the cells. In the presence of 3x BBG (15 μM), viability recovered to 93% ($P < 0.001$), which is similar to the viability of 3x BBG dye alone without A β monomer (95%). This finding suggests the possibility that 3x BBG inhibits toxic aggregate formation of A β monomers (5 μM) during

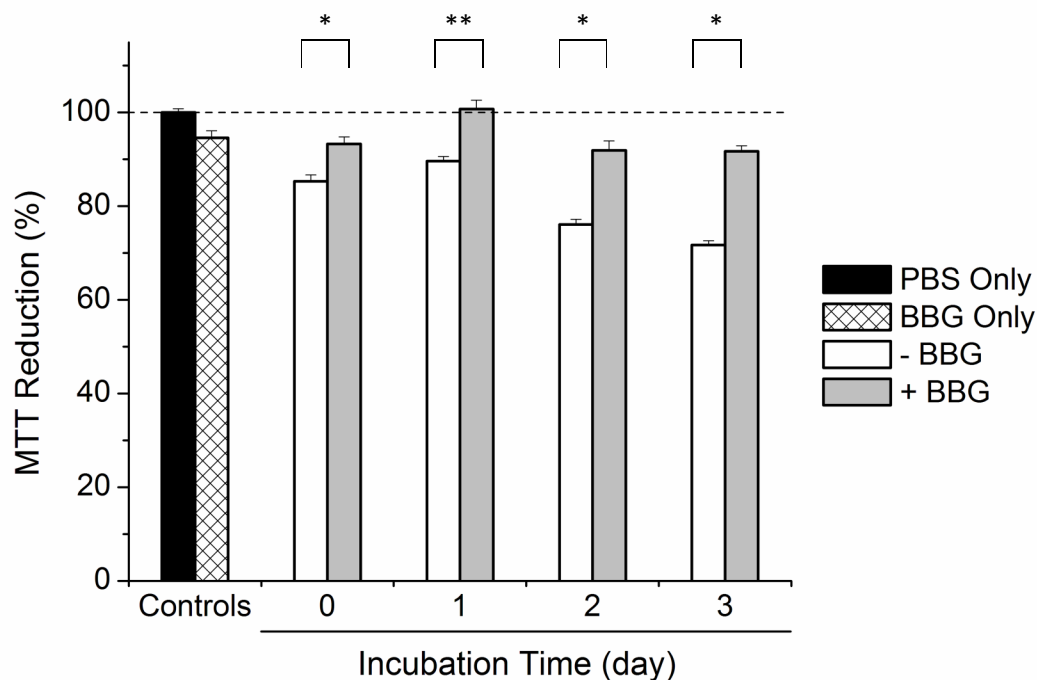


Figure 2.8. Viability of neuroblastoma SH-SY5Y cells incubated with preformed A β samples in the absence or presence of BBG. Preformed A β aggregates were prepared by incubating 50 μ M of A β monomer in the absence or presence of BBG at 37 °C for 0 to 3 days, as indicated in the graph. Aggregates were then administered to SH-SY5Y cells at a final concentration of 5 μ M. After 48 hours, mitochondrial metabolic activity was measured using MTT reduction. Cells administered with PBS as a control (*Black*), 3x BBG (15 μ M) dye only (*White with pattern*), A β incubated without BBG (*White*), A β incubated with 3x BBG (*Grey*). Values represent means \pm standard deviation ($n \geq 3$). Values are normalized to the viability of cells administered with PBS only. Two-sided Student's t-tests were applied to the data. * $P < 0.001$, ** $P < 0.005$.

the 48 hr incubation with the cells. At day 1, in the presence of 3x BBG, the A β sample exhibited cell viability of 101 %, significantly higher than the cell viability (90%) of A β samples without BBG ($P < 0.001$) (Figure 2.8). These findings support the hypothesis that BBG can counteract the A β sample cytotoxicity and that BBG-induced A β aggregates observed by TEM were non-toxic.

At day 2, in the absence of BBG, cell viability decreased to 76%. This can likely be attributed to an increased concentration of A11-reactive toxic oligomers and to the emergence of amyloid fibrils (Figure 2.8). Although amyloid fibrils are less toxic than A11-reactive toxic oligomers, the toxicity of amyloid fibrils is reportedly higher than that of monomers (8, 9). In the presence of BBG, cell viability significantly improved to 92% ($P < 0.001$), consistent with the reduction of A11-reactive A β species in the dot-blot results (Figure 2.2) and lack of observable fibrils in the TEM image (Figure 2.3). These results suggest that a decrease in the concentration of A11-reactive species correlates with a decrease in A β -associated toxicity.

At day 3, in the absence of BBG, addition of the preformed A β aggregates reduced the cell viability to 72%. Although the A11-reactive signal dropped after day 2, the reduced viability was most probably caused by the predominant amyloid fibrils converted from both small fraction of toxic A11-reactive aggregates and probably more dominant toxic non-A11 reactive large intermediates. Ishii and co-workers showed that A β aggregates larger than 50 kDa were five times less toxic than A β aggregates smaller than 50 kDa (9). Based on dot-blotting, TEM and fluorescence, the vast majority of fibrils were formed almost exclusively after day 2 (Figure 2.2, 2.3, and 2.5). Consequently, at day 3, fibrils were the major toxic moieties. However, when A β was incubated with 3x BBG, cell viability significantly recovered to 92% ($P < 0.001$), which is comparable to the viability of cells incubated only with 3x BBG, without A β . Based on the cell

viability results, we conclude that 3x BBG completely mitigates A β -associated cytotoxicity. Moreover, these findings suggest that the majority of oligomers and protofibrils formed in the presence of 3x BBG observed in TEM in fact are non-toxic and structurally distinct from toxic A β species formed in the absence of BBG. This confirms that BBG reduces A β -associated toxicity by promoting the conversion of A β monomer to off-pathway, non-toxic intermediates.

Although an MTT reduction assay has been widely used to determine A β -associated cytotoxicity on numerous cell lines (21, 45, 71-75), the MTT reduction assay results should be carefully interpreted due to a potential issue of A β -induced expedited exocytosis of the reduced MTT. There have been several reports indicating that A β aggregates can increase export of the reduced MTT and promote buildup of the crystalline form of the reduced MTT on the cell surface leading to a reduced MTT uptake (76-78). Considering other researchers have reported a good correlation between a MTT reduction and other viability assay results, including oxidative stress (73) and lactate dehydrogenase (LDH) release (75), the increased MTT exocytosis may be dependent on the cell type and A β preparation method used.

In order to confirm the correlation of the MTT assay results with A β -associated cytotoxicity, an Alamar Blue reduction assay was also performed. Alamar Blue reducing cellular activity has been considered an indication of cell viability and used to measure A β -associated cytotoxicity (79-81). Since Alamar Blue is a soluble dye, it does not cause an issue of crystal dye buildup on the cell surface. A β samples incubated for 0 to 3 days at 37 °C were added to SH-SY5Y cells to determine Alamar Blue reducing activities. Similar to the MTT reduction assay results, the cells treated with A β aggregates incubated for 2 days exhibited significantly ($P < 0.05$) lowered Alamar Blue reducing activity compared to the cells without A β treatment (Control) or cells treated with A β monomers (Day 0) (Figure A2.2). Furthermore, co-

incubation of 3x BBG with A β for 2 days inhibited the A β -associated reduction of the Alamar Blue reducing activity ($P < 0.05$) (Figure A2.2), which is also consistent with the MTT reduction assay results. However, there were two factors making it difficult to detect a subtle change in the Alamar Blue reducing activity under the other conditions used in our studies. First, the differences in the Alamar Blue reducing cellular activities with different A β samples were smaller than those in the MTT reducing activities at similar conditions. Second, the standard deviations of the measured Alamar Blue reducing activities (5 to 11%) were greater than those in the MTT reducing activities (usually less than 5%). Despite the limitations, the Alamar Blue assay results support the idea that the reduction in the MTT reducing activity of cells treated with A β aggregates (at least at day 2) indicates the A β -associated cytotoxicity and inhibition of the A β -associated cytotoxicity by co-incubation of 3x BBG under the conditions used in our studies. Therefore, we believe that the MTT reduction assay results have a good correlation with the cell viabilities treated with the A β samples, though we do not completely exclude the possibility of the promoted crystal buildup of the reduced MTT contributes to the MTT reduction results.

Dose-Dependent Inhibition of A β -Associated Cytotoxicity by BBG. In order to evaluate dose-dependent ability of BBG to inhibit A β -associated cytotoxicity, preformed A β aggregates were prepared by incubating A β monomer in the absence (control) or presence of varying concentrations of BBG from 0.001x to 10x at 37 °C for 2 days. The resulting preformed species were administered to SH-SY5Y cells and viability was measured after 48 hours using MTT reduction. From 0.001x (5.0 nM) to 0.1x (0.5 μ M) BBG, cell viability (approximately 72%) was comparable to that of the control. However, cell viability dramatically improved when 0.5x BBG (2.5 μ M) or greater was co-incubated with A β (Figure 2.9). Consequently, from 3x to

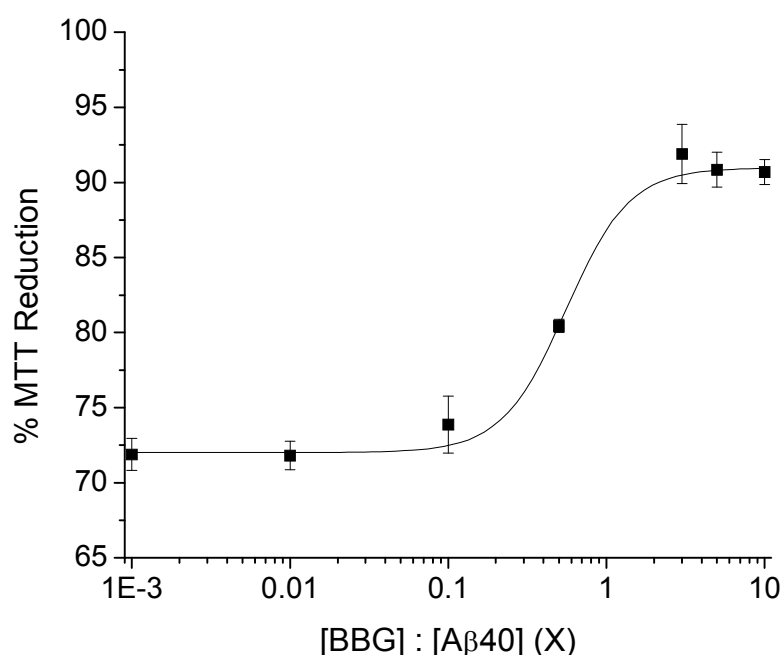


Figure 2.9. Dose-dependence of inhibition of A β -associated cytotoxicity by BBG. Preformed A β aggregates were prepared by incubating 50 μ M of A β monomer in the presence of varying concentrations of BBG (0.001x, 0.01x, 0.1x, 0.5x, 1x, 3x, 5x, and 10x) at 37 °C for 2 days. A β aggregates were then administered to SH-SY5Y cells at a final concentration of 5 μ M. After incubation, mitochondrial metabolic activity was measured after 48 hours using MTT reduction. Values represent means \pm standard deviation ($n \geq 3$). Values are normalized to the viability of cells administered with PBS only. The data were fitted to a sigmoid curve ($R^2 = 0.99$).

10x BBG, cell viability was maintained in the range of 91 to 93%. When the data were fitted to a sigmoid dose-dependent curve ($R^2 = 0.99$), a half maximal effective concentration (EC_{50}) value of 0.55x BBG was obtained. This value corresponded almost exactly to the significant reduction in the A β -associated cytotoxicity observed at 0.5x BBG. These results clearly demonstrate that BBG inhibits A β -associated cytotoxicity in a dose-dependent manner.

Based on the results described earlier, it is obvious that BBG inhibits formation of A11-reactive A β species and A β -associated cytotoxicity in a dose-dependent manner. Furthermore, the EC_{50} value (0.55x BBG) derived from A β -associated cytotoxicity sigmoidal regression (Figure 2.9) corresponds well to the IC_{50} values (0.72x BBG) derived from the sigmoidal regression of inhibition of A11-reactive A β species formation by BBG (Figure 2.6D). Therefore, we conclude that the inhibition of A β -associated cytotoxicity directly correlates with BBG aggregation modulation effects. Furthermore, considering that BBG-induced aggregates are non-toxic, A β -associated cytotoxicity reduction is attributed to BBG-induced, non-toxic aggregate formation.

Bias of ThT Fluorescence Reading at High BBG Concentrations. We used ThT binding to verify the onset of fibril formation at varying BBG concentrations. As BBG concentration was increased ThT fluorescence of A β sample decreased accordingly (Figure 2.5), consistent with our findings and observations at 3x BBG. In order to quantify the inhibition of ThT fluorescence by BBG, we plotted ThT fluorescence versus BBG concentrations from 10^{-5} x to 10x BBG (Figure A2.1). Data fitting to a sigmoid curve ($R^2 = 0.99$) generated an IC_{50} value of 0.03x BBG, which is one order of magnitude lower than those determined for the inhibition of A11-reactive species formation by BBG. To explain this discrepancy, we hypothesized that the

ThT fluorescence reading was biased due to either spectral interference of BBG on ThT fluorescence measurement or competitive binding of BBG to ThT binding sites on amyloid fibrils. Carver et al. reported that curcumin and quercetin significantly skewed ThT fluorescence measurements via spectral interference, where alternatively resveratrol introduced a measurement bias by competing with ThT for amyloid fibril binding sites (82). Since BBG at neutral pH has negligible absorbance at both 450 nm (excitation wavelength of ThT fluorescence) and 485 nm (emission wavelength of ThT fluorescence) (83), spectral interference was ruled out as a source of the bias. Next, to determine whether BBG and ThT competitively bind to the same sites, we measured the ThT fluorescence of preformed amyloid fibrils that were momentarily mixed with varying BBG concentrations immediately prior to adding ThT (Figure A2.4). As BBG concentration increased, ThT fluorescence decreased accordingly. When the data were fitted to a sigmoidal curve ($R^2 = 0.99$), an IC_{50} value of 0.16x BBG was obtained. From this we conclude that the ThT fluorescence measurements of A β samples co-incubated with BBG can be biased since BBG at high concentrations can interfere with ThT binding to amyloid fibrils. Consequently, the ThT fluorescence assay should be used with caution at high concentrations of BBG.

Comparison of the A β aggregates formed in the presence or in the absence of BBG.

TEM, ThT fluorescence, immune-blotting, and cellular reducing activity assays have demonstrated various differences between the A β aggregates formed with BBG and those formed without BBG. In particular, the A β aggregates incubated for 2 days with and without 3x BBG exhibited several noticeable differences. The TEM images clearly indicate that 3x BBG inhibits long fibril formation but promotes ~ 100 nm-long curvilinear protofibril formation (Figure 2.3

top middle and bottom middle). At day 2, A β aggregates formed without BBG exhibited a moderate increase in ThT fluorescence compared to A β monomers (Figure 2.5), which suggests that fibrillar and non-fibrillar aggregates exist together. Unfortunately, the reduction in the ThT fluorescence value of the A β aggregates formed with 3x BBG cannot be directly interpreted as an indication of a reduction of A β fibrils due to the interference issue. The A β aggregates formed with 3x BBG showed very weak A11-reactivity, whereas the A β aggregates formed without BBG exhibited a substantial A11-reactivity. The protofibrils (Figure 2.3 top middle) look similar to the A11-reactive A β 40 protofibrils that Kim et al. recently reported (39). In the presence of 3x BBG, the 4G8-reactivity of the A β aggregates decreased (Figure 2.2), which suggests that one of the BBG binding sites might be located to near the 4G8 epitope, the hydrophobic patch of A β at the 3x BBG concentration.

At day 2, the A β aggregates formed without BBG exhibited a significant decrease in the cellular reducing activity in both MTT (Figure 2.8) and Alamar Blue (Figure A2.2) assays. These two assays indicate the reduced cell viability is correlated with the substantial A11-reactivity (Figure 2.2). The very weak A11-reactivity of the A β aggregates formed with 3x BBG suggests its correlation with the substantial increase in the cellular reducing activity on both MTT (Figure 2.8) and Alamar Blue (Figure A2.2). A11-reactivity is defined by immuno-reactivity of A β aggregates but not by size or morphology. Therefore, it remains unclear whether there is any correlation between the A11-reactivity and the size or morphology of A β aggregates. Considering that the BBG-induced A β aggregates do not form A β fibrils or at least substantially slow down fibril formation process, we speculate that BBG binding causes conformation changes of A β protofibrils or blocking the nuclei leading to inhibition of fibril formation. However, further investigation is required to clarify the relationship between the

BBG-induced A β aggregate morphology change and the change in the cellular reducing activity using MTT and Alamar Blue.

Modulation of A β aggregation by BBG analogs. In order to determine whether any structural features of BBG are critical in modulating A β aggregation and cytotoxicity, A β aggregation modulation by three close structural analogs of BBG (BBR, BBF and FGF) were examined using dot blotting and TEM analysis. The four compounds (BBG, BBR, BBF, and FGF) are congeners sharing the common triphenylmethane structure. Both BBF and FGF are FDA-approved food dyes (84). Similar to BBG, BBR is commonly used to stain proteins in protein electrophoresis. However, the chemical structure of BBR differs from BBG by the lack of two methyl groups attached to triphenylmethane (Figure 2.1). Both BBF and FGF have three benzenesulfonate functional groups, whereas BBG and BBR have two benzenesulfonate functional groups and one uncharged diphenylamine group. FGF differs from BBF with only one hydroxyl functional group attached to one of the benzenesulfonate functional groups (Figure 2.1).

Three different concentrations (1x, 3x, and 10x) of each BBG analog were co-incubated with 50 μ M of A β up to three days and the immuno-reactivities of the A β samples were monitored by A11, 4G8, and 6E10 A β -specific antibodies. Similar to BBG, BBR reduced toxic A11-reactive A β species. In the presence of 3x BBR, the A11-reactive A β signal became less than half the A11-reactive signal of A β sample incubated without any dye, though 1x BBR did not make a substantial change in the A11-reactive signal (Figure 2.10A). Co-incubation of 10x BBR with the A β samples led to almost complete elimination of the A11-reactive species. However, considering that even 1x BBG substantially reduced A11-reactive signal (Figure

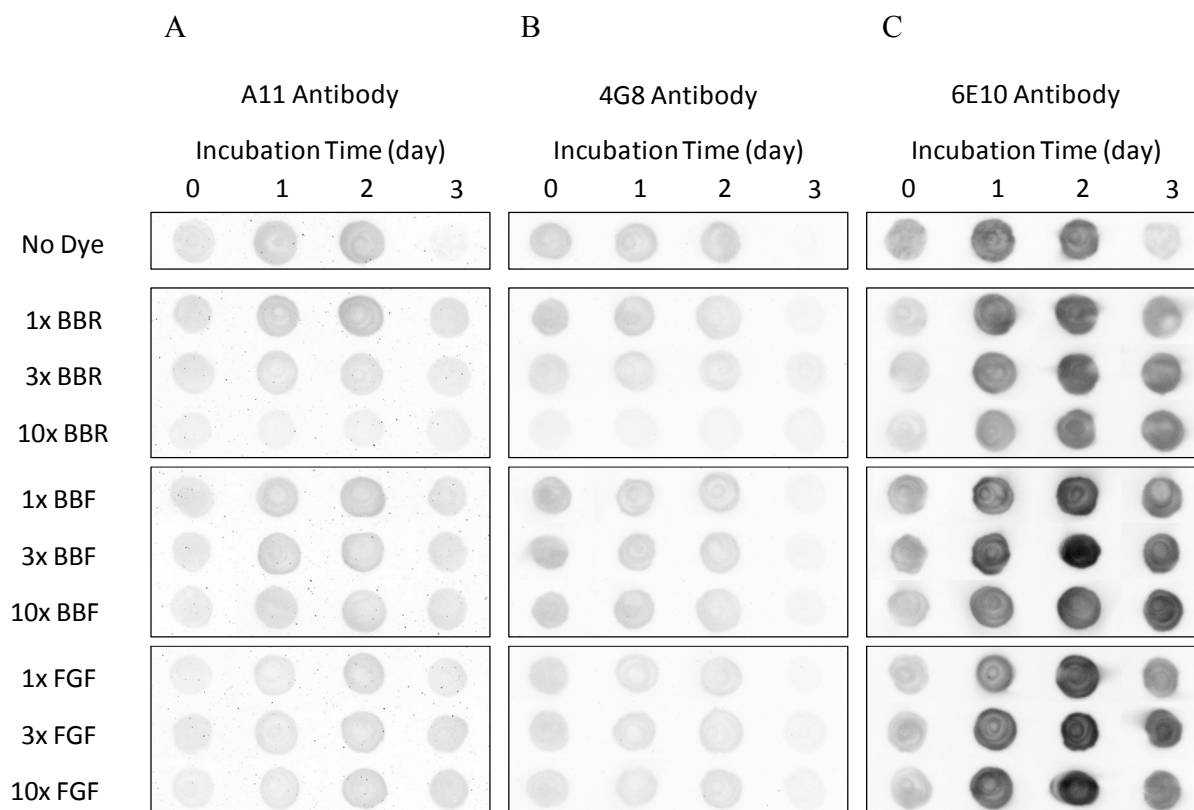


Figure 2.10. Modulation of A β aggregation by BBR, BBF and FGF. 50 μ M of A β monomer was incubated at 37 °C in the absence (No Dye) or presence of the indicated concentrations of BBR, BBF or FGF (1x, 3x, and 10x) for up to three days. Samples were taken on the indicated day and spotted onto a nitrocellulose membrane. Each membrane was immunostained with the A11 (A), 4G8 (B), or 6E10 (C) antibody.

2.10A), BBR is less effective than BBG in reducing A11-reactive species. Similarly to 10x BBG, 10x BBR substantially reduced the 4G8-reactive signal, suggesting that both BBR and BBG bind to the A β hydrophobic patch (4G8 epitope) in a similar fashion (Figure 2.10B). In contrast, even at 10x BBR, there was no substantial reduction of the 6E10-reactive signal, which suggests that the BBR interaction mode of A β is different from that of BBG (Figure 2.6C and 2.10C). These results suggest that BBR reduces A11-reactive toxic species, but the interaction mode of BBR with A β is different from that of BBG.

In sharp contrast to BBG, both BBF and FGF exhibited little or minor changes in the immuno-reactivities of the A β samples against the A11 and 4G8 antibodies from the A β samples incubated without any dye (Figure 2.10A to C). In particular, even 10x BBF and 10x FGF did not show any substantial reduction of the neurotoxic A11-reactive A β species. At day 3, the A β samples incubated with either BBF or FGF exhibited strong 6E10 signals, whereas A β aggregates formed in the absence of any dye exhibited very weak 6E10 signals (Figure 2.10C). These 6E10 epitope accessibility results suggest that BBF- or FGF-induced A β protofibrils and fibrils have conformations different from those of A β protofibrils and fibrils formed in the absence of any dye.

Morphology of A β aggregates formed after two days in the absence (no dye control) or in the presence of one of the BBG congeners was analyzed by negative-stain TEM (Figure 2.4). Similar to BBG, co-incubation of 10x BBR promoted protofibril formation (less than 100 nm), but inhibited amyloid fibril formation (Figure 2.4B and C). In contrast, both BBF and FGF induced formation of the mixture of long fibrils and protofibrils, whereas the A β aggregates incubated with BBG for two days were predominantly curvilinear protofibrils (Figure 2.4B, D, and E). In contrast, morphology of the A β aggregates formed in the presence of either BBF

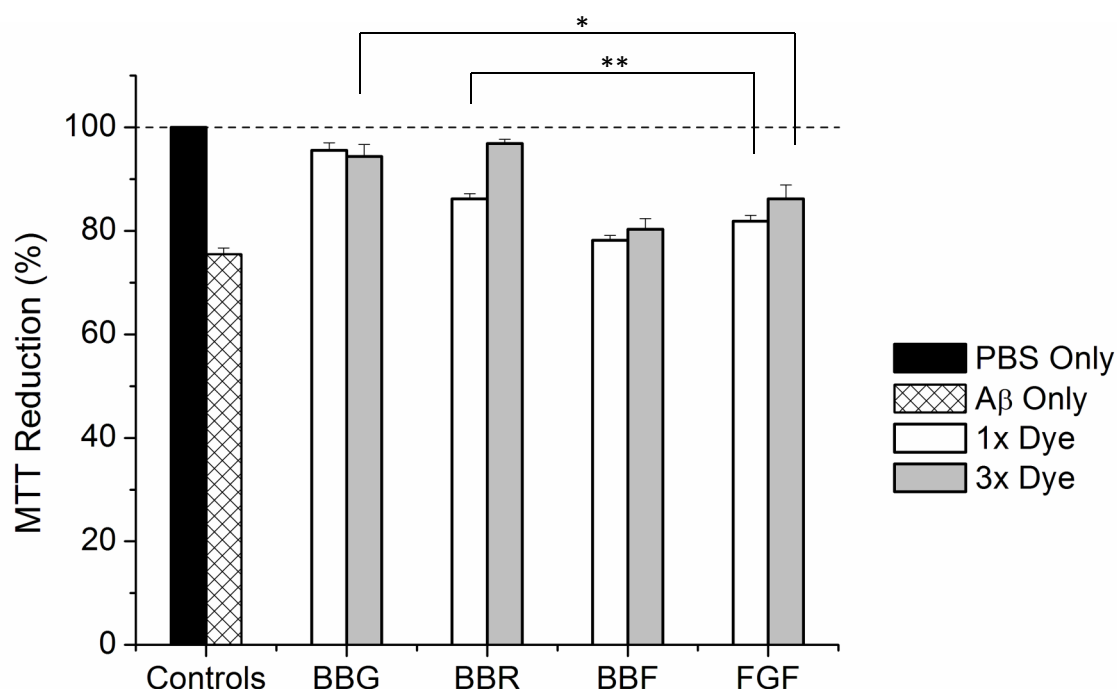


Figure 2.11. Viability of neuroblastoma SH-SY5Y cells incubated with preformed A β samples in the presence of BBG or BBG analogs (BBR, BBF, and FGF). Preformed A β aggregates were prepared by incubating 50 μ M of A β monomer in the presence of BBG or BBG analogs at 37 °C for two days, as indicated in the graph. Aggregates were then administered to SH-SY5Y cells at a final concentration of 5 μ M. After 48 hours, mitochondrial metabolic activity was measured using MTT reduction. Cells administered with PBS as a control (*Black*), A β samples incubated without BBG (*White with pattern*), A β samples incubated with 1x dye (*White*) or 3x dye (*Grey*). Values represent means \pm standard deviation ($n \geq 3$). Values are normalized to the viability of cells administered with PBS only. Two-sided Student's t-tests were applied to the data. * $P < 0.001$, ** $P < 0.01$.

(Figure 2.4D) or FGF (Figure 2.4E) were similar to that of the A β aggregates formed in the absence of any dye (Figure 2.4A), which is consistent with the dot-blot results that there are little or minor differences in the immuno-reactivities of the A β aggregates formed in the absence or in the presence of BBF or FGF.

These results strongly suggest that the both BBG and BBR effectively modulate A β aggregation by promoting protofibril formation but inhibiting fibril formation. In contrast, both BBF and FGF are not as effective in modulating A β aggregation as BBG and BBR, but promote formation of the mixture of protofibrils and fibrils.

Modulation of A β cytotoxicity by BBG analogues. Modulating effects of the BBG analogs on A β -associated cytotoxicity were also evaluated by MTT reduction assay of SH-SY5Y cells (Figure 2.11). Similarly to 3x BBG, co-incubation of 3x BBR with A β samples recovered the viability of SH-SY5Y cells from 76% to 97% (Figure 2.11), which is consistent with the reduced neurotoxic A11-reactive signal of the A β aggregates at 3x BBR (Figure 2.10A). However, compared with 1x BBG, co-incubation of 1x BBR exhibits less increase in the SH-SY5Y cell viability (86%) consistent with lower reduction of A11-reactive signal. These findings support the idea that BBR reduces A β -associated cytotoxicity but is less effective than BBG.

In contrast, BBF and FGF are less effective in modulating the A β -cytotoxicity than BBG and BBR. Even at 3x BBF and FGF, the SH-SY5Y cell viability was 80% and 86%, respectively, which is higher than the cell viability without any dye but 10% lower than the cell viability with either 3x BBG or 3x BBR. A moderate reduction of A β cytotoxicity produced by BBF or FGF may be due to promoted formation of fibrils less toxic than oligomers/protofibrils (Figure 2.4D and E). Investigations are underway to reveal the underlying mechanisms for this behavior.

2.5 Conclusion

Our research is geared towards the discovery of potential therapies for Alzheimer's disease. To this end, our efforts have focused on discovering practically applicable small molecules that can modulate amyloid-beta cytotoxicity and elucidating their mode of action. While expanding the pool of potential candidates, we also compared molecular analogues to identify unique structural features responsible for imparting modulating activity.

Comprehensively, our results conclusively demonstrate that BBG inhibits A β -associated cytotoxicity. BBG inhibits the formation of neurotoxic A11-reactive A β intermediates in a dose-dependent manner, by promoting the formation of non-toxic A β aggregates. The half-maximal BBG concentration for inhibition of A11-reactive A β aggregate formation (IC₅₀) after a two-day incubation was 0.72x. Moreover, negative-stain TEM, ThT fluorescence and dot-blotting assay results demonstrate that BBG promotes the formation of A11-unreactive, off-pathway A β oligomers and protofibrils, and also consequently inhibits the formation of amyloid fibrils. 15 μ M of BBG (3x BBG) was marginally cytotoxic (5%) to neuroblastoma SH-SY5Y cells, which is approximately one third the cytotoxicity of 5 μ M of A β monomer. 3x BBG also completely suppressed A β -associated cytotoxicity throughout the duration of our study (three days). The half-maximal BBG concentration for the inhibition of A β -associated cytotoxicity (EC₅₀) was 0.55x. These results strongly supports that the inhibition of A β -associated cytotoxicity directly correlates with the reduction of neurotoxic A11-reactive A β aggregates by BBG.

Based on our findings, we identified several structural features that are important to the modulating activity of the triphenylmethane derivatives. In particular, the electron withdrawing sulfur atom on the sulfonated aryl groups are expected to perturb *pi-pi* stacking interaction.

Moreover, although all four triphenylmethane derivatives exhibit modulating activity towards A β aggregation, the structural difference between BBG and BBR, and BBF and FGF dictate their characteristic interaction mode and level of activity. The 4-ethoxy aniline group is structurally unique to BBG and BBR and likely imparts the ability to strongly modulate both A β aggregation and cytotoxicity by reducing the formation of toxic aggregates. A comparison between BBG and BBR also revealed the potential importance of two additional methyl groups on the core triphenylmethane structure that may allow BBG to inhibit A β toxicity at lower stoichiometric concentrations.

The inhibitory effects of BBG on A β -associated cytotoxicity as well as highly favorable biocompatibility and BBB-permeability make BBG a promising lead compound for future AD therapeutic development.

2.6 Literature Cited

1. Brookmeyer, R., Gray, S., and Kawas, C. (1998) Projections of Alzheimer's disease in the United States and the public health impact of delaying disease onset, *Am. J. Public Health* 88, 1337-1342.
2. Alzheimer's Association. (2010) 2010 Alzheimer's Disease Facts and Figures, In *Alzheimer's & Dementia*.
3. Sinha, S., and Lieberburg, I. (1999) Cellular mechanisms of beta-amyloid production and secretion, *Proc. Natl. Acad. Sci. USA* 96, 11049-11053.
4. Bitan, G., Kirkitadze, M. D., Lomakin, A., Vollers, S. S., Benedek, G. B., and Teplow, D. B. (2003) Amyloid beta-protein (A beta) assembly: A beta 40 and A beta 42 oligomerize through distinct pathways, *Proc. Natl. Acad. Sci. U. S. A.* 100, 330-335.
5. Hardy, J. A., and Higgins, G. A. (1992) Alzheimers disease - the amyloid cascade hypothesis, *Science* 256, 184-185.
6. Hardy, J., and Selkoe, D. J. (2002) Medicine - The amyloid hypothesis of Alzheimer's disease: Progress and problems on the road to therapeutics, *Science* 297, 353-356.

7. McLean, C. A., Cherny, R. A., Fraser, F. W., Fuller, S. J., Smith, M. J., Beyreuther, K., Bush, A. I., and Masters, C. L. (1999) Soluble pool of A beta amyloid as a determinant of severity of neurodegeneration in Alzheimer's disease, *Ann. Neurol.* **46**, 860-866.
8. Ladiwala, A. R. A., Lin, J. C., Bale, S. S., Marcelino-Cruz, A. M., Bhattacharya, M., Dordick, J. S., and Tessier, P. M. (2010) Resveratrol Selectively Remodels Soluble Oligomers and Fibrils of Amyloid A beta into Off-pathway Conformers, *J. Biol. Chem.* **285**, 24228-24237.
9. Chimon, S., Shaibat, M. A., Jones, C. R., Calero, D. C., Aizezi, B., and Ishii, Y. (2007) Evidence of fibril-like beta-sheet structures in a neurotoxic amyloid intermediate of Alzheimer's beta-amyloid, *Nat. Struct. Mol. Biol.* **14**, 1157-1164.
10. Hawkes, C. A., Ng, V., and McLaurin, J. (2009) Small Molecule Inhibitors of A beta-Aggregation and Neurotoxicity, *Drug Dev. Res.* **70**, 111-124.
11. Hamaguchi, T., Ono, K., and Yamada, M. (2006) Anti-amyloidogenic therapies: strategies for prevention and treatment of Alzheimer's disease, *Cell. Mol. Life Sci.* **63**, 1538-1552.
12. Thapa, A., Woo, E. R., Chi, E. Y., Sharoar, M. G., Jin, H. G., Shin, S. Y., and Park, I. S. Biflavonoids Are Superior to Monoflavonoids in Inhibiting Amyloid-beta Toxicity and Fibrillogenesis via Accumulation of Nontoxic Oligomer-like Structures, *Biochemistry* **50**, 2445-2455.
13. Necula, M., Kayed, R., Milton, S., and Glabe, C. G. (2007) Small molecule inhibitors of aggregation indicate that amyloid beta oligomerization and fibrillization pathways are independent and distinct, *J. Biol. Chem.* **282**, 10311-10324.
14. Bose, P. P., Chatterjee, U., Xie, L., Johansson, J., Gothelid, E., and Arvidsson, P. I. (2010) Effects of Congo Red on A beta(1-40) Fibril Formation Process and Morphology, *ACS Chem. Neurosci.* **1**, 315-324.
15. Burgevin, M. C., Daniel, N., Passat, M., Messence, K., Bertrand, P., Doble, A., and Blanchard, J. C. (1994) Neurotoxicity of beta-amyloid analog peptides on rat hippocampal neuronal cultures, *J. Neurochem.* **63**, S74-S74.
16. Lorenzo, A., and Yankner, B. A. (1994) Beta-amyloid neurotoxicity requires fibril formation and is inhibited by congo red, *Proc. Natl. Acad. Sci. U. S. A.* **91**, 12243-12247.
17. Pedersen, M. O., Mikkelsen, K., Behrens, M. A., Pedersen, J. S., Enghild, J. J., Skrydstrup, T., Malmendal, A., and Nielsen, N. C. (2010) NMR Reveals Two-Step

- Association of Congo Red to Amyloid beta in Low-Molecular-Weight Aggregates, *J. Phys. Chem. B* 114, 16003-16010.
18. Podlisny, M. B., Walsh, D. M., Amarante, P., Ostaszewski, B. L., Stimson, E. R., Maggio, J. E., Teplow, D. B., and Selkoe, D. J. (1998) Oligomerization of endogenous and synthetic amyloid beta-protein at nanomolar levels in cell culture and stabilization of monomer by congo red, *Biochemistry* 37, 3602-3611.
 19. McLaurin, J., Golomb, R., Jurewicz, A., Antel, J. P., and Fraser, P. E. (2000) Inositol stereoisomers stabilize an oligomeric aggregate of Alzheimer amyloid beta peptide and inhibit A beta-induced toxicity, *J. Biol. Chem.* 275, 18495-18502.
 20. McLaurin, J., Kierstead, M. E., Brown, M. E., Hawkes, C. A., Lambermon, M. H. L., Phinney, A. L., Darabie, A. A., Cousins, J. E., French, J. E., Lan, M. F., Chen, F. S., Wong, S. S. N., Mount, H. T. J., Fraser, P. E., Westaway, D., and St George-Hyslop, P. (2006) Cyclohexanehexol inhibitors of A beta aggregation prevent and reverse Alzheimer phenotype in a mouse model, *Nat. Med.* 12, 801-808.
 21. Ehrnhoefer, D. E., Bieschke, J., Boeddrich, A., Herbst, M., Masino, L., Lurz, R., Engemann, S., Pastore, A., and Wanker, E. E. (2008) EGCG redirects amyloidogenic polypeptides into unstructured, off-pathway oligomers, *Nat. Struct. Mol. Biol.* 15, 558-566.
 22. Feng, Y., Wang, X.-P., Yang, S.-G., Wang, Y.-J., Zhang, X., Du, X.-T., Sun, X.-X., Zhao, M., Huang, L., and Liu, R.-t. (2009) Resveratrol inhibits beta-amyloid oligomeric cytotoxicity but does not prevent oligomer formation, *Neurotoxicology* 30, 986-995.
 23. Reinke, A. A., and Gestwicki, J. E. (2007) Structure-activity relationships of amyloid beta-aggregation inhibitors based on curcumin: Influence of linker length and flexibility, *Chem. Biol. Drug Design* 70, 206-215.
 24. Yang, F. S., Lim, G. P., Begum, A. N., Ubeda, O. J., Simmons, M. R., Ambegaokar, S. S., Chen, P. P., Kayed, R., Glabe, C. G., Frautschy, S. A., and Cole, G. M. (2005) Curcumin inhibits formation of amyloid beta oligomers and fibrils, binds plaques, and reduces amyloid in vivo, *J. Biol. Chem.* 280, 5892-5901.
 25. Moss, M. A., Varvel, N. H., Nichols, M. R., Reed, D. K., and Rosenberry, T. L. (2004) Nordihydroguaiaretic Acid Does Not Disaggregate beta-Amyloid(1-40) Protofibrils but Does Inhibit Growth Arising from Direct Protofibril Association, *Mol. Pharmacol.* 66, 592-600.
 26. Pardridge, W. A. (2009) Alzheimer's disease drug development and the problem of the blood-brain barrier, *Alzheimers Dement.* 5, 427-432.

27. Frid, P., Anisimov, S. V., and Popovic, N. (2007) Congo red and protein aggregation in neurodegenerative diseases, *Brain Res. Rev.* 53, 135-160.
28. Ladiwala, A. R. A., Dordick, J. S., and Tessier, P. M. (2010) Aromatic Small Molecules Remodel Toxic Soluble Oligomers of Amyloid beta through Three Independent Pathways, *J. Biol. Chem.* 286, 3209-3218.
29. Zini, A., Del Rio, D., Stewart, A. J., Mandrioli, J., Merelli, E., Sola, P., Nichelli, P., Serafini, M., Brighenti, F., Edwards, C. A., and Crozier, A. (2006) Do flavan-3-ols from green tea reach the human brain?, *Nutr. Neurosci.* 9, 57-61.
30. Yazawa, K., Kihara, T., Shen, H. L., Shimmyo, Y., Niidome, T., and Sugimoto, H. (2006) Distinct mechanisms underlie distinct polyphenol-induced neuroprotection, *FEBS Lett.* 580, 6623-6628.
31. Diniz, A., Escuder-Gilabert, L., Lopes, N. P., Gobbo-Neto, L., Villanueva-Camanas, R. M., Sagrado, S., and Medina-Hernandez, M. J. (2007) Permeability profile estimation of flavonoids and other phenolic compounds by biopartitioning micellar capillary chromatography, *J. Agric. Food Chem.* 55, 8372-8379.
32. Remy, M., Thaler, S., Schumann, R. G., May, C. A., Fiedorowicz, M., Schuettauf, F., Gruterich, M., Priglinger, S. G., Nentwich, M. M., Kampik, A., and Haritoglou, C. (2008) An in vivo evaluation of Brilliant Blue G in animals and humans, *Br. J. Ophthalmol.* 92, 1142-1147.
33. Peng, W. G., Cotrina, M. L., Han, X. N., Yu, H. M., Bekar, L., Blum, L., Takano, T., Tian, G. F., Goldman, S. A., and Nedergaard, M. (2009) Systemic administration of an antagonist of the ATP-sensitive receptor P2X7 improves recovery after spinal cord injury, *Proc. Natl. Acad. Sci. U. S. A.* 106, 12489-12493.
34. Borzelleca, J. F., Depukat, K., and Hallagan, J. B. (1990) Lifetime toxicity carcinogenicity studies of FD&C blue No.1 (brilliant blue FCF) in rats and mice, *Food Chem. Toxicol.* 28, 221-234.
35. Borzelleca Joseph, F., and Hallagan John, B. (1992) Safety and Regulatory Status of Food, Drug, and Cosmetic Color Additives, In *Food Safety Assessment*, pp 377-390, American Chemical Society.
36. Ryu, J. K., and McLarnon, J. G. (2008) Block of purinergic P2X(7) receptor is neuroprotective in an animal model of Alzheimer's disease, *Neuroreport* 19, 1715-1719.
37. Matute, C., Torre, I., Perez-Cerda, F., Perez-Samartin, A., Alberdi, E., Etxebarria, E., Arranz, A. M., Ravid, R., Rodriguez-Antiguedad, A., Sanchez-Gomez, M. V., and

- Domercq, M. (2007) P2X(7) receptor blockade prevents ATP excitotoxicity in oligodendrocytes and ameliorates experimental autoimmune encephalomyelitis, *J. Neurosci.* 27, 9525-9533.
38. Kayed, R., Head, E., Thompson, J. L., McIntire, T. M., Milton, S. C., Cotman, C. W., and Glabe, C. G. (2003) Common structure of soluble amyloid oligomers implies common mechanism of pathogenesis, *Science* 300, 486-489.
 39. Hu, Y., Su, B. H., Kim, C. S., Hernandez, M., Rostagno, A., Ghiso, J., and Kim, J. R. (2010) A strategy for designing a peptide probe for detection of beta-amyloid oligomers, *ChemBioChem* 11, 2409-2418.
 40. Khurana, R., Coleman, C., Ionescu-Zanetti, C., Carter, S. A., Krishna, V., Grover, R. K., Roy, R., and Singh, S. (2005) Mechanism of thioflavin T binding to amyloid fibrils, *J. Struct. Biol.* 151, 229-238.
 41. LeVine, H. (1999) Quantification of beta-sheet amyloid fibril structures with thioflavin T, In *Amyloid, Prions, and Other Protein Aggregates*, pp 274-284.
 42. Dahlgren, K. N., Manelli, A. M., Stine, W. B., Baker, L. K., Krafft, G. A., and LaDu, M. J. (2002) Oligomeric and fibrillar species of amyloid-beta peptides differentially affect neuronal viability, *J. Biol. Chem.* 277, 32046-32053.
 43. Shafirir, Y., Durell, S. R., Anishkin, A., and Guy, H. R. (2010) Beta-barrel models of soluble amyloid beta oligomers and annular protofibrils, *Proteins* 78, 3458-3472.
 44. Chen, Y. R., and Glabe, C. G. (2006) Distinct early folding and aggregation properties of Alzheimer amyloid-beta peptides A beta 40 and A beta 42 - Stable trimer or tetramer formation by A beta 42, *J. Biol. Chem.* 281, 24414-24422.
 45. Kaye, R., Head, E., Sarsoza, F., Saing, T., Cotman, C. W., Necula, M., Margol, L., Wu, J., Breydo, L., Thompson, J. L., Rasool, S., Gurlo, T., Butler, P., and Glabe, C. G. (2007) Fibril specific, conformation dependent antibodies recognize a generic epitope common to amyloid fibrils and fibrillar oligomers that is absent in prefibrillar oligomers, *Mol. Neurodegener.* 2, 18.
 46. Wu, J. W., Breydo, L., Isas, J. M., Lee, J., Kuznetsov, Y. G., Langen, R., and Glabe, C. (2010) Fibrillar oligomers nucleate the oligomerization of monomeric amyloid beta but do not seed fibril formation, *J. Biol. Chem.* 285, 6071-6079.
 47. Iijima, K., Liu, H. P., Chiang, A. S., Hearn, S. A., Konsolaki, M., and Zhong, Y. (2004) Dissecting the pathological effects of human A beta 40 and A beta 42 in Drosophila: A potential model for Alzheimer's disease, *Proc. Natl. Acad. Sci. U. S. A.* 101, 6623-6628.

48. Kimura, N., Yanagisawa, K., Terao, K., Ono, F., Sakakibara, I., Ishii, Y., Kyuwa, S., and Yoshikawa, Y. (2005) Age-related changes of intracellular A beta in cynomolgus monkey brains, *Neuropathol. Appl. Neurobiol.* 31, 170-180.
49. Klyubin, I., Walsh, D. M., Lemere, C. A., Cullen, W. K., Shankar, G. M., Betts, V., Spooner, E. T., Jiang, L. Y., Anwyl, R., Selkoe, D. J., and Rowan, M. J. (2005) Amyloid beta protein immunotherapy neutralizes A beta oligomers that disrupt synaptic plasticity in vivo, *Nat. Med.* 11, 556-561.
50. Thakker, D. R., Weatherspoon, M. R., Harrison, J., Keene, T. E., Lane, D. S., Kaemmerer, W. F., Stewart, G. R., and Shafer, L. L. (2009) Intracerebroventricular amyloid-beta antibodies reduce cerebral amyloid angiopathy and associated micro-hemorrhages in aged Tg2576 mice, *Proc. Natl. Acad. Sci. U. S. A.* 106, 4501-4506.
51. Sarroukh, R., Cerf, E., Derclaye, S., Dufrêne, Y., Goormaghtigh, E., Ruyschaert, J.-M., and Raussens, V. (2010) Transformation of amyloid β (1-40) oligomers into fibrils is characterized by a major change in secondary structure, *Cell. Mol. Life Sci.*, 1-10.
52. Mamikonyan, G., Necula, M., Mkrtichyan, M., Ghochikyan, A., Petrushina, I., Movsesyan, N., Mina, E., Kiyatkin, A., Glabe, C. G., Cribbs, D. H., and Agadjanyan, M. G. (2007) Anti-A beta(1-11) antibody binds to different beta-amyloid species, inhibits fibril formation, and disaggregates preformed fibrils but not the most toxic oligomers, *J. Biol. Chem.* 282, 22376-22386.
53. Schmidt, M., Sachse, C., Richter, W., Xu, C., Fandrich, M., and Grigorieff, N. (2009) Comparison of Alzheimer A beta(1-40) and A beta(1-42) amyloid fibrils reveals similar protofilament structures, *Proc. Natl. Acad. Sci. U. S. A.* 106, 19813-19818.
54. Findeis, M. A. (2000) Approaches to discovery and characterization of inhibitors of amyloid beta-peptide polymerization, *BBA Mol. Basis Dis.* 1502, 76-84.
55. Findeis, M. A., and Molineaux, S. M. (1999) Design and testing of inhibitors of fibril formation, In *Amyloid, Prions, and Other Protein Aggregates*, pp 476-488.
56. Morinaga, A., Ono, K., Takasaki, J., Ikeda, T., Hirohata, M., and Yamada, M. (2011) Effects of sex hormones on Alzheimer's disease-associated beta-amyloid oligomer formation in vitro, *Exp. Neurol.* 228, 298-302.
57. Ono, K., Condron, M. M., Ho, L., Wang, J., Zhao, W., Pasinetti, G. M., and Teplow, D. B. (2008) Effects of Grape Seed-derived Polyphenols on Amyloid beta-Protein Self-assembly and Cytotoxicity, *J. Biol. Chem.* 283, 32176-32187.

58. Geng, J., Li, M., Ren, J., Wang, E., and Qu, X. (2011) Polyoxometalates as Inhibitors of the Aggregation of Amyloid β -Peptides Associated with Alzheimer's Disease, *Angew. Chem. Int. Ed.*, n/a-n/a.
59. Qi, W., Zhang, A., Patel, D., Lee, S., Harrington, J. L., Zhao, L. M., Schaefer, D., Good, T. A., and Fernandez, E. J. (2008) Simultaneous monitoring of peptide aggregate distributions, structure, and kinetics using amide hydrogen exchange: Application to A beta(1-40) fibrillogenesis, *Biotechnol. Bioeng.* 100, 1214-1227.
60. Qi, W., Zhang, A. M., Good, T. A., and Fernandez, E. J. (2009) Two Disaccharides and Trimethylamine N-Oxide Affect A beta Aggregation Differently, but All Attenuate Oligomer-Induced Membrane Permeability, *Biochemistry* 48, 8908-8919.
61. Zhang, A., Qi, W., Good, T. A., and Fernandez, E. J. (2009) Structural differences between A beta(1-40) intermediate oligomers and fibrils elucidated by proteolytic fragmentation and hydrogen/deuterium exchange, *Biophys. J.* 96, 1091-1104.
62. Sandberg, A., Luheshi, L. M., Sollvander, S., de Barros, T. P., Macao, B., Knowles, T. P. J., Biverstal, H., Lendel, C., Ekholm-Petterson, F., Dubnovitsky, A., Lannfelt, L., Dobson, C. M., and Hard, T. (2010) Stabilization of neurotoxic Alzheimer amyloid-beta oligomers by protein engineering, *Proc. Natl. Acad. Sci. U. S. A.* 107, 15595-15600.
63. Sohl, J. L., and Splittgerber, A. G. (1991) The binding of Coomassie brilliant blue to Bovine Serum Albumin: A physical biochemistry experiment, *J. Chem. Educ.* 68, 262-null.
64. Feng, Y., Yang, S. G., Du, X. T., Zhang, X., Sun, X. X., Zhao, M., Sun, G. Y., and Liu, R. T. (2009) Ellagic acid promotes A beta 42 fibrillization and inhibits A beta 42-induced neurotoxicity, *Biochem. Biophys. Res. Commun.* 390, 1250-1254.
65. Pollack, S. J., Sadler, I. I. J., Hawtin, S. R., Tailor, V. J., and Shearman, M. S. (1995) Sulfonated dyes attenuate the toxic effects of beta-amyloid in a structure-specific fashion, *Neurosci. Lett.* 197, 211-214.
66. Avramovich-Tirosh, Y., Amit, T., Bar-Am, O., Zheng, H., Fridkin, M., and Youdim, M. B. (2007) Therapeutic targets and potential of the novel brain- permeable multifunctional iron chelator-monoamine oxidase inhibitor drug, M-30, for the treatment of Alzheimer's disease, *J Neurochem* 100, 490-502.
67. Avramovich-Tirosh, Y., Reznichenko, L., Mit, T., Zheng, H., Fridkin, M., Weinreb, O., Mandel, S., and Youdim, M. B. (2007) Neurorescue activity, APP regulation and amyloid-beta peptide reduction by novel multi-functional brain permeable iron-

- chelating- antioxidants, M-30 and green tea polyphenol, EGCG, *Curr. Alzheimer Res.* 4, 403-411.
68. Lee, S., Fernandez, E. J., and Good, T. A. (2007) Role of aggregation conditions in structure, stability, and toxicity of intermediates in the A beta fibril formation pathway, *Protein Sci.* 16, 723-732.
 69. Reznichenko, L., Amit, T., Zheng, H., Avramovich-Tirosh, Y., Youdim, M. B., Weinreb, O., and Mandel, S. (2006) Reduction of iron-regulated amyloid precursor protein and beta-amyloid peptide by (-)-epigallocatechin-3-gallate in cell cultures: implications for iron chelation in Alzheimer's disease, *J. Neurochem.* 97, 527-536.
 70. Ward, R. V., Jennigs, K. H., Jepras, R., Neville, W., Owen, D. E., Hawkins, J., Christie, G., Davis, J. B., George, A. J., Karran, E. H., and Howlett, D. R. (2000) Fractionation and characterization of oligomeric, protofibrillar and fibrillar forms of b-amyloid peptide, *Biochem. J.* 348, 137-144.
 71. Datki, Z., Juhász, A., Gálfi, M., Soós, K., Papp, R., Zádori, D., and Penke, B. (2003) Method for measuring neurotoxicity of aggregating polypeptides with the MTT assay on differentiated neuroblastoma cells, *Brain Res. Bull.* 62, 223-229.
 72. Nishimura, S., Murasugi, T., Kubo, T., Kaneko, I., Meguro, M., Marumoto, S., Kogen, H., Koyama, K., Oda, T., and Nakagami, Y. (2003) RS-4252 Inhibits Amyloid β -Induced Cytotoxicity in HeLa Cells, *Pharmacol. Toxicol.* 93, 29-32.
 73. Olivieri, G., Otten, U., Meier, F., Baysang, G., Dimitriadis-Schmutz, B., Müller-Spahn, F., and Savaskan, E. (2003) [beta]-amyloid modulates tyrosine kinase B receptor expression in SHSY5Y neuroblastoma cells: influence of the antioxidant melatonin, *Neuroscience* 120, 659-665.
 74. Ono, K., Yoshiike, Y., Takashima, A., Hasegawa, K., Naiki, H., and Yamada, M. (2003) Potent anti-amyloidogenic and fibril-destabilizing effects of polyphenols in vitro: implications for the prevention and therapeutics of Alzheimer's disease, *J. Neurochem.* 87, 172-181.
 75. Wang, S. S.-S., Rymer, D. L., and Good, T. A. (2001) Reduction in Cholesterol and Sialic Acid Content Protects Cells from the Toxic Effects of β -Amyloid Peptides, *J. Biol. Chem.* 276, 42027-42034.
 76. Liu, Y., and Schubert, D. (1997) Cytotoxic Amyloid Peptides Inhibit Cellular 3-(4,5-Dimethylthiazol-2-yl)-2,5-Diphenyltetrazolium Bromide (MTT) Reduction by Enhancing MTT Formazan Exocytosis, *J. Neurochem.* 69, 2285-2293.

77. Abe, K., and Saito, H. (1998) Amyloid [beta] protein inhibits cellular MTT reduction not by suppression of mitochondrial succinate dehydrogenase but by acceleration of MTT formazan exocytosis in cultured rat cortical astrocytes, *Neurosci. Res.* 31, 295-305.
78. Hertel, C., Hauser, N., Schubengel, R., Seilheimer, B., and Kemp, J. A. (1996) β -Amyloid-Induced Cell Toxicity: Enhancement of 3-(4,5-Dimethylthiazol-2-yl)-2,5-Diphenyltetrazolium Bromide-Dependent Cell Death, *J. Neurochem.* 67, 272-276.
79. Estus, S., Tucker, H. M., van Rooyen, C., Wright, S., Brigham, E. F., Wogulis, M., and Rydel, R. E. (1997) Aggregated amyloid-b protein induces cortical neuronal apoptosis and concomitant "apoptotic" pattern of gene induction, *J. Neurosci.* 17, 7736-7745.
80. Lindhagen-Persson, M., Brännström, K., Vestling, M., Steinitz, M., and Olofsson, A. (2010) Amyloid- β Oligomer Specificity Mediated by the IgM Isotype – Implications for a Specific Protective Mechanism Exerted by Endogenous Auto-Antibodies, *PLoS ONE* 5, e13928.
81. McLaurin, J., Cecal, R., Kierstead, M. E., Tian, X., Phinney, A. L., Manea, M., French, J. E., Lambermon, M. H. L., Darabie, A. A., Brown, M. E., Janus, C., Chishti, M. A., Horne, P., Westaway, D., Fraser, P. E., Mount, H. T. J., Przybylski, M., and St George-Hyslop, P. (2002) Therapeutically effective antibodies against amyloid-[beta] peptide target amyloid-[beta] residues 4-10 and inhibit cytotoxicity and fibrillogenesis, *Nat. Med.* 8, 1263-1269.
82. Hudson, S. A., Ecroyd, H., Kee, T. W., and Carver, J. A. (2009) The thioflavin T fluorescence assay for amyloid fibril detection can be biased by the presence of exogenous compounds, *FEBS J.* 276, 5960-5972.
83. Georgiou, C. D., Grintzalis, K., Zervoudakis, G., and Papapostolou, I. (2008) Mechanism of Coomassie brilliant blue G-250 binding to proteins: a hydrophobic assay for nanogram quantities of proteins, *Anal. Bioanal. Chem.* 391, 391-403.
84. Hansen, W. H., Long, E. L., Davis, K. J., Nelson, A. A., and Fitzhugh, O. G. (1966) Chronic toxicity of three food colourings: Guinea Green B, Light Green SF Yellowish and Fast Green FCF in rats, dogs and mice, *Food Cosmet. Toxicol.* 4, 389-410.
85. Bradford, M. M. (1976) Rapid and sensitive method for quantitation of microgram quantities of protein utilizing principle of protein-dye binding, *Anal. Biochem.* 72, 248-254.
86. Congdon, R. W., Muth, G. W., and Splittgerber, A. G. (1993) The Binding Interaction of Coomassie Blue with Proteins, *Anal. Biochem.* 213, 407-413.

2.7 Appendix

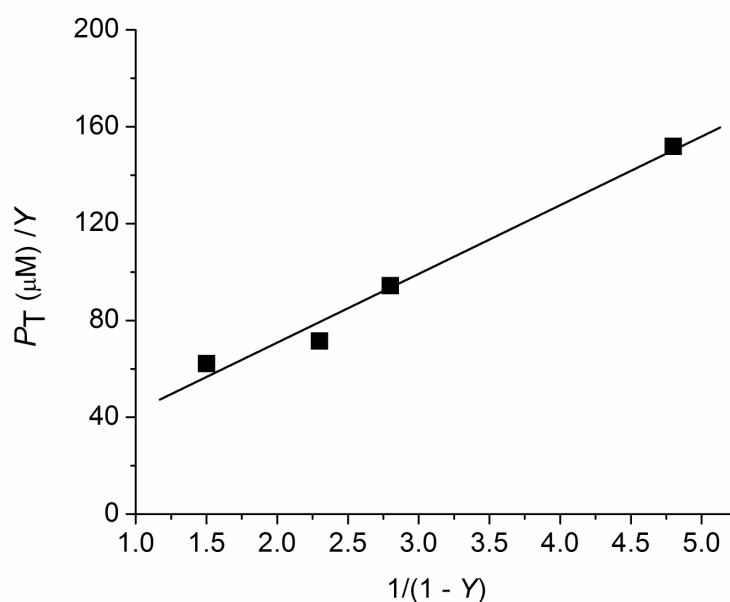


Figure A2.1. The data on the BBG-A β binding saturation curve (Figure 2.7) were fitted into a straight-line according to the equation, $P_T/Y = 1/(nk) [1/(1 - Y)] + D_T/n$ derived from $Y = nk(D)(P_T/D_T)/(1 + k(D))$ where Y , n , k , D , D_T , and P_T mean the fractional saturation of ligand binding sites, the number of binding sites, the binding constant, the dye concentration in solution, the total dye concentration, and the total protein concentration, respectively (*1*). The BBG concentration (D_T) was fixed at 49 μM . The A β concentration (P_T) was varied from 0 to 300 μM . The data at four P_T values between 20 μM and 120 μM were used for the fitting to a straight-line ($R^2 = 0.98$). The values of n and k were 3.2 and $1.1 \times 10^4 \text{ (M}^{-1}\text{)}$, respectively.

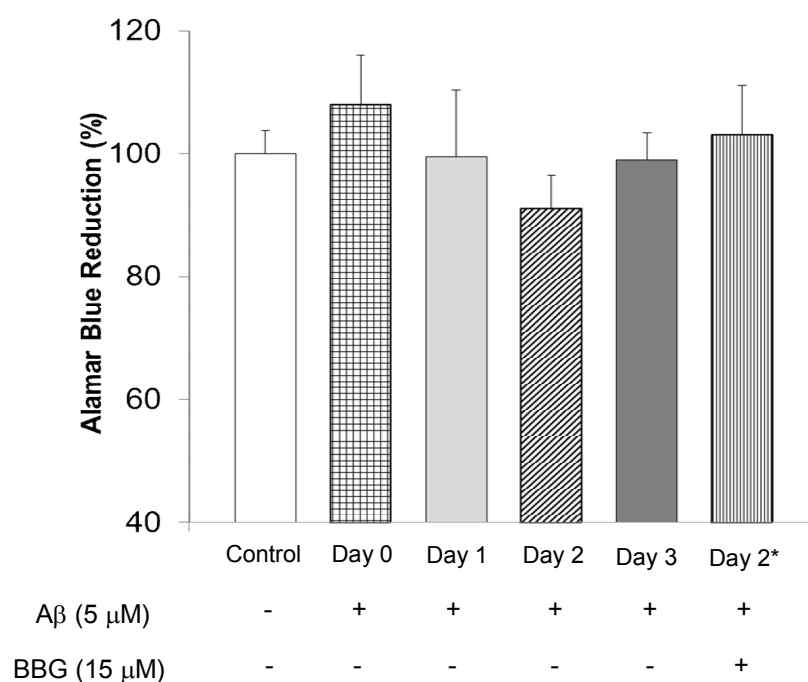


Figure A2.2. Alamar blue reducing activities of neuroblastoma SH-SY5Y cells incubated with pre-formed A β samples in the absence or presence of 3x BBG. Preformed A β aggregates were prepared by incubating 50 μ M of A β monomer in the absence of BBG at 37 °C for 0 to 3 days or in the presence of 3x BBG for 2 days, as indicated in the graph. The A β aggregates were then administered to SH-SY5Y cells at a final concentration of 5 μ M. After 3 days, cell viability was measured using alamar blue reduction. Cells administered with PBS as a control (*Control*), A β incubated without BBG for 0 (*Day 0*), 1 (*Day 1*), 2 (*Day 2*), or 3 days (*Day 3*), or A β incubated with 3x BBG for 2 days (*Day 2**). Values represent means \pm standard deviation ($n \geq 3$). Values are normalized to the viability of cells administered with PBS only. One-sided Student's t-tests were applied to the data. * $P < 0.05$.

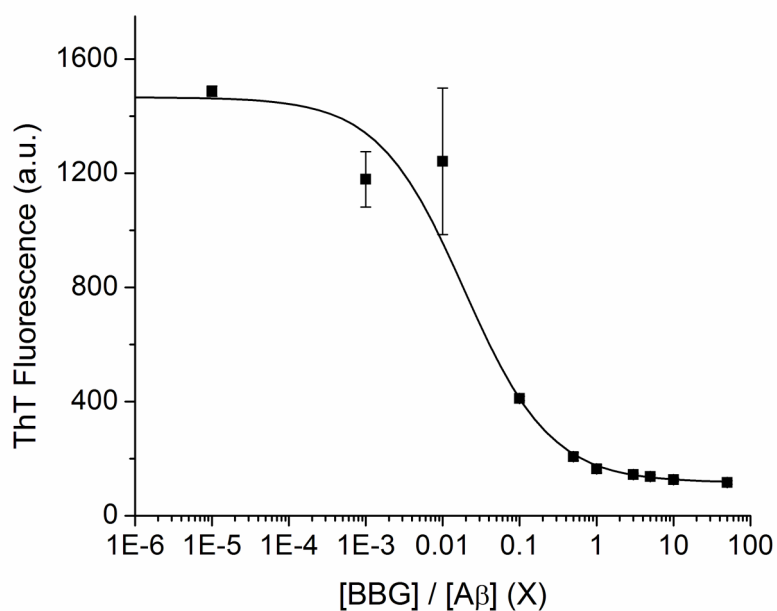


Figure A2.3. Dose-dependence inhibition of ThT fluorescence of A β samples by BBG. 50 μ M of A β monomer was incubated at 37 °C in the absence (no BBG) or presence of the indicated concentrations of BBG (from $10^{-5}x$ to $50x$). 5 μ L of A β sample was taken at 72 hours of incubation. ThT fluorescence was measured in arbitrary units (a.u.). Values represent means \pm standard deviation ($n = 3$). The data were fitted to a sigmoid curve ($R^2 = 0.99$).

Chapter 3

Xanthene Food Dye, a Modulator of Amyloid-beta-associated Neuronal Cell Function

Impairment and Aggregation

3.1 Abstract

Alzheimer's disease (AD) is the most common form of dementia. AD is a degenerative brain disorder that causes problems with memory, cognition and behavior. It has been suggested that aggregation of amyloid-beta peptide ($A\beta$) is closely linked to the development of AD pathology. In the search for safe, effective modulators, we evaluated the modulating capabilities of erythrosine B (ER), a Food and Drug Administration (FDA)-approved red food dye, on $A\beta$ aggregation and $A\beta$ -associated impaired neuronal cell function.

In order to evaluate the modulating ability of ER on $A\beta$ aggregation, we employed transmission electron microscopy (TEM), thioflavin T (ThT) fluorescence assay, and immunoassays using $A\beta$ -specific antibodies. TEM images and ThT fluorescence of $A\beta$ samples indicate that protofibrils are predominantly generated and persist for at least 3 days. The average length of the ER-induced protofibrils is inversely proportional to the concentration of ER above the stoichiometric concentration of $A\beta$ monomers. Immunoassay results using $A\beta$ -specific antibodies suggest that ER binds to the N-terminus of $A\beta$ and inhibits amyloid fibril formation. In order to evaluate $A\beta$ -associated toxicity we determined the reducing activity of SH-SY5Y neuroblastoma cells treated with $A\beta$ aggregates formed in the absence or in the presence of ER. As the concentration of ER increased above the stoichiometric concentration of $A\beta$, cellular reducing activity increased and reducing activity loss was negligible at 500 μ M ER.

Our findings show that ER is a novel modulator of $A\beta$ aggregation and reduces $A\beta$ -associated impaired cell function. Our findings also suggest that xanthene dyes can be a new type of small molecule modulator of $A\beta$ aggregation. With demonstrated safety profiles and blood-brain permeability, ER represents a particularly attractive aggregation modulator for amyloidogenic proteins associated with neurodegenerative diseases.

3.2 Introduction

Growing evidence suggests that protein misfolding and aggregation closely correlate to the onset of numerous neurodegenerative diseases, such as Alzheimer's disease (AD), Parkinson's disease (PD), and Huntington's disease (HD). A common pathological hallmark of these neurodegenerative diseases is the accumulation of insoluble protein aggregates in the brain. Amyloidogenic protein associated with AD, PD, and HD is amyloid-beta peptide ($A\beta$), α -synuclein, and huntingtin protein, respectively. Although the exact cellular and molecular mechanisms of protein aggregation remain unclear, there is increasing evidence supporting the idea that aggregation of peptides/proteins associated with the neurodegenerative diseases have common cellular and molecular mechanisms [1,2]. Therefore, it is hypothesized that protein aggregates associated with neurodegenerative disease have common structural features. Glabe et al. discovered that an oligomer-specific antibody raised using amyloid-beta peptide recognizes soluble oligomers of other types of amyloids including α -synuclein, insulin, and polyglutamine [1], demonstrating that soluble oligomers of amyloidoigenic proteins share common conformation. Numerous small molecules have been tested for their ability to reduce toxic $A\beta$ aggregates [3,4,5,6,7,8,9,10,11]. Recently Wanker et al. reported that (-)-epigallocatechin gallate preferentially binds to unfolded monomeric α -synuclein and $A\beta$ and induces formation of non-toxic oligomers, suggesting that small molecules modulate aggregation of amyloidogenic proteins through a common molecular mechanism [7]. However, the modulation of amyloidgenic protein aggregation by the same small molecule via a common mechanism has not been extensively explored. In order to validate this concept, we chose one α -synuclein aggregation modulator, erythrosine B (ER), considering its demonstrated safety profiles evidenced by FDA

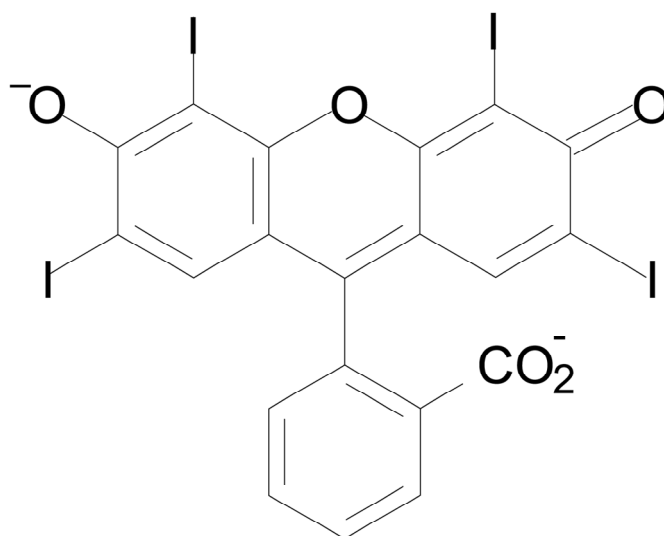


Figure 3.1. Chemical structure of erythrosine B (ER)

approval as a food dye [12,13]. To our knowledge, A β modulating capacities of xanthene dyes including ER have not been reported. Herein, we evaluate the modulating capacities of ER on A β aggregation and A β -induced impaired cellular reducing activity in neuronal cells, and investigate whether there are any common features in the interaction mode of erythrosine B with between α -synuclein and A β .

ER is a xanthene dye and is commonly used in coloring candies and cakes (Figure 3.1). ER is listed in the US as FD&C Red No. 3, in the EU as E127, and also in many other countries as a food coloring dye. It exhibits no observable toxicity up to a daily dose of 149 mg/kg body mass in healthy animals [13]. Likewise, a daily dose of 60 mg/kg does not exhibit any toxicity to humans [14]. ER is highly lipid soluble and so crosses the blood-brain barrier (BBB) [15,16]. The *in vivo* BBB permeability value of ER is 39 μ l/min/g brain, though the condition of the subject can affect plasma protein binding to ER leading to restricted brain uptake [16]. With demonstrated safety profiles and BBB permeability, ER represents a particularly attractive aggregation modulator for amyloidogenic proteins associated with neurodegenerative diseases.

3.3 Material and Methods

A β 40 was purchased from Anaspec, Inc. (Fremont, CA). SH-SY5Y Human neuroblastoma cells were obtained from ATCC (Manassas, VA). Polyclonal A11 anti-oligomer and horseradish peroxidase (HRP)-conjugated anti-rabbit IgG antibodies were obtained from Invitrogen (Carlsbad, CA). 4G8 antibody was obtained from Abcam (Cambridge, MA). Monoclonal 6E10 was obtained from Millipore (Billerica, MA). ECL advance chemiluminescence kit was obtained from GE Healthcare Life Sciences. All other chemicals were obtained from Sigma-Aldrich (St. Louis, MO) unless otherwise noted.

A β Sample Preparation. A β 40 powder (Anaspec, Inc.) was added to 0.1 % trifluoroacetic acid (TFA) to obtain a 1.0 mM stock solution, which was then incubated for one hour without agitation for complete dissolution as described previously [17,18,19]. The freshly prepared 1.0 mM stock A β solution was diluted with phosphate buffered saline (PBS) solution (10 mM NaH₂PO₄ and 150 mM NaCl at pH 7.4) to obtain a 50 μ M A β solution. 50 μ M A β samples were then incubated at 37 °C for the specified time duration.

Transmission Electron Microscopy (TEM). 10 μ L A β sample was spread onto a formvar mesh grid and incubated for one min. The grids were then negatively stained with 2% uranyl acetate for 45 sec., dried and viewed on a Jeol JEM1230 Transmission Electron Microscope (80 kV) located at the Advanced Microscopy Laboratory at the University of Virginia.

Thioflavin T (ThT) Fluorescence Assay. 5 μ L of 50 μ M A β 40 sample in the absence or in the presence of ER was diluted in 250 μ L of 10 μ M ThT in 96-well plates. ThT fluorescence was measured using a Synergy 4 UV-Vis/fluorescence multi-mode microplate reader (Biotek, VT) at an emission wavelength of 485 nm using an excitation wavelength of 450 nm.

Dot Blotting. 2 μ L of A β samples were spotted onto a nitrocellulose membrane and were dried at room temperature. The nitrocellulose membrane was incubated in 5% skim milk dissolved in 0.1% Tween 20, Tris-buffered saline (TBS-T) solution for one hour. The 5% milk TBS-T solution was removed and the membrane was washed three times (each time for five minutes) with TBS-T solution. The membrane was then incubated with antibody for one hour. Polyclonal

A11 anti-oligomer antibody and horseradish peroxidase (HRP)-conjugated anti-rabbit antibody were obtained from Invitrogen (Carlsbad, CA). 4G8 antibody was obtained from Abcam (Cambridge, MA). Monoclonal 6E10 and polyclonal OC antibodies were obtained from Millipore (Billerica, MA). The 4G8, OC, A11 and 6E10 antibodies were diluted in 0.5% milk TBS-T solution according to the manufacturer's protocols. After incubation the membrane was washed three times for 5 minutes using TBS-T solution. In the case of the HRP-conjugated antibody (4G8), membranes were coated with 2 mL of detection agent from the ECL Advance Detection Kit (GE Healthcare, NJ) and the fluorescence was visualized. Otherwise, the membrane was incubated in (1:5000 dilution in 0.5% milk TBS-T) HRP-conjugated secondary antibody solution for one hour. Then the membrane was washed three times (each time for 5 minutes) with TBS-T solution and the same detection method as previously described was used. The blot images were taken using a BioSpectrum imaging system (UVP, CA).

MTT Reduction Assay. Viability of Human neuroblastoma SH-SY5Y cells (American Type Culture Collection) was determined by 3-(4,5-Dimethylthiazol-2-yl)-2,5-diphenyltetrazolium bromide (MTT) reduction. 50 mg of MTT (Millipore, MA) was dissolved overnight at 4 °C in 10 mL of PBS. The MTT solution was then sterile filtered. SH-SY5Y cells were cultured in a humidified 5% CO₂/air incubator at 37 °C in DMEM/F 12:1:1 modified media with 10% fetal bovine serum and 1% penicillin-streptomycin (Thermo Scientific, MA). 20,000 to 25,000 SH-SY5Y cells were seeded into each well of 96-well plates and incubated for 48 hours. Then, the culture medium was replaced with 100 µL of fresh media, and 10 µL of the A β sample was added to each well to obtain a final A β concentration of 5 µM. Cells were incubated for an additional 48 hours. After replacing the culture medium with a fresh medium, 10 µL of the

sterile MTT solution was added, and cells were incubated for 6 hours at 37 °C in the dark. After dissolution of the reduced MTT using 200 μ L of DMSO, the absorbance was measured at 506 nm using a Synergy 4 UV-Vis/fluorescence multi-mode microplate reader.

3.4 Results and Discussion

Stabilization of A β protofibrils and Inhibition of A β fibril formation by ER. In order to monitor morphological changes of A β aggregates and formation of amyloid fibrils, we employed TEM and ThT fluorescence assays. TEM has been widely used to obtain morphological information on A β aggregates [20,21,22,23]. A β intermediates as well as fibrils can be directly visualized with negative-stain TEM. ThT fluoresces at 485 nm when bound to amyloid fibrils [9,24,25]. Therefore, ThT fluorescence is used to monitor the progression of amyloid fibril formation. A β samples were prepared by incubating 50 μ M of A β monomer either in the absence (control) or presence of ER from 0 to 3 days at 37 °C without shaking as described previously [17,18,19].

A β sample TEM images clearly show distinct differences in morphology among A β samples incubated in the absence and in the presence of ER (Figure 3.2). In the absence of ER, oligomers, protofibrils, and amyloid fibril mesh network were sequentially observed throughout the study (Figure 3.2, far-left panels). The onset of fibril formation at day 2 was confirmed by a dramatic increase in ThT fluorescence from 48 to 72 hr (Figure 3.3A). At day 1, in the presence of 50 μ M of ER (1x ER), protofibrils were the predominant species (Figure 3.2, top 1x ER panel), whereas oligomers were dominant in the absence of ER (Figure 3.2, top far-left panel). Furthermore, these protofibrils were observed until day 3 and appeared to have morphological homogeneity characterized by similarity in length and width (Figure 3.2, 1x ER panels). To

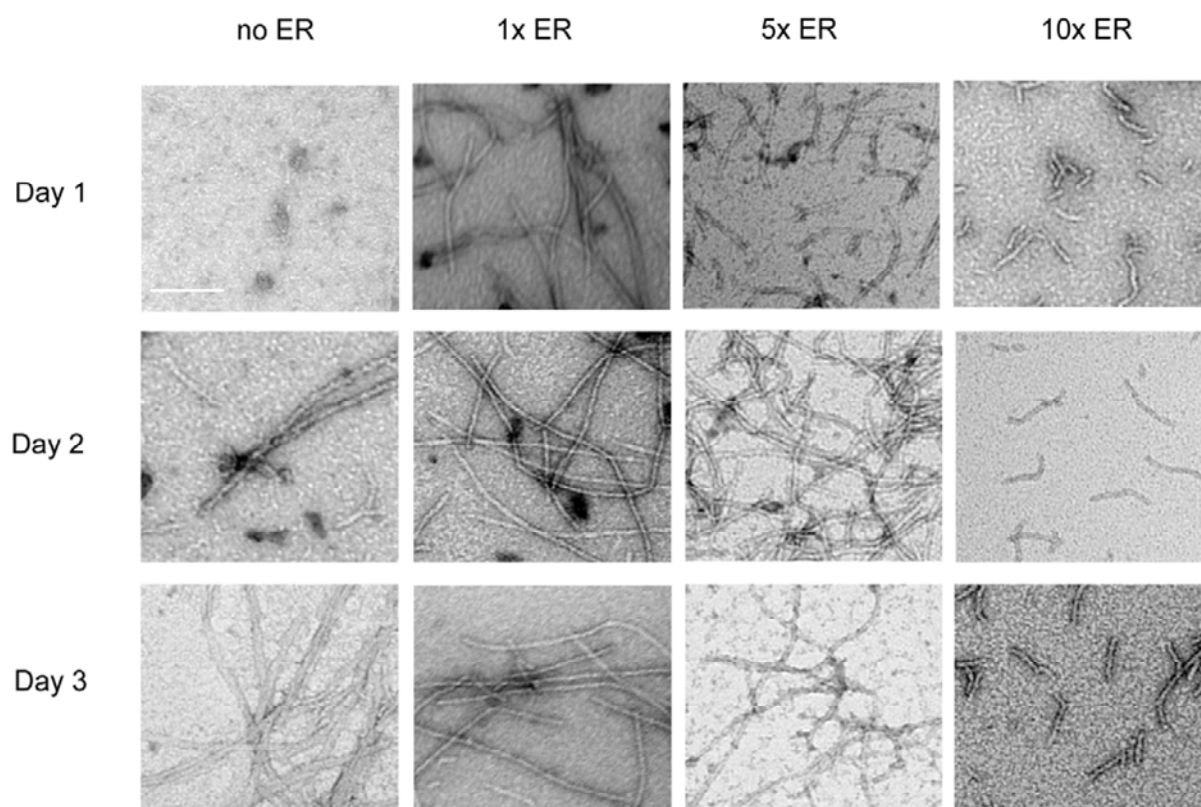


Figure 3.2. TEM images of A β aggregates. A β monomers were incubated for one to three days in the absence (no ER) (far-left panels) and the presence of 1x (middle-left panels), 5x (middle-right panels), or 10x ER (far-right panels) and visualized by TEM. Scale bars are 100 nm.

Table 1. Length distribution of A β aggregates incubated in the presence of 1x, 5x, and 10x for one, two, and three days.^a

ER		Length of A β aggregates (μ m) ^b															Average
conc.		0.1	0.2	0.3	0.4	0.5	0.6	0.7	0.8	0.9	1.0	1.1	1.2	1.3	1.4	>1.4	(nm)
Day 1	1x	ND	20	17	27	17	22	11	21	7	13	7	7	9	4	18	690 \pm 430
	5x	1	25	68	63	25	15	3	ND	ND	ND	ND	ND	ND	ND	ND	320 \pm 110
	10x	187	12	1	ND	ND	ND	ND	ND	ND	ND	ND	ND	ND	ND	ND	55 \pm 27
Day 2	1x	ND	9	20	25	24	16	17	18	21	15	9	4	5	2	15	702 \pm 424
	5x	ND	ND	1	9	21	28	28	34	28	25	7	3	5	8	3	758 \pm 263
	10x	162	37	1	ND	ND	ND	ND	ND	ND	ND	ND	ND	ND	ND	ND	73 \pm 37
Day 3	1x	1	16	13	18	15	21	16	20	17	9	9	9	6	5	25	784 \pm 485
	5x	ND	3	8	23	25	31	31	33	16	18	4	3	5	ND	ND	642 \pm 233
	10x	151	45	4	ND	ND	ND	ND	ND	ND	ND	ND	ND	ND	ND	ND	83 \pm 41

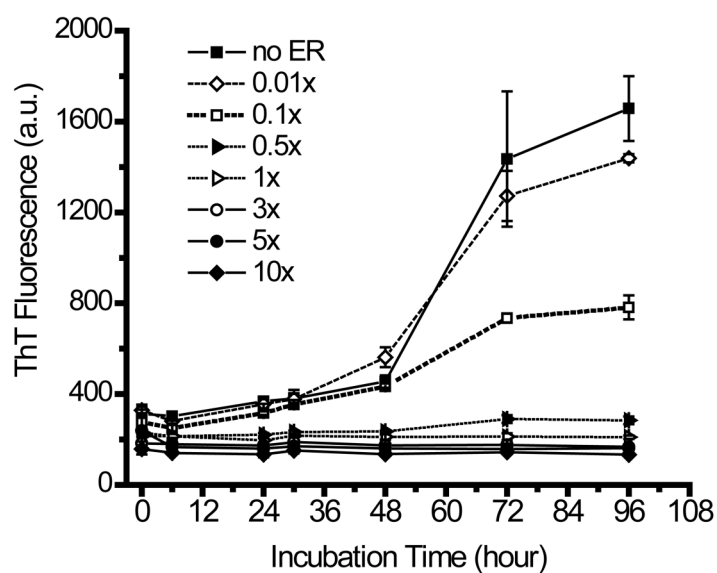
a. Two hundred A β aggregates observed in negative-stain TEM images at each concentration of ER were analyzed.

b. Each bin has a 100 nm interval in the length of A β aggregates. The number indicates the maximum length of A β aggregates in each bin. ND: Not Detected

evaluate this quantitatively, the length of two hundred A β aggregates including protofibrils and fibrils in TEM images at each ER concentration were manually measured using ImageJ (NIH). The length distribution of the two hundred A β aggregates at 1x, 5x, or 10x ER concentration is described in Table 3.1. At day 1, in the presence of 1x ER, the average protofibril length was 690 nm. In the presence of 1x ER, the average length protofibrils did not change substantially on subsequent days (Table 3.1). At day 1, increasing the ER concentration from 1x to 10x decreased the average length of A β aggregates from 690 nm to 55 nm. At days 2 and 3, the average length of protofibrils in the presence of 5x was 758 and 641 nm, respectively, but short protofibrils of length less than 100 nm were predominantly observed in the presence of 10x (Table 3.1). These findings support the idea that ER promoted the formation of stable intermediate protofibrils.

Furthermore, ER likely limited the capability to form longer fibrils. Therefore, next we determined whether the inhibition of fibril formation was dependent on ER concentration using ThT fluorescence assay. In the absence of ER, there was a steady increase in the ThT fluorescence of A β samples throughout the study (Figure 3.3A). In particular, a steep increase in the fluorescence was observed from 48 to 72 hr, indicating amyloid fibril formation. However, as the ER concentration varied from 0.01x to 10x, a substantial reduction in the ThT fluorescence was observed (Figure 3.3A). However, the ThT data of the A β aggregates formed with ER should be interpreted with caution due to interference of ER with the ThT fluorescence measurement. In order to investigate the interference of ER with the ThT fluorescence, three different ER concentrations (1x, 3x, and 10x) were added to the A β aggregates incubated without any ER for 3 days displaying a high ThT fluorescence intensity. Addition of 1x, 3x, or 10x ER caused 66%, 81%, and 88% reduction in the A β aggregate fluorescence, respectively (Figure 3.3B), suggesting that ER competitively binds to ThT bindings sites on A β fibrils. However, the

A



B

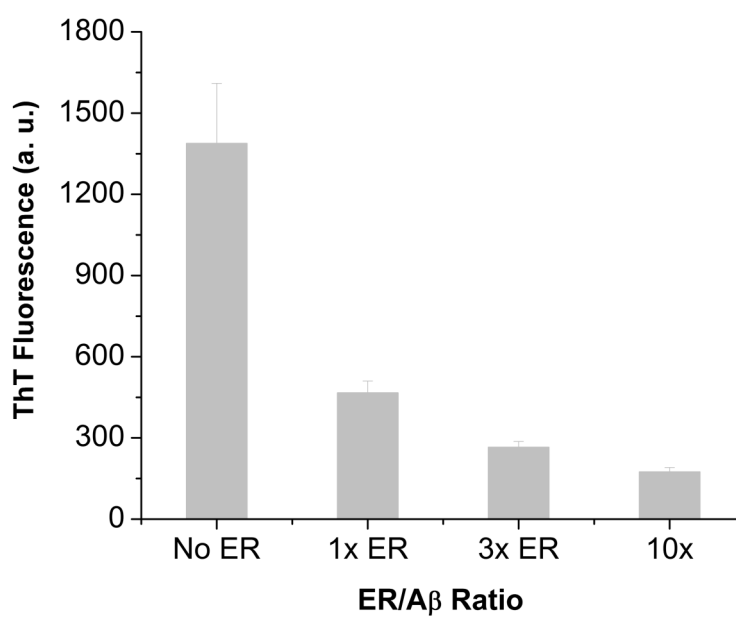


Figure 3.3. ThT fluorescence of A β samples. A β monomers were incubated for four days in the absence (no ER) or in the presence of 0.01x, 0.1x, 0.5x, 1x, 3x, 5x, or 10x of ER (A). Values represent means \pm standard deviation ($n = 3$). Preformed amyloid fibrils (72 hours) were mixed with varying concentrations of ER (1x, 3x, and 10x ER) (B). ThT fluorescence was measured in arbitrary units (a.u.). Values represent means \pm standard deviation ($n = 3$).

ThT fluorescence of the A β aggregates formed with 1x or 3X ER for 3 days was twice lower than that of the A β aggregates at day 3 mixed with 1x or 3x ER respectively, suggesting that the ER-induced A β protofibrils weakly bind ThT compared to A β fibrils. Glabe et al. also reported that A β fibrillar oligomers with stacked β -sheet structure are OC-antibody reactive but weakly bind ThT [26].

In summary, co-incubation of A β with ER concentrations of 1x or greater inhibits high-molecular weight A β fibril formation and leads to formation of protofibrils and stabilization of the protofibrils at least up to 3 days. At day 1, the average length of A β protofibrils is inversely proportional to the concentration of ER at the concentration of 1x ER or greater (Table 3.1).

Changes in A β -aggregate immunoreactivity caused by ER. Dot blotting with A β -specific antibodies was also used to monitor A β aggregate formation. These assays were performed to obtain an integrated picture of A β aggregation modulation by ER. With A β -specific antibodies, dot blotting has become an effective method for monitoring A β aggregate formation [1,26,27,28,29,30]. Four A β -specific antibodies were utilized for this purpose. 4G8 is an A β -sequence-specific monoclonal antibody [31,32,33,34] that binds to amino acids 17 to 24 of A β , the hydrophobic patch of A β . 6E10 is a monoclonal antibody that recognizes A β residues 1-16 [28,35]. A11 is a polyclonal antibody that reacts with soluble toxic oligomers and protofibrils [7,28,30]. OC is a polyclonal antibody that reacts with aggregates with fibrillar structure, including fibrillar oligomers, protofibrils and fibrils [28,29].

In the absence of ER, 4G8-reactive species were detected from day 0 to 2, whereas 4G8-reactivity was nearly negligible at day 3. Considering that the 4G8 epitope lies in a hydrophobic patch of the A β peptide that is known to be buried during amyloid fibril formation, a dramatic

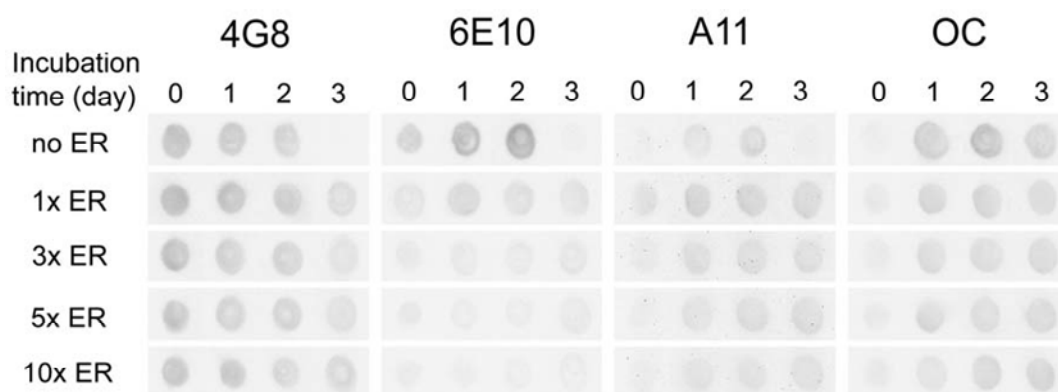


Figure 3.4. Dot-blotting of A β samples using four A β -specific antibodies. A β monomers were incubated at 37 °C in the absence (no ER) or presence of the indicated concentrations of ER (from 1x to 10x) for up to 3 days. Samples were spotted onto a nitrocellulose membrane and immunostained with the 4G8, 6E10, A11, or OC antibody.

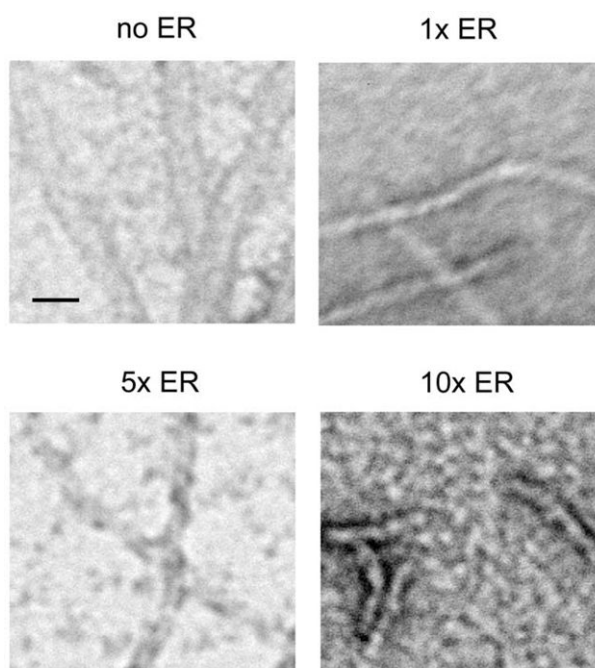


Figure 3.5. TEM images of A β aggregates after three day incubation. A β monomers were incubated for three days in the absence (no ER) or in the presence of 1x, 5x, or 10x ER and visualized by TEM. Scale bars are 20 nm.

loss of the 4G8 signal was regarded as the onset of extensive fibril-mesh networking [35]. The loss of 4G8 signal corresponding to the formation of fibril-mesh networks was also confirmed by TEM results (Figure 3.2, far-left panels). In contrast, in the presence of 1x ER or greater, there was prominent 4G8-reactivity even at day 3 indicating that fibril-mesh networks were not readily formed, which is consistent with TEM results. In the absence of ER, significant 6E10 reactivity was observed from day 0 to 2. Under these conditions, the N-terminus of A β , the 6E10 epitope, is easily accessible to the 6E10 antibody. At day 3, only very weak 6E10 signal was detected, which is most probably due to A β conformation change restricting 6E10 antibody binding similar to 4E8. However, as ER concentration was increased from 1x to 10x, 6E10 reactivity decreased significantly even at day 1 and 2. At ER 10x concentration, 6E10 reactivity was significantly weaker than reactivity in the absence of ER (Figure 3.4). This suggests that ER interaction with A β inhibits 6E10 binding. There are two possible mechanisms. First ER competitively binds to the 6E10 epitope. Second, ER alters the conformation of A β limiting antibody accessibility to the 6E10 epitope, essentially hiding the N-terminus. According to the structural model of A β 40 fibril proposed by Grigorieff et. al., two pairs of A β protofibrils intertwine adjacently to form a fibril with a 20 nm cross-sectional width [36], which is consistent with the 20 nm A β -fibril cross-sectional width observed in Figure 3.5 (no ER panel). In their model, the N-terminus of each protofibril is laterally exposed and interlocked to form a fibril. Based on this A β 40 fibril structural model, we speculate that ER binding disrupts the coalescence of two protofibrils leading to inhibition of amyloid fibril formation. This is also consistent with the results that ER-induced oligomers/protofibrils (7 nm cross-sectional width) are stable and do not form fibrils (Figure 3.5).

In the absence of ER, significant A11-signals were detected at day 1 and 2 but not at day 3 indicating the A11-reactive species were formed until day 2 but converted into amyloid fibrils between day 2 and 3. In contrast, when 1x ER was present, A11-signal was detected even at day 0 and persisted until day 3. In the presence of 3x, 5x, and 10x ER, substantial A11-signal was detected from day 1 to 3, which is consistent with predominant protofibrils but no fibrils were observed in the TEM images. In the absence or the presence of ER, OC-reactive signals remain unchanged (Figure 3.4) indicating that ER-induced protofibrils still have a fibrillar aspect. These dot-blotting results support the idea that ER induces formation of both A11- and OC-reactive oligomers but inhibits fibril formation.

Modulation of A β and α -synuclein aggregation by ER. All of these findings strongly support the idea that ER is an efficient aggregation modulator. ER promotes the formation of A β protofibrils and stabilizes them for at least three days, which in turn inhibits fibril formation. Based on the A β 40 fibril structural model proposed by Grigorieff et. al. and the immunoassay results using the A β N-terminus specific antibody, inhibition of A β fibril formation is at least partly due to ER binding to the A β N-terminus by blocking binding of two protofibrils to form one fibril. As mentioned earlier, it is worthwhile to compare modulation of aggregation of α -synuclein and A β by ER. Previous studies on α -synuclein aggregation [12] and our findings indicate that ER promotes protofibril formation of both α -synuclein and A β . ER binding sites were found to be predominantly on the hydrophobic region of non-A β component of AD amyloid (NAC) [12]. Therefore, the authors speculate that ER facilitates hydrophobic interaction of α -synuclein leading to fast protofibril formation. Similarly ER aromatic rings might play a key role in the promotion of A β aggregation at 1x ER concentration. However,

although the concentration of ER increased up to 10x, the hydrophobic patch of A β (4G8 epitope) was not completely buried, suggesting that the interaction mode of ER with A β is different from that with α -synuclein. A bigger difference was found in the effects of xanthene dyes on fibril formation of α -synuclein and A β . Although xanthene dyes lead to formation of α -synuclein fibrils, ER clearly inhibits formation of A β fibrils. These comparisons suggest that ER promotes protofibril formation of both α -synuclein and A β most probably due to the interaction of xanthene aromatic rings with the hydrophobic region of each protein. However, ER is thought to bind to the N-terminus of A β leading to the inhibition of A β fibril formation, which distinguishes the ER interaction with A β from that with α -synuclein.

Inhibition of A β -induced cellular impairment by ER. Modulation of A β aggregation by ER was clearly demonstrated in the previous sections. However, since A β oligomers and protofibrils are normally considered toxic species, we wanted to determine whether ER-induced A β protofibrils perturb cellular activities of neuronal cells. In order to determine the detrimental effects of ER-induced A β aggregates on cellular functions, we chose the cellular MTT reducing activity of SH-SY5Y neuroblastoma cells. MTT reducing activity has been widely considered as an indication of cell viability [8,29,37,38]. Therefore, the MTT reducing activity loss has often been interpreted as the A β -associated cytotoxicity [7,28,39,40,41,42,43]. However, due to a potential issue of the promoted export of the reduced MTT from the cells upon A β aggregate treatment leading to reduction of the MTT signal [44,45,46], we avoided direct interpretation of the reduced MTT signal as A β -associated cytotoxicity but considered the reduced MTT signal as an indication of impaired cellular functions. Cells were administered A β aggregates preformed in the absence or presence of ER. Preformed A β aggregates were prepared by incubating 50 μ M A β

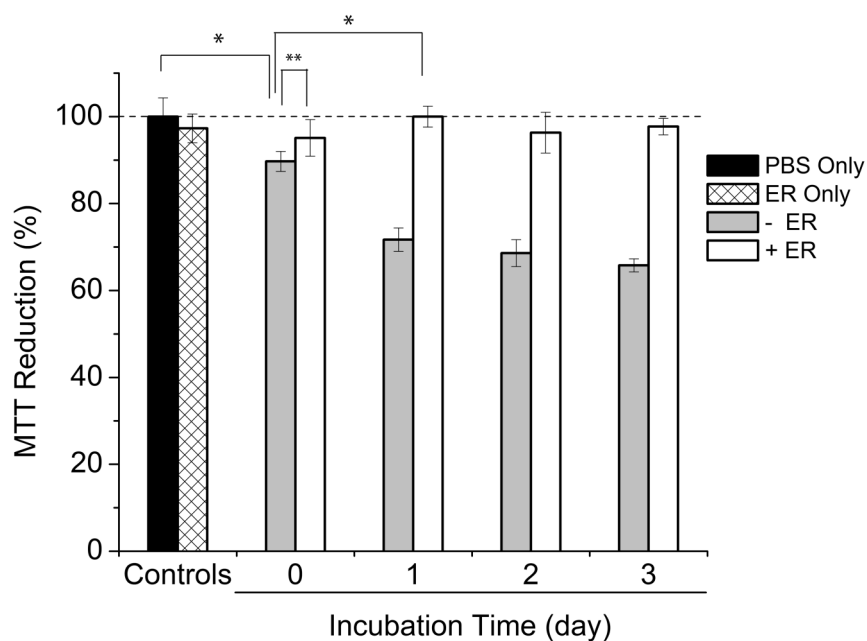


Figure 3.6. Viability of neuroblastoma SH-SY5Y cells treated with Aβ samples (5 μM) formed in the absence or presence of 10x ER incubated at 37 °C for one to three days, measured by MTT reduction. Values represent means ± standard deviation (n ≥ 3). Values are normalized to the viability of cells administered with PBS only. Two-sided Student's t-tests were applied to the data (* P < 0.001; ** P < 0.005).

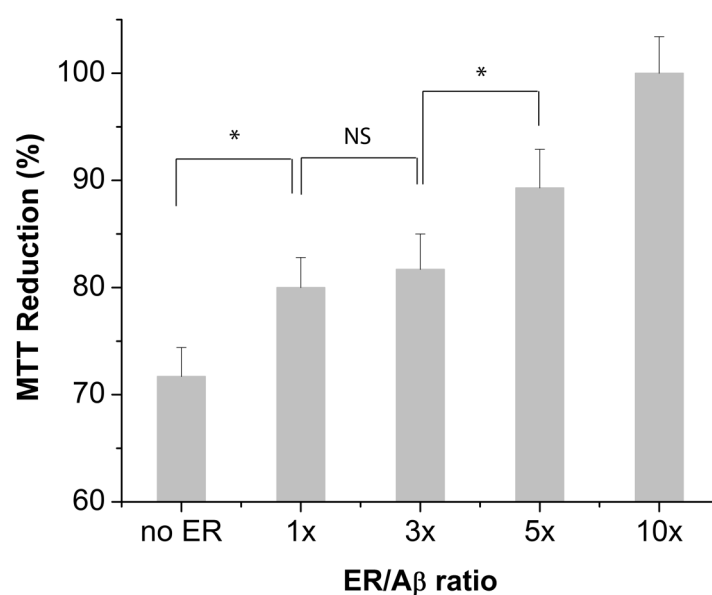


Figure 3.7. Viability of neuroblastoma SH-SY5Y cells treated with A β samples (5 μ M) incubated at 37 $^{\circ}$ C for one day in the absence of (no ER) or in the presence of 1x, 3x, 5x, or 10x ER, measured by MTT reduction. Values represent means \pm standard deviation ($n \geq 3$). Values are normalized to the viability of cells administered with PBS only. Two-sided Student's t-tests were applied to the data (* $P < 0.001$; NS: not significant).

monomers in the absence or presence of various concentrations of ER (1x to 10x) at 37 °C for the specified time duration. SH-SY5Y cells were incubated with 5 μ M preformed aggregates for 48 hours, and subsequently MTT reducing activity was determined.

As a control, the MTT reducing activity of cells treated with varying concentrations of ER was measured. Up to 10x ER (500 μ M), there was only slight reduction (5%) in the MTT reduction. At day 0, A β monomers (5 μ M) caused 10% reduction ($P < 0.001$) in the MTT reduction probably due to the toxic A β aggregate formation during the A β monomer incubation with the cells for 48 hr (Figure 3.6). However, in the presence of 10x ER, the MTT reducing activity was recovered to 95%. At day 1, preformed A β species formed in the absence of ER significantly reduced the MTT reducing activity by 28%. This loss of the MTT reducing activity likely resulted from the formation of both A11- and OC-reactive protofibrils (Figure 3.4). However, preformed A β species prepared in the presence of 10x ER showed an MTT reducing activity significantly higher than those of the A β incubated without any ER at days 0 and 1 ($P < 0.001$ and < 0.005 , respectively) up to the level of a negative control without any A β (Figure 3.6). At day 1, ER reduced the A β -induced loss of the MTT reducing activity in a dose-dependent manner (Figure 3.7). At 1x ER, there was only 8% recovery of the MTT reducing activity ($P < 0.001$). However, the MTT reduction reaches close to 100% in the presence of 10x ER. Similar results were shown with preformed A β on subsequent days. The cellular MTT reducing activity with A β (5 μ M) incubated for 2 and 3 days decreased to 69% and 66%, respectively. In particular, co-incubation of 10x ER raised the MTT reducing activity to 96% and 98% at day 2 and 3, respectively (Figure 3.6).

3.5 Conclusion

Erythrosine B (ER) was able to significantly inhibit A β -associated cytotoxicity by improving the cellular reduction activity of SH-SY5Y neuroblastoma cells in a dose-dependent manner. TEM images and ThT fluorescence revealed that protofibrils were predominantly generated and persisted throughout the duration of the study. Furthermore their average length is inversely proportional to the concentration of ER. Immunoassay results using A β -specific antibodies suggest that ER binds to the N-terminus of A β and inhibits amyloid fibril formation. Collectively the results suggest that ER inhibits A β -associated cytotoxicity by promoting the formation of non-toxic aggregates. However at the same time, we have not excluded the possibility that ER binding may block A β sites that confers cytotoxicity.

Here we demonstrated that ER is a novel modulator of A β aggregation and reduces A β -associated impaired cell function. Our findings also suggest that xanthene dyes may be a novel group of small-molecule modulators of A β aggregation. With demonstrated safety and blood-brain permeability, ER represents a particularly attractive aggregation modulator for amyloidogenic proteins associated with neurodegenerative diseases.

3.6 Literature Cited

1. Kayed R, Head E, Thompson JL, McIntire TM, Milton SC, et al. (2003) Common structure of soluble amyloid oligomers implies common mechanism of pathogenesis. *Science* 300: 486-489.
2. Bucciantini M, Giannoni E, Chiti F, Baroni F, Formigli L, et al. (2002) Inherent toxicity of aggregates implies a common mechanism for protein misfolding diseases. *Nature* 416: 507-511.
3. Hawkes CA, Ng V, McLaurin J (2009) Small Molecule Inhibitors of A beta-Aggregation and Neurotoxicity. *Drug Dev Res* 70: 111-124.

4. Hamaguchi T, Ono K, Yamada M (2006) Anti-amyloidogenic therapies: strategies for prevention and treatment of Alzheimer's disease. *Cell Mol Life Sci* 63: 1538-1552.
5. McLaurin J, Golomb R, Jurewicz A, Antel JP, Fraser PE (2000) Inositol stereoisomers stabilize an oligomeric aggregate of Alzheimer amyloid beta peptide and inhibit A beta-induced toxicity. *J Biol Chem* 275: 18495-18502.
6. McLaurin J, Kierstead ME, Brown ME, Hawkes CA, Lambermon MHL, et al. (2006) Cyclohexanehexol inhibitors of A beta aggregation prevent and reverse Alzheimer phenotype in a mouse model. *Nat Med* 12: 801-808.
7. Ehrnhoefer DE, Bieschke J, Boeddrich A, Herbst M, Masino L, et al. (2008) EGCG redirects amyloidogenic polypeptides into unstructured, off-pathway oligomers. *Nat Struct Mol Biol* 15: 558-566.
8. Feng Y, Wang X-P, Yang S-G, Wang Y-J, Zhang X, et al. (2009) Resveratrol inhibits beta-amyloid oligomeric cytotoxicity but does not prevent oligomer formation. *Neurotoxicology* 30: 986-995.
9. Reinke AA, Gestwicki JE (2007) Structure-activity relationships of amyloid beta-aggregation inhibitors based on curcumin: Influence of linker length and flexibility. *Chemical Biology & Drug Design* 70: 206-215.
10. Yang FS, Lim GP, Begum AN, Ubeda OJ, Simmons MR, et al. (2005) Curcumin inhibits formation of amyloid beta oligomers and fibrils, binds plaques, and reduces amyloid in vivo. *J Biol Chem* 280: 5892-5901.
11. Moss MA, Varvel NH, Nichols MR, Reed DK, Rosenberry TL (2004) Nordihydroguaiaretic Acid Does Not Disaggregate beta-Amyloid(1-40) Protofibrils but Does Inhibit Growth Arising from Direct Protofibril Association. *Molecular Pharmacology* 66: 592-600.
12. Shin HJ, Lee EK, Lee JH, Lee D, Chang CS, et al. (2000) Eosin interaction of alpha-synuclein leading to protein self-oligomerization. *Biochimica Et Biophysica Acta-Protein Structure and Molecular Enzymology* 1481: 139-146.
13. Borzelleca JF, Hallagan JB (1990) Multigeneration study of FD & C Red No. 3 (erythrosine) in Sprague-Dawley rats. *Food Chem Toxicol* 28: 813-819.
14. Gardner DF, Utiger RD, Schwartz SL, Witorsch P, Meyers B, et al. (1987) Effects of oral erythrosine (2',4',5',7'-tetraiodofluorescein) on thyroid-function in normal men. *Toxicology and Applied Pharmacology* 91: 299-304.

15. Hirohashi T, Terasaki T, Shigetoshi M, Sugiyama Y (1997) In vivo and in vitro evidence for nonrestricted transport of 2',7'-bis(2-carboxyethyl)-5(6)-carboxyfluorescein tetraacetoxymethyl ester at the blood-brain barrier. *J Pharmacol Exp Ther* 280: 813-819.
16. Levitan H, Ziylan Z, Smith QR, Takasato Y, Rapoport SI (1984) Brain uptake of a food dye, erythrosine B, prevented by plasma-protein binding. *Brain Research* 322: 131-134.
17. Lee S, Fernandez EJ, Good TA (2007) Role of aggregation conditions in structure, stability, and toxicity of intermediates in the A beta fibril formation pathway. *Protein Science* 16: 723-732.
18. Qi W, Zhang A, Patel D, Lee S, Harrington JL, et al. (2008) Simultaneous monitoring of peptide aggregate distributions, structure, and kinetics using amide hydrogen exchange: Application to A beta(1-40) fibrillogenesis. *Biotechnol Bioeng* 100: 1214-1227.
19. Qi W, Zhang AM, Good TA, Fernandez EJ (2009) Two Disaccharides and Trimethylamine N-Oxide Affect A beta Aggregation Differently, but All Attenuate Oligomer-Induced Membrane Permeability. *Biochemistry* 48: 8908-8919.
20. Chen B, Thurber KR, Shewmaker F, Wickner RB, Tycko R (2009) Measurement of amyloid fibril mass-per-length by tilted-beam transmission electron microscopy. *Proc Natl Acad Sci U S A* 106: 14339-14344.
21. Komatsu H, Feingold-Link E, Sharp KA, Rastogi T, Axelsen PH (2010) Intrinsic Linear Heterogeneity of Amyloid beta Protein Fibrils Revealed by Higher Resolution Mass-per-length Determinations. *J Biol Chem* 285: 41843-41851.
22. Paravastu AK, Leapman RD, Yau WM, Tycko R (2008) Molecular structural basis for polymorphism in Alzheimer's beta-amyloid fibrils. *Proc Natl Acad Sci U S A* 105: 18349-18354.
23. Chimon S, Shaibat MA, Jones CR, Calero DC, Aizezi B, et al. (2007) Evidence of fibril-like beta-sheet structures in a neurotoxic amyloid intermediate of Alzheimer's beta-amyloid. *Nat Struct Mol Biol* 14: 1157-1164.
24. Khurana R, Coleman C, Ionescu-Zanetti C, Carter SA, Krishna V, et al. (2005) Mechanism of thioflavin T binding to amyloid fibrils. *J Struct Biol* 151: 229-238.
25. LeVine H (1999) Quantification of beta-sheet amyloid fibril structures with thioflavin T. *Amyloid, Prions, and Other Protein Aggregates*. pp. 274-284.
26. Wu JW, Breydo L, Isas JM, Lee J, Kuznetsov YG, et al. (2010) Fibrillar oligomers nucleate the oligomerization of monomeric amyloid beta but do not seed fibril formation. *J Biol Chem* 285: 6071-6079.

27. Chen YR, Glabe CG (2006) Distinct early folding and aggregation properties of Alzheimer amyloid-beta peptides A beta 40 and A beta 42 - Stable trimer or tetramer formation by A beta 42. *J Biol Chem* 281: 24414-24422.
28. Kaye R, Head E, Sarsoza F, Saing T, Cotman CW, et al. (2007) Fibril specific, conformation dependent antibodies recognize a generic epitope common to amyloid fibrils and fibrillar oligomers that is absent in prefibrillar oligomers. *Mol Neurodegener* 2: 18.
29. Ladiwala ARA, Lin JC, Bale SS, Marcelino-Cruz AM, Bhattacharya M, et al. (2010) Resveratrol Selectively Remodels Soluble Oligomers and Fibrils of Amyloid A beta into Off-pathway Conformers. *J Biol Chem* 285: 24228-24237.
30. Hu Y, Su BH, Kim CS, Hernandez M, Rostagno A, et al. (2010) A strategy for designing a peptide probe for detection of beta-amyloid oligomers. *ChemBioChem* 11: 2409-2418.
31. Iijima K, Liu HP, Chiang AS, Hearn SA, Konsolaki M, et al. (2004) Dissecting the pathological effects of human A beta 40 and A beta 42 in *Drosophila*: A potential model for Alzheimer's disease. *Proc Natl Acad Sci U S A* 101: 6623-6628.
32. Kimura N, Yanagisawa K, Terao K, Ono F, Sakakibara I, et al. (2005) Age-related changes of intracellular A beta in cynomolgus monkey brains. *Neuropathol Appl Neurobiol* 31: 170-180.
33. Klyubin I, Walsh DM, Lemere CA, Cullen WK, Shankar GM, et al. (2005) Amyloid beta protein immunotherapy neutralizes A beta oligomers that disrupt synaptic plasticity in vivo. *Nat Med* 11: 556-561.
34. Thakker DR, Weatherspoon MR, Harrison J, Keene TE, Lane DS, et al. (2009) Intracerebroventricular amyloid-beta antibodies reduce cerebral amyloid angiopathy and associated micro-hemorrhages in aged Tg2576 mice. *Proc Natl Acad Sci U S A* 106: 4501-4506.
35. Sarroukh R, Cerf E, Derclaye S, Dufrêne Y, Goormaghtigh E, et al. (2010) Transformation of amyloid β (1-40) oligomers into fibrils is characterized by a major change in secondary structure. *Cell Mol Life Sci*: 1-10.
36. Schmidt M, Sachse C, Richter W, Xu C, Fandrich M, et al. (2009) Comparison of Alzheimer A beta(1-40) and A beta(1-42) amyloid fibrils reveals similar protofilament structures. *Proc Natl Acad Sci U S A* 106: 19813-19818.
37. Feng Y, Yang SG, Du XT, Zhang X, Sun XX, et al. (2009) Ellagic acid promotes A beta 42 fibrillization and inhibits A beta 42-induced neurotoxicity. *Biochem Biophys Res Commun* 390: 1250-1254.

38. Pollack SJ, Sadler III, Hawtin SR, Tailor VJ, Shearman MS (1995) Sulfonated dyes attenuate the toxic effects of beta-amyloid in a structure-specific fashion. *Neuroscience Letters* 197: 211-214.
39. Datki Z, Juhász A, Gálfi M, Soós K, Papp R, et al. (2003) Method for measuring neurotoxicity of aggregating polypeptides with the MTT assay on differentiated neuroblastoma cells. *Brain Res Bull* 62: 223-229.
40. Nishimura S, Murasugi T, Kubo T, Kaneko I, Meguro M, et al. (2003) RS-4252 Inhibits Amyloid β -Induced Cytotoxicity in HeLa Cells. *Pharmacol Toxicol* 93: 29-32.
41. Olivieri G, Otten U, Meier F, Baysang G, Dimitriadis-Schmutz B, et al. (2003) [beta]-amyloid modulates tyrosine kinase B receptor expression in SHSY5Y neuroblastoma cells: influence of the antioxidant melatonin. *Neuroscience* 120: 659-665.
42. Ono K, Yoshiike Y, Takashima A, Hasegawa K, Naiki H, et al. (2003) Potent anti-amyloidogenic and fibril-destabilizing effects of polyphenols in vitro: implications for the prevention and therapeutics of Alzheimer's disease. *J Neurochem* 87: 172-181.
43. Wang SS-S, Rymer DL, Good TA (2001) Reduction in Cholesterol and Sialic Acid Content Protects Cells from the Toxic Effects of β -Amyloid Peptides. *J Biol Chem* 276: 42027-42034.
44. Liu Y, Schubert D (1997) Cytotoxic Amyloid Peptides Inhibit Cellular 3-(4,5-Dimethylthiazol-2-yl)-2,5-Diphenyltetrazolium Bromide (MTT) Reduction by Enhancing MTT Formazan Exocytosis. *J Neurochem* 69: 2285-2293.
45. Abe K, Saito H (1998) Amyloid [beta] protein inhibits cellular MTT reduction not by suppression of mitochondrial succinate dehydrogenase but by acceleration of MTT formazan exocytosis in cultured rat cortical astrocytes. *Neurosci Res* 31: 295-305.
46. Hertel C, Hauser N, Schubnel R, Seilheimer B, Kemp JA (1996) β -Amyloid-Induced Cell Toxicity: Enhancement of 3-(4,5-Dimethylthiazol-2-yl)-2,5-Diphenyltetrazolium Bromide-Dependent Cell Death. *J Neurochem* 67: 272-276.

Chapter 4

Halogenated Xanthene Benzoate Dyes Can Potently Modulate Amyloid-beta Aggregation and
Neurotoxicity

4.1 Abstract

Amyloid-beta ($A\beta$) aggregates have been implicated in causing the onset of Alzheimer's disease (AD). A number of $A\beta$ aggregates, including fibrils, are known to be toxic, while certain soluble $A\beta$ oligomers are highly neurotoxic. Together they cause a cascade of events that leads to cell death. A promising strategy to combat AD is the modulation of toxic $A\beta$ species. Although halogenation is widely used to enhance specific qualities and the efficacy of therapeutic small-molecules and peptides, its effect on $A\beta$ aggregation modulation has rarely been investigated. More importantly, a halogenated aromatic small-molecule, with the ability to strongly modulate $A\beta$ -associated cytotoxicity, to our knowledge, has only recently been identified through our previous work. To potentially expand the pool of such molecules we investigated erythrosine B and its family of halogenated xanthene benzoate derivatives. Here, we demonstrate that erythrosine B and eosin Y eliminated $A\beta$ -associated toxicity by promoting the formation of non-toxic aggregates and by inhibiting fibrillogenesis. Alternatively, eosin B (EB) and phloxine B were less effective, and Rose Bengal (RB) and ethyl eosin (EE) were not significantly effective at modulating $A\beta$ cytotoxicity. Despite close structural similarity, groups of molecules modulated $A\beta$ aggregation via unique pathways, and all were able to inhibit fibril formation. Except for EB, each of the dyes inhibited fibrillar oligomer formation. Comparison between structure and modulating activity showed that a benzoate attached to the xanthene was more effective at modulating $A\beta$ cytotoxicity than a tetrachlorobenzoate or an ethyl benzoate attached to xanthene. Our results suggest that halogenated xanthene benzoates are a novel family of $A\beta$ modulators. At the same time this body of work opens the door to exciting new small-molecules with diverse chemistry.

4.2 Introduction

Alzheimer's disease (AD) is the most common form of senile dementia and has become the 6th leading cause of death in the United States. Patients progressively suffer loss of cognitive capacity and experience dramatic behavioral changes. Death is inevitable as bodily functions decline.

Extracellular plaques and brain lesions are pathological hallmarks of AD and form from the deposition and accumulation of a protein called amyloid-beta ($A\beta$). $A\beta$ is generated from the sequential cleavage of the amyloid precursor protein by a group of secretases. Multiple isoforms can be created depending on the cleavage site. However, the two most physiologically abundant isoforms are $A\beta_{40}$ and $A\beta_{42}$. After generation, $A\beta$ undergoes a complex aggregation process to form amyloid fibrils.

While a number of aggregate conformers, including fibrils, are known to be toxic, growing evidence has shown that certain soluble $A\beta$ oligomers are highly neurotoxic. They cause a cascade of events, including oxidative stress that leads to cell death. Most importantly their presence strongly correlates with disease. Consequently, the reduction of toxic $A\beta$ oligomers and fibrils is a promising strategy to inhibit $A\beta$ -induced toxicity.

Numerous small-molecules have been investigated for their ability to modulate the formation of toxic $A\beta$ species and reduce $A\beta$ -associated toxicity. The majority of effective molecules contain multiple aryl groups with functional moieties attached to the aromatic constituents. These molecules are believed to bind $A\beta$ through *pi-pi* interactions with the two adjacent phenylalanine residues that dictate self-association. However, not all aromatic molecules are effective $A\beta$ modulators. Currently, polyphenols, which have an acidic electron withdrawing hydroxyl group attached to the benzene ring, contain the most known modulators.

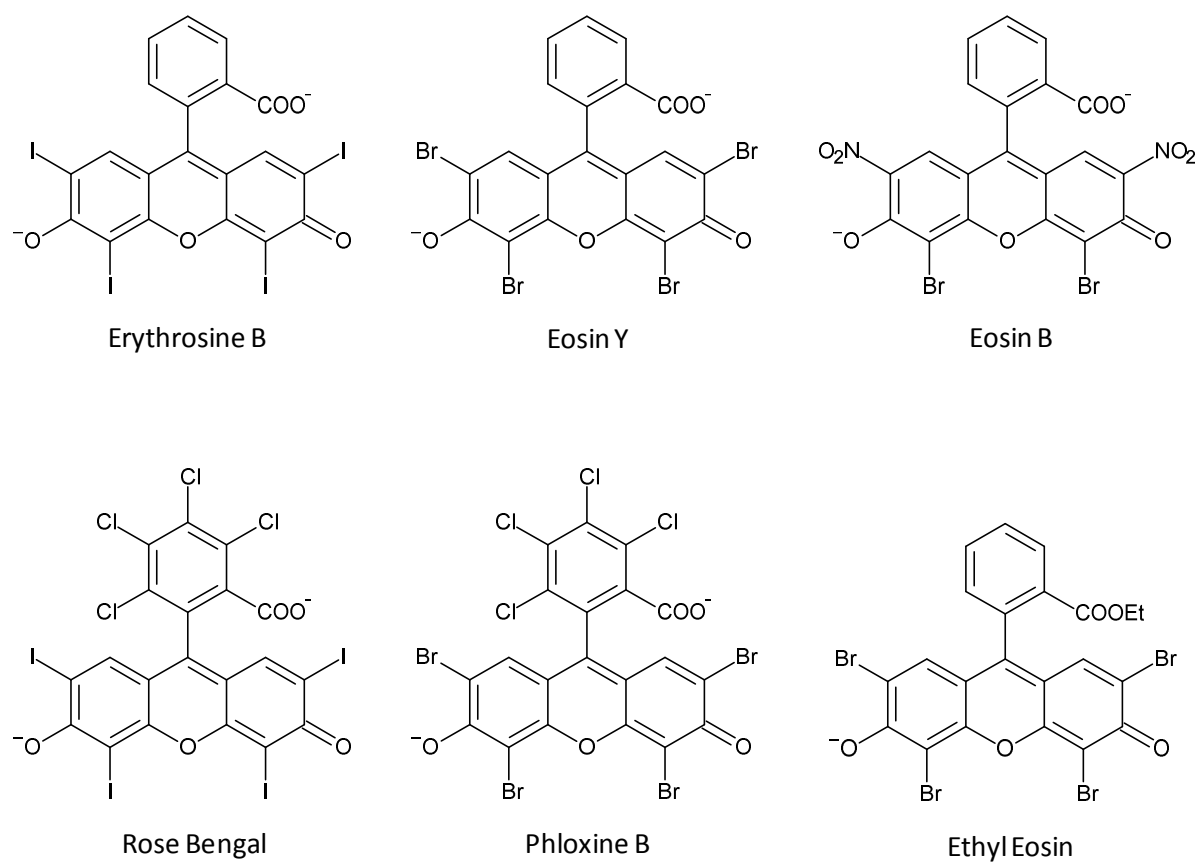


Figure 4.1. The structure of erythrosine B and its halogenated xanthene benzoate analogues at pH=7.

Depending on the type and degree, halogenation can also alter the electronics of the benzene ring which in theory allows manipulation of *pi-pi* interactions between A β and potential lead compounds. Although halogenation has been favorably employed to enhance specific qualities and the efficacy of therapeutic small-molecules and peptides, its effect on A β aggregation modulation has rarely been investigated. Sood et al and Torok et al have shown that halogenated molecules can modulate A β aggregation. However, to our knowledge, a halogenated aromatic small-molecule with the ability to strongly modulate A β -associated cytotoxicity has only recently been identified through our previous endeavors. In order to potentially broaden the population of these compounds that possess such rich chemistry, we investigated erythrosine B and its family of halogenated xanthene benzoate derivatives. To this end, we characterized the modulating activity of, erythrosine B (ER), eosin Y (EY), eosin B (EB), Rose Bengal (RB), phloxine B (PH), and ethyl eosin (EE) (Figure 4.1). We also compared structure to function to identify moieties that are central to modulating activity.

4.3. Materials and Methods

A β 40 was purchased from Anaspec Inc. (Fremont, CA). Human neuroblastoma SH-SY5Y cells were obtained from the American Type Culture Collection (ATCC; Manassas, VA). Polyclonal A11 antioligomer and horseradish peroxidase (HRP)-conjugated anti-rabbit IgG antibodies were obtained from Invitrogen (Carlsbad, CA). 4G8 antibody was obtained from Abcam (Cambridge, MA). Monoclonal 6E10 antibody and 3-(4,5-dimethylthiazol-2-yl)-2,5-diphenyltetrazolium bromide (MTT) were obtained from Millipore (Billerica, MA). Nitrocellulose membranes and ECL advance chemiluminescence detection kit were obtained from GE Healthcare Life Sciences (Uppsala, SE). Eosin Y was purchased from Acros Organics

(Geel, Belgium). All other chemicals were obtained from Sigma-Aldrich (St. Louis, MO) unless otherwise noted.

Dye Stock Solution Preparation. Erythrosine B, eosin Y, eosin B, Rose Bengal, phloxine B or ethyl eosin were dissolved in phosphate buffered saline (PBS).

A β Sample Preparation. A β 40 was dissolved in 100 % hexafluoroisopropanol (HFIP) (2 mg/mL) and incubated at room temperature for 2 hours. HFIP was evaporated under a constant stream of nitrogen, and the peptide was reconstituted in PBS solution (10 mM NaH₂PO₄ and 150 mM NaCl, pH 7.4) to a concentration of 50 μ M. If needed, concentrated dye stock solutions (1 – 10 mM) were added. The peptide samples were incubated at 37 °C.

Thioflavin T (ThT) Assay. 5 μ L of A β sample (50 μ M) was dissolved in 250 μ L of ThT (10 μ M). Fluorescence was measured in 96-well microtiter plates (Fisher Scientific, Pittsburgh, PA) using a Synergy 4 UV-Vis/fluorescence multi-mode microplate reader (Biotek, VT) with an excitation and emission wavelength of 450 nm and 485 nm, respectively.

Transmission Electron Microscopy (TEM). 10 μ L of A β sample (50 μ M) was spotted onto a formvar mesh grid and incubated for 1 min and wicked. The grids were then stained with 2 % uranyl acetate for 45 sec, wicked, allowed to air dry and viewed on a Jeol JEM1230 Transmission Electron Microscope. To determine mean aggregate lengths, 200 aggregate species were measured from at least one representative TEM image.

Dot Blotting. 2 μ L A β samples were spotted onto nitrocellulose membranes and were dried at room temperature. A solution of 0.1 % Tween 20 in Tris-buffered saline (TBS-T) solution (0.1% Tween 20, 20 mM Tris, 150 mM NaCl, pH 7.4) was prepared. Each nitrocellulose membrane was blocked at room temperature for 1 hour (5 % milk TBS-T) and washed with TBS-T. Each membrane was then incubated with antibody (oxidase (HRP)-conjugated 4G8, 6E10, A11, or OC antibody) in 0.5% milk TBS-T for 1 hour at room temperature and washed with TBS-T. After immunostaining with HRP-conjugated 4G8, the membranes were coated with 2 mL of ECL advance detection agent (based on manufacturer specifications) and visualized. Alternatively, all other membranes were incubated with HRP-conjugated anti-rabbit IgG in 0.5 % milk TBS-T for 1 hour and washed with TBS-T. Signal detection was performed as aforementioned using the ECL Advance Detection kit and was visualized using a Biospectrum imaging system (UVP, Upland, CA). HRP-conjugated 4G8, 6E10, and OC were applied at a 1:25000 dilution while A11 and HRP-conjugated anti-rabbit IgG were applied at a 1:10000 dilution.

MTT Reduction Assay. 50 mg of 3-(4,5-Dimethylthiazol-2-yl)-2,5-diphenyltetrazolium bromide (MTT) obtained from Millipore (Billerica, MA) was dissolved overnight at 4 °C in 10 mL of PBS. The MTT solution was then sterile filtered. SH-SY5Y human neuroblastoma cells were cultured in a humidified 5 % CO₂/air incubator at 37 °C in DMEM/F 12:1:1 containing 10 % fetal bovine serum and 1 % penicillin-streptomycin. 20,000 cells were seeded into each well of a 96-well microtiter plate (BD, Franklin Lakes, NJ) and allowed to acclimate for 3 days. 10 μ L of A β sample was added to each well and incubated for 2 days. The cells were washed by replacing the culture media with fresh media and incubating for 1 hour. The wash media was replaced with fresh media. 10 μ L of MTT was added to each well and incubated for 6 hours at 37

°C in the dark. After incubation, reduced MTT was dissolved by adding 200 μ L of dimethylsulfoxide (DMSO). After reduced MTT dissolution, the absorbance was measured at 506 nm using a Synergy 4 UV-Vis/fluorescence multi-mode microplate reader (Biotek, VT).

Circular Dichroism (CD). A β sample was diluted 1:10 using double distilled water. Samples were measured using a Jasco J710 spectropolarimeter with a 1 mm path length. The reported spectrum for each sample was the average of at least 5 measurements. Peptide spectra were obtained by subtracting background spectra.

4.4 Results and Discussion

In order to determine if the erythrosine B and its family of xanthene benzoate analogues are capable of modulating aggregation, transmission electron microscopy (TEM), circular dichroism (CD) and dot blotting analysis were employed. TEM is widely used to visualize A β aggregate morphology and can differentiate large aggregates, protofibrils and fibrils. Circular dichroism was employed to detect peptide secondary structure and to confirm fibril β -sheet secondary structure. Dot blotting was performed with a panel of sequence-specific and conformation-specific antibodies. The A11 and OC antibody were used to detect prefibrillar oligomers and fibrillar species, respectively. And the 4G8 and 6E10 sequence-specific antibodies were used to detect A β moieties. Peptide sample was prepared by incubating 50 μ M A β monomer in the absence or presence of 1x, 3x and 10x dye at 37°C for up to 6 days.

The commonality of fibril inhibition. Fibrils are a significant part of extracellular plaques and are neurotoxic. Therefore the ability of Erythrosine B (ER) and its analogues to

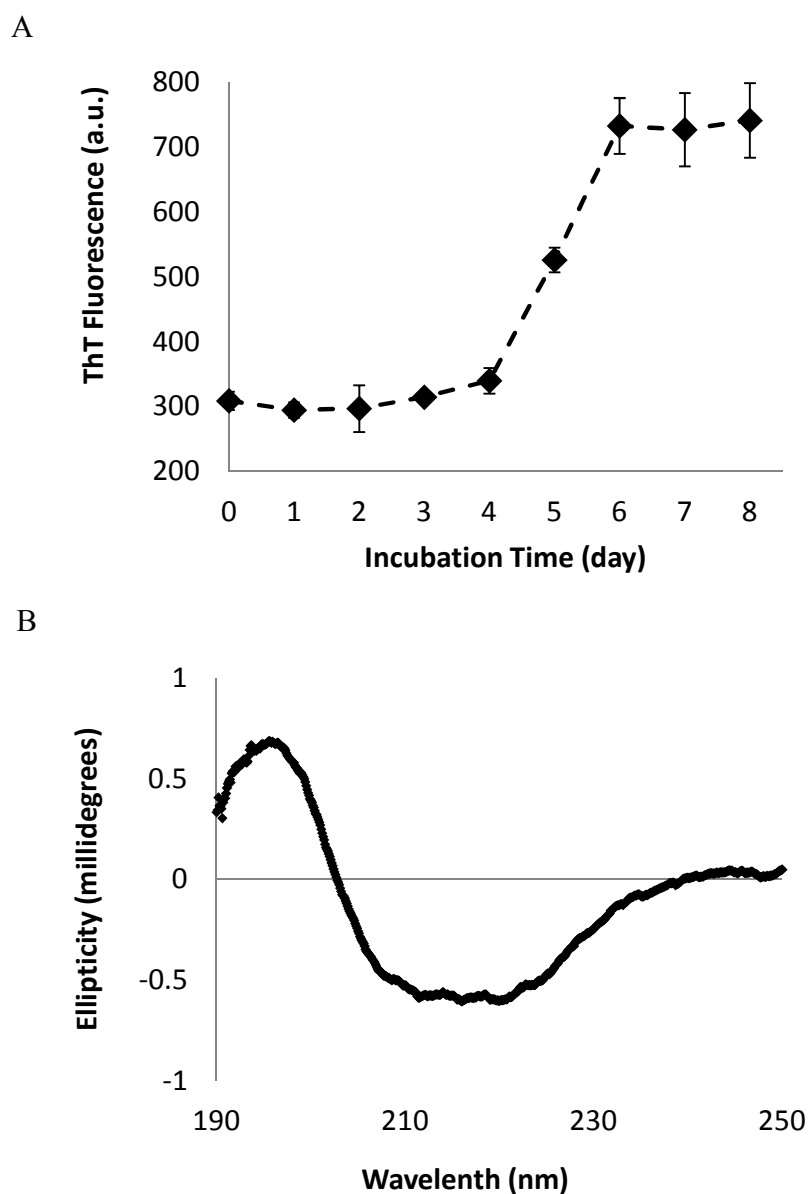


Figure 4.2. Confirmation of fibril formation by ThT fluorescence and CD. ThT (A) and CD (B) results were obtained by sampling A β incubated at 37°C in the absence of dye. CD was performed on day 5 and shows the characteristic β -sheet structure present in protofibrils and fibrils. The CD spectra is the average of five readings.

inhibit fibril formation was tested. 500 μ M dye was used to confer even the most subtle modulating effects and to improve the likelihood that every A β moiety was interacting with dye moiety. Samples were incubated in the absence (control sample) or presence of 10x dye for 5 days. Fibril formation was confirmed at day 5 using ThT fluorescence, CD and TEM. A sharp increase in ThT signal was observed on day 5 which is consistent with fibril formation (Figure 4.2A). The presence of β -sheets prominent in fibrillar species was detected by CD (Figure 4.2B). TEM also confirmed the presence of laterally-paired protofibrils which is characteristic of fibrils.

By comparing TEM images of A β samples coincubated with and without dye at day 5, it is apparent that coincubation of A β with dyes promotes noticeably shorter aggregates (Figure 4.3A-G). To quantitatively evaluate the difference, aggregate lengths from representative TEM images were manually measured (Figure 4.4). A downward shift in the distribution of aggregate lengths was observed when dyes were coincubated with A β (Figure 4.4). The dyes dramatically reduced the number of aggregates greater than a 100 nm cutoff, compared to the control sample, by at least 81% and up to 95% (Table 4.1). At a 150 nm cutoff, the dyes diminished the number of larger aggregates by 86% and up to 100% (Table 4.1). These results indicate that the dyes are highly effective in inhibiting the lengthening of aggregates which suggests their underlying potential to inhibit fibril formation.

Examination of TEM images found that fibrils were present in the A β control sample, while fibril and fibril-like species were not observed with dyes except (Figure 4.3D-G) for with ER and eosin Y (EY) (Figure 4.3B, 4.3C). Based on the size distribution, compared to the A β control, the fibril-like aggregates present with ER and EY were a minor component comprising no more than 4% (150 nm cutoff) of the total aggregates (Table 4.1). Based on these results, we concluded that all of the dyes are capable of inhibiting fibril formation.

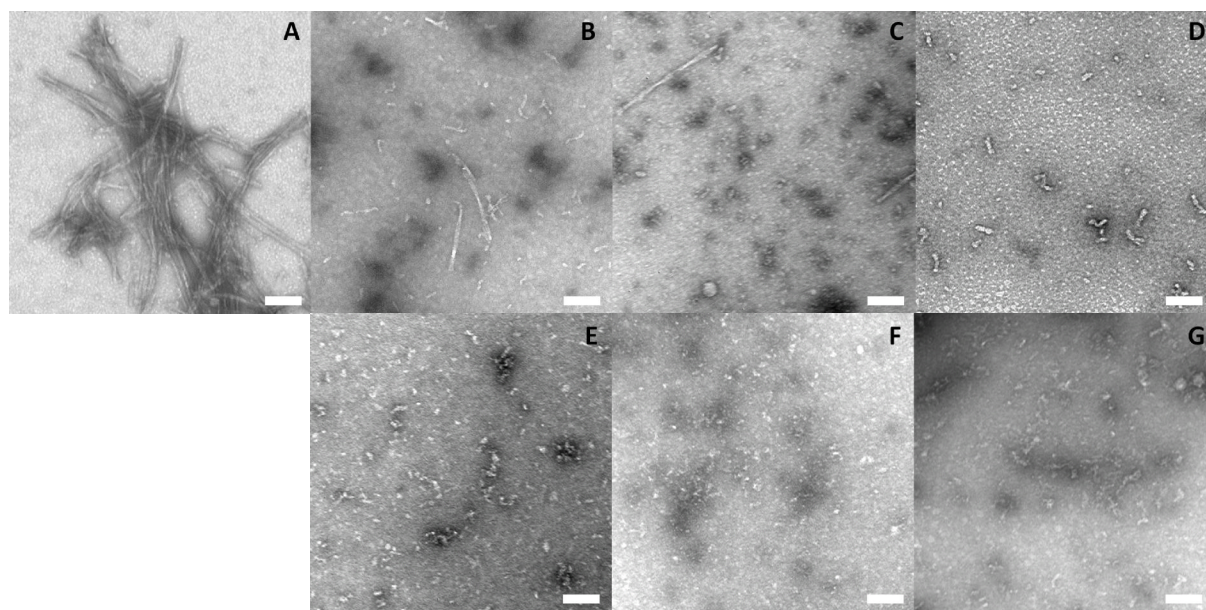


Figure 4.3. TEM images of A β aggregates formed after a three day incubation. A β monomer was incubated for 5 days at 37°C in the absence (A) or in the presence of 10x ER (B), EY (C), EB (D), RB (E), PH (F), and EE (F) and visualized by TEM. Scale bar is 100 nm.

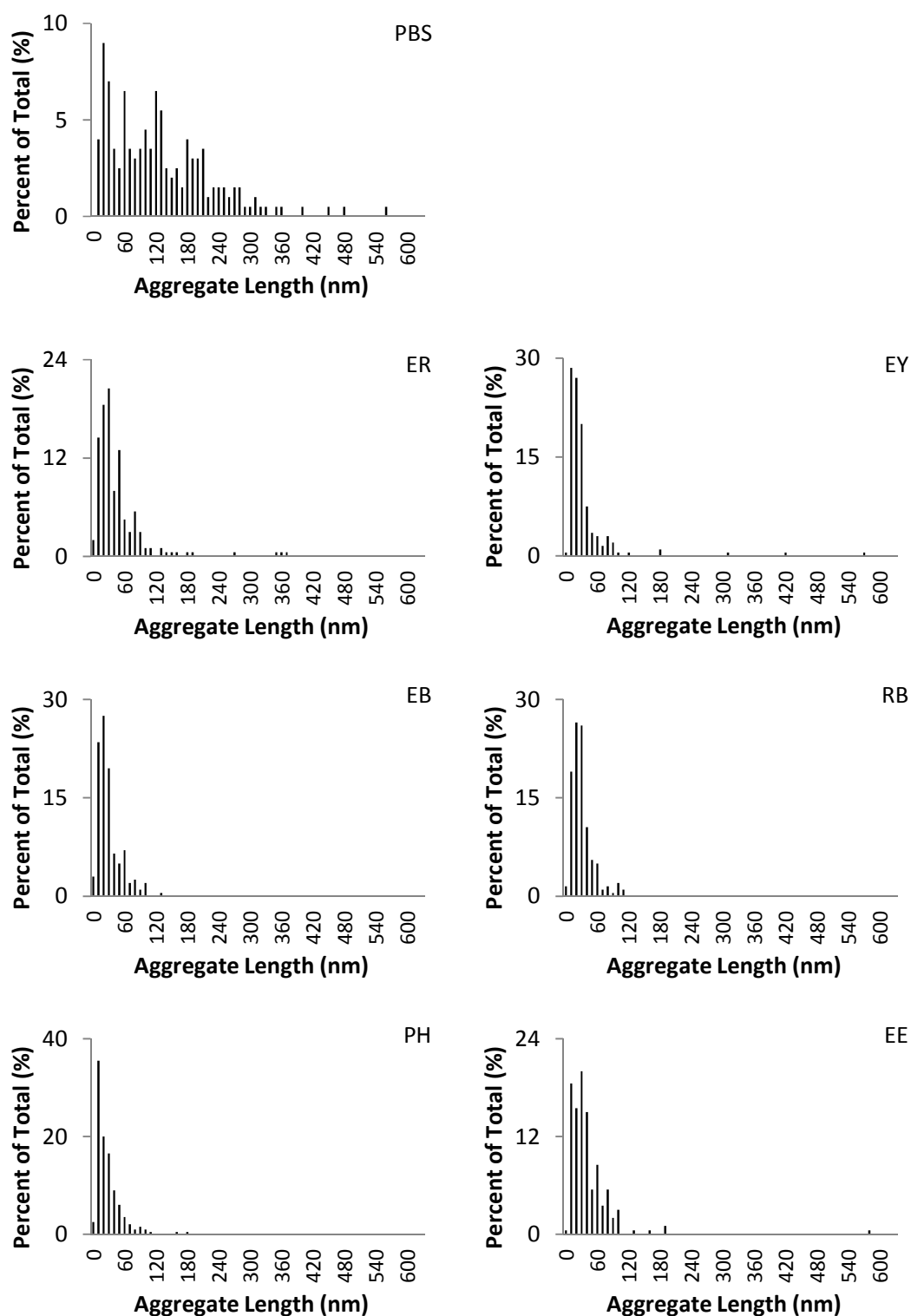


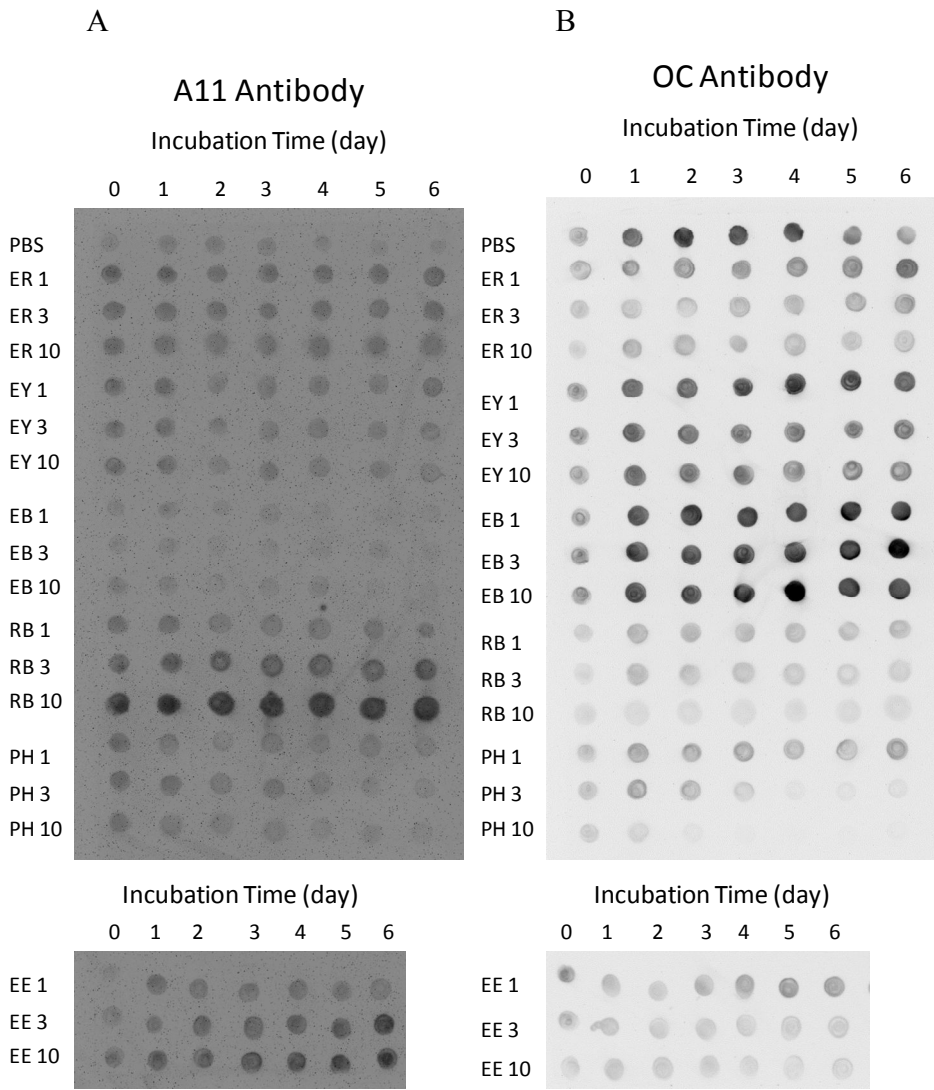
Figure 4.4. Comparison of Aggregate Length Distributions. Aggregate lengths were measured manually using representative TEM images for each of the dyes ($n = 200$). Aggregate lengths were binned in 10 nm length intervals.

Table 4.1. Comparison of long aggregate inhibition by each dye.

Dye	Percent of Aggregates Above 100 nm	Percent reduction of Aggregates < 100 nm (compared to control)	Percent of Aggregates Above 150 nm	Percent reduction of Aggregates < 150 nm (compared to control)
No Dye	58	—	35	—
ER	8	86	4	89
EY	5	91	2	96
EB	3	95	0	100
RB	3	95	0	100
PH	3	95	1	97
EE	11	81	2	94

Each molecule has unique aggregation modulating activity. Since these dyes inhibited fibril formation, logically, we investigated the mechanism by which these dyes modulate aggregation. Dot blotting was employed to determine the apparent concentration of prefibrillar and fibrillar species. The A11 and OC antibodies were used to detect prefibrillar and fibrillar species, respectively. 6E10 and 4G8, two sequence-specific dyes were also used. A β aggregates were prepared by incubating A β monomer in the absence (control sample) or presence of 1x, 3x or 10x dye at 37°C for up to 6 days.

Eosin B (EB) was the only dye that enhanced OC-reactivity compared to the control sample at all concentrations from day 1 to 6 (Figure 4.5B). This corresponded to an inverse response in A11-reactivity, where EB exhibited the lowest A11-reactivity from day 1 to 6 when compared with the other dye-induced aggregates (Figure 4.5A). This indicates that EB stabilizes fibrillar aggregates and inhibits the formation of prefibrillar species. The size of the aggregates suggests that EB is capable of stabilizing fibrillar oligomers but prevents the formation of prototypical amyloid fibrils (Figure 4.4). Interestingly, EB also induced a significant reduction in 4G8-reactivity at day 5 (Figure 4.5C). Previously we observed that a sudden loss in 4G8 reactivity was associated with protofibril and fibril formation, where β -sheet stacking obstructs accessibility to the 4G8 epitope. Similarly, fibril formation was also found to be accompanied by a decrease in both OC- and 6E10-reactivity associated with the lateral pairing of protofibril strands (Figure 4.5B, 4.5D). However, interestingly, EB induced the loss of the both 4G8- and 6E10-reactivity without aggregate elongation and without inhibiting OC-reactivity (Figure 4.5B-D). This suggests that the loss of 4G8- and 6E10-reactivity may not result directly from β -sheet stacking. Instead it may originate from a conformation change that is obligate for β -sheet stacking. As the



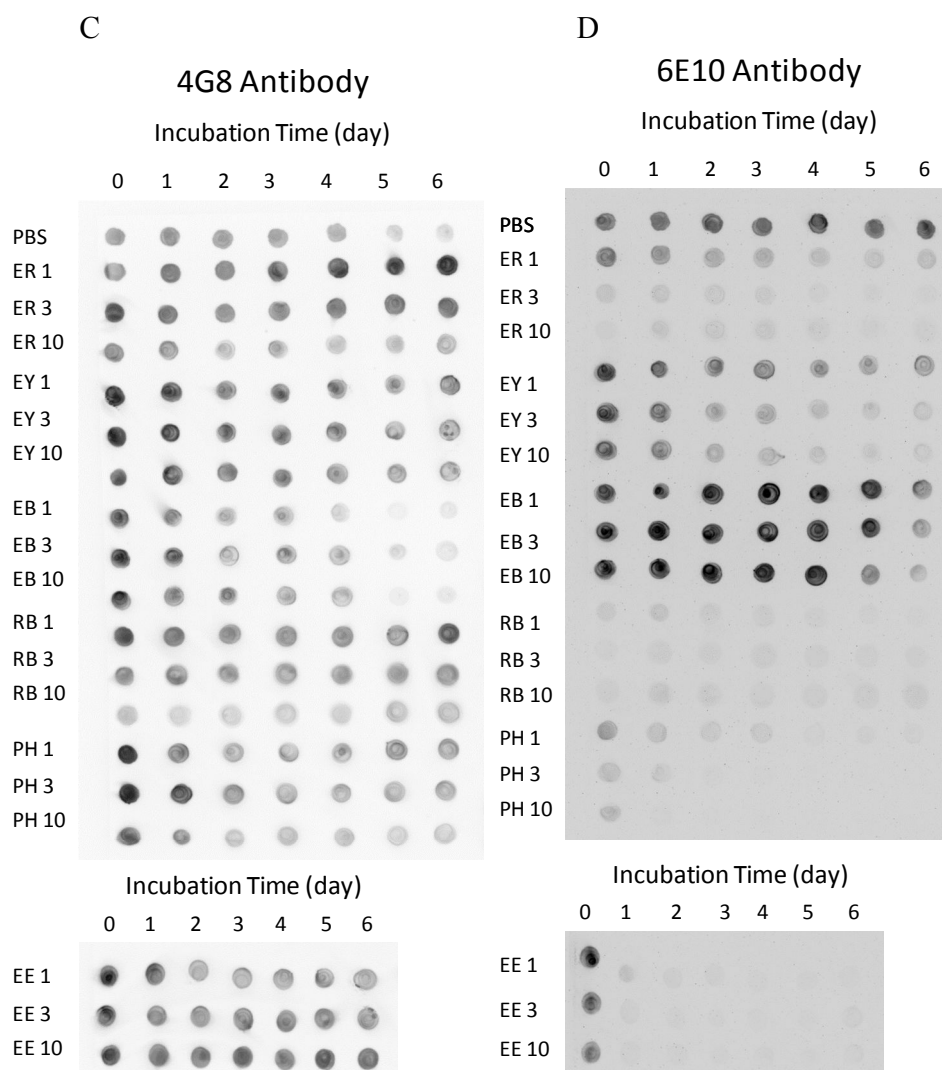


Figure 4.5. Monitoring A β aggregation by dot blotting. Conformational-specific antibodies A11 and OC were used to detect prefibrillar oligomers and fibrillar species, respectively. A β -sequence specific antibodies, 4G8 and 6E10, were used. 50 μ M A β was incubated in the absence or presence of 1x, 3x or 10x dye for 6 days at 37 $^{\circ}$ C. Samples were obtained on the indicated day and spotted onto a nitrocellulose membrane. Each membrane were immunostained with the A11 (A), OC (B), 4G8 (B), or 6E10 (C) antibody.

only dye with a NO₂ group on the xanthene constituent, the results also demonstrate that the NO₂ group likely played a pivotal role in stabilizing fibrillar species (Figure 4.1).

ER inhibited OC-reactivity starting from day 1 in a dose-dependent manner (Figure 4.5B). At 1x and 3x ER concentration, OC-reactivity was observed to increase with the time of incubation. This indicates that while ER can inhibit fibrillogenesis, it may not suspend it indefinitely. ER promoted A11-reactivity at all concentrations for the entire duration of the study (Figure 4.5A). These results suggest that ER strongly stabilizes and promotes prefibrillar oligomers which in turn inhibits fibrillogenesis. These results are consistent with previously observations (REF).

At 1x, EY maintained a strong constant OC-reactivity comparable to the highest level of the A β control from day 1 to 6 (Figure 4.5B). However, at higher concentrations EY was able to marginally inhibit OC reactivity and it is most apparent at day 3 to 6. On the other hand, EY also promoted A11-reactivity similarly at all concentrations, comparable to the strongest signal of the A β control throughout the entire duration of the study (Figure 4.5A). These findings along with the size distributions suggest that EY stabilizes both prefibrillar species and short fibrillar species which consequently inhibit fibril formation.

Ethyl eosin (EE) inhibited OC reactivity at all concentrations despite having fairly constant signal strength temporally at each concentration (Figure 4.5B). OC reactivity was comparable at 3x and 10x but still lower than at 1x. Interestingly, A11-reactivity was enhanced by EE, compared to the control in a dose-dependent manner (Figure 4.5A). Furthermore, the A11 signal strength was maintained at independently at each concentration from day 1 to 6. These results suggest that EE stabilizes prefibrillar oligomers and while inhibiting the formation of fibrillar species.

Phloxine B (PH) inhibited OC- reactivity starting from day 1 in a dose-dependent manner (Figure 4.5B). At 1x OC-reactivity was weaker than the A β control and was constant from day 1 to 6. At 3x concentration, OC reactivity is inhibited to the same degree as 1x PH, but the signal decreases significantly after day 2. At 10x concentration, OC-reactivity decreases significantly after day 0 (Figure 4.5B). On the other hand, PH did not seem to modulate A11-reactivity in a dose-dependent manner (Figure 4.5A). PH did however enhance A11-reactivity from day 0 at each concentration tapers off at later time points similarly to the A β control. This suggest that PH inhibits the formation of fibrillar species.

Rose Bengal (RB) was shown to inhibit OC-reactivity starting from day 1 at all concentrations in a dose-dependent manner (Figure 4.5B). Consequently, RB promoted A11-reactivity in a dose dependent manner for the entire duration of the study (Figure 4.5A). However in supplemental work, RB was shown to artificially enhance A11-reactivity. When RB alone was spotted onto nitrocellulose and immunostained, it was capable of producing positive A11 signal (data not shown). In order to quantitatively evaluate the degree of artificial enhancement, we integrated dot blots intensities. The signal enhancement from 3x over 1x RB was found to be 13 arbitrary units (a.u.) which suggest that the enhancement at 1x is approximately 4 a.u. Adjusting for the enhancement, places the A11 signal intensity of A β -aggregates induced by 1x RB and 1x PH at a nearly equivalent level. The enhancement from 10x over 3x was found to be 37 a.u. which is approximately a 2.8-fold increase, indicating that RB might artificially enhance A11-reactivity in a dose-dependent manner. Therefore, we hypothesize, that had RB not had this artificial A11-reactivity enhancement property RB and PH would have similar A11 signal profiles.

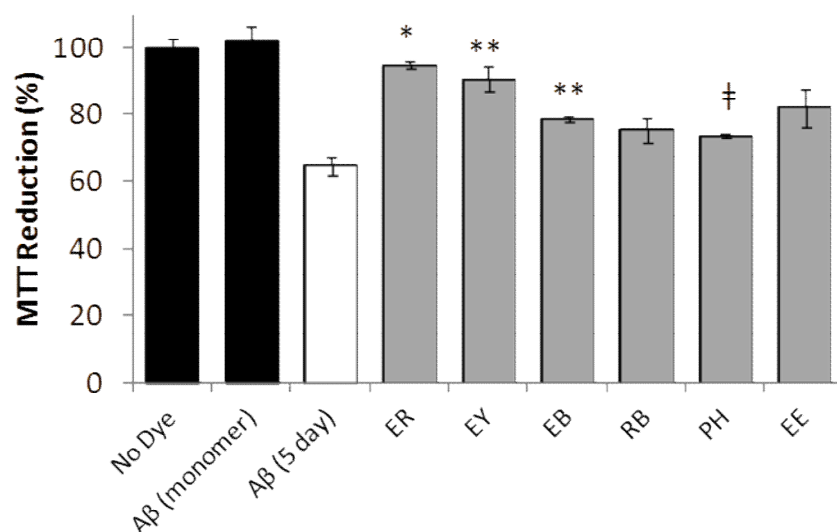


Figure 4.6. Viability of neuroblastoma SH-SY5Y cells incubated with preformed A β samples in the absence or presence of 1x dyes. Mitochondrial metabolic activity was measured by MTT reduction. Preformed A β aggregates were prepared by incubating 50 μ M of A β monomer in the absence or presence of ER, EY, EB, RB, PH or EE at 37 °C for 5 days. A β monomer was prepared using the sample preparation method outlined in Materials and Methods. *P < 0.0001, **P < 0.005, †P < 0.05; t-test between A β (5 day) dye-induced aggregates.

Halogenated xanthene benzoate dyes can potently inhibit A β -associated toxicity.

Previously we reported that ER was able to modulate cytotoxicity. To potentially expand the pool of effective A β cytotoxicity modulators, we wanted determine if the analogues could perform similarly. A β aggregates were prepared by incubating 50 μ M of A β monomer in the absence or presence of 1x dye at 37 °C for 5 days. The resulting aggregates were administered to SH-SY5Y cells and MTT reduction was employed to measure cell viability. At 1x dye concentration, when compared with the A β control, ER and EY were highly effective and significantly improved cell viability from 65% to 95% ($P < 0.001$) and 91% ($P < 0.005$), respectively (Figure 4.6). Based on the two-tailed t-test, the cell viability accompanying the ER- and EY-induced aggregates was not statistically different from the PBS control which suggests that ER and EY might completely eliminate A β -associated toxicity. Alternatively, while less effective, EB and PH showed an improvement to cell viability from 65% to 79% ($P < 0.005$) and 74% ($P < 0.05$), respectively, compared to the A β control (Figure 4.6). Coincubation with RB and EE exhibited cell viability of 75% and 82%, respectively.

Erythrosine B and eosin Y modulate A β cytotoxicity by inhibiting fibrillogenesis and promoting the formation of non-toxic aggregates. Next we wanted to look for evidence that might explain the neuroprotective properties of some of these dyes. When MTT reduction was examined and compared to the 1x dot blotting results, we found that for ER, EY and EB, the apparent concentration of A11-reactivity species did not trend with toxicity (Figure 4.6, 4.7A). Instead, OC-reactivity did (Figure 4.6, 4.7B). All of these molecules were able to either maintain or promote OC-reactivity compared to the control. Despite having the highest A11-reactivity and comparable OC-reactivity to the A β control, ER demonstrated the highest recovery in cell

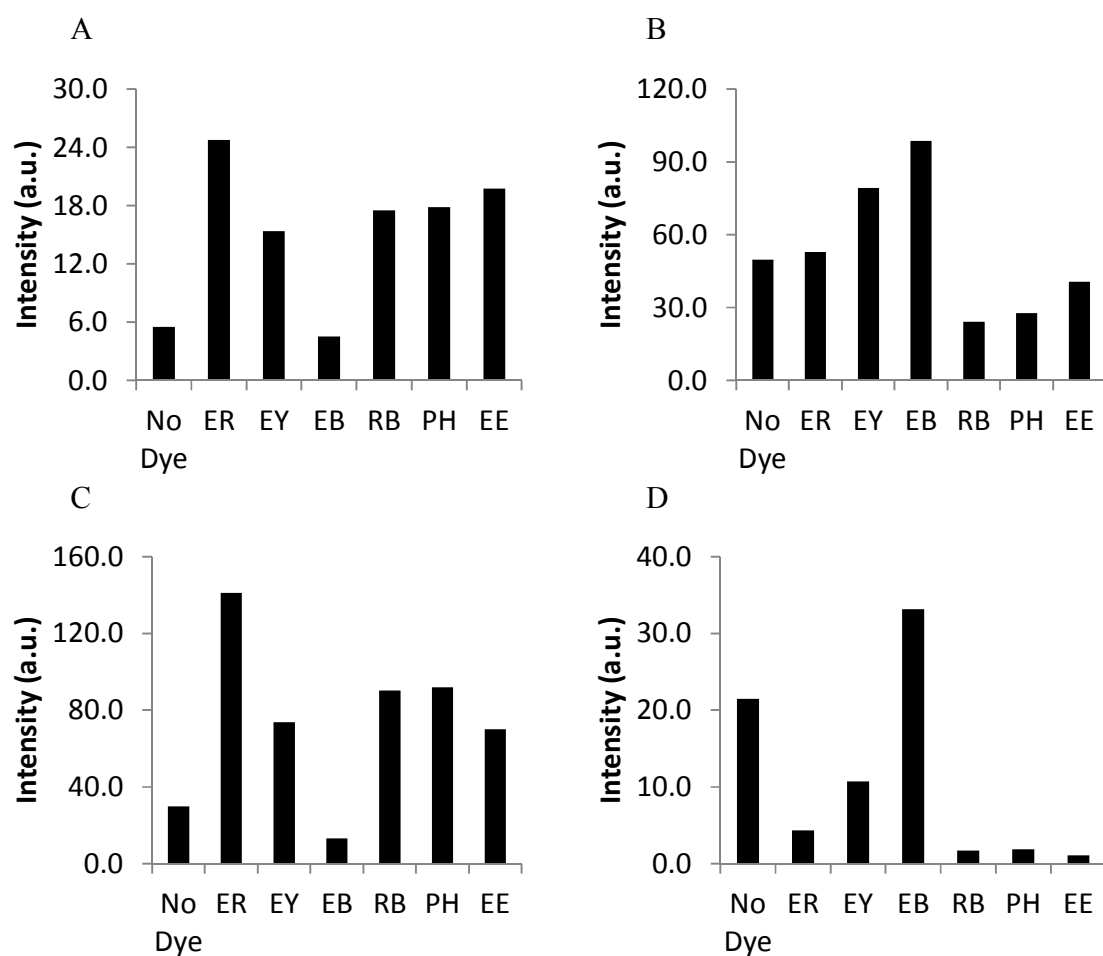


Figure 4.7. Comparison of dot blot intensities at 1x dye concentration from day 5. A11 (A), OC (B), 4G8 (C), 6E10 (E). Dot blot intensities were obtained by integrating dots using ImageJ. Arbitrary units is denoted by a.u.

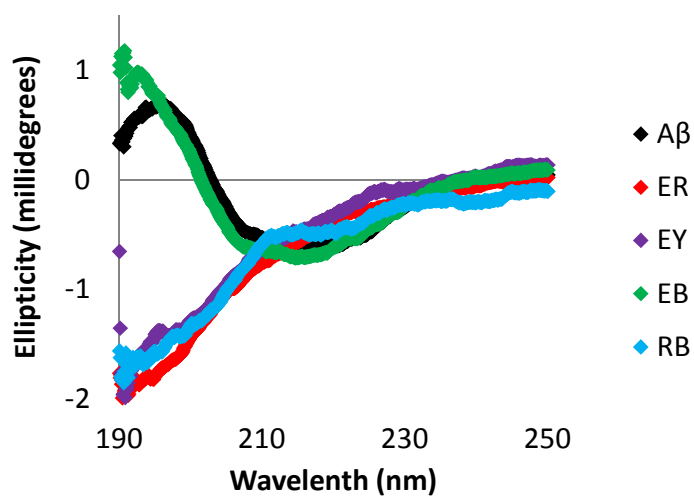


Figure 4.8. Secondary Structure of A β , and ER-, EY-, EB- and RB-induced aggregates on day 5. The secondary structure of A β aggregates formed in the absence or presence of dye were obtained by CD. Since the dyes absorb within the measured wavelengths, peptide spectra were obtained by subtracting the background spectra that were obtained separately. Each spectrum is the average of five readings. A β and EB resemble the spectra for β -sheet structure. A β aggregates induced by ER, EY and RB resemble the spectra for random coil structure.

viability (Figure 4.6, 4.7A, 4.7B). Since both ER and EY exhibited higher A11-reactivity than the A β control, while significantly inhibiting toxicity, this suggests that the A11-reactive species induced by ER and EY were innocuous. More specifically, the results indicate that both ER and EY demonstrated similar modulating activity, where they inhibited fibrillogenesis and promoted the formation of non-toxic, prefibrillar species. On the other hand, EB showed the highest OC-reactivity and A11-reactivity lower than the A β control (Figure 4.7A, 4.7B). With negligible A11-reactivity at all time points, the results indicate that EB inhibits fibrillogenesis but is unable to promote the formation of non-toxic A11-reactive species.

Alternatively, RB, PH and EE seemed to induce a different modulating effect. At day 5, these three dyes inhibited OC-reactivity compared to the A β control (Figure 4.7B). At the same time, they demonstrated comparable A11-reactivity to ER and EY (Figure 4.7A). However, RB and PH exhibited the lowest recovery to cell viability. Although EE seemed to improve cell viability more than RB and PH, its modulating activity at 1x was similar to theirs with respect to OC-reactivity and A11-reactivity (Figure 4.7A, 4.7B). This suggests that the A11-reactive species induced by RB, PH and EE were toxic. Therefore, RB, PH, and EE were not able to promote the formation of non-toxic prefibrillar species.

To further validate these observations we also wanted to gauge the relative concentration of A11- and OC-reactive species present with each of the dyes at 1x concentration. To accomplish this, OC-reactivity and A11-reactivity were compared to those of the two sequence specific antibodies. The sequence-specific antibody dyes if uninterrupted by dye binding or fibril formation should give consistent signal. We found that the A11-reactivity pattern trended well with 4G8-reactivity (Figure 4.7A, 4.7C). Alternatively, the OC-reactivity profile seemed to trend accordingly with 6E10-reactivity (Figure 4.7B, 4.7D). While 4G8 signal was observed at nearly

all dots where A11- and OC-reactivity were present, the 6E10 antibody could not detect the A11-reactive and OC-reactive species induced by RB, PH and EE at day 5 at all concentrations, suggesting its limited utility for detecting A β moieties (Figure 4.5C, 4.5D). Since the OC-reactivity did not trend with 4G8-reactivity while A11-reactivity did (Figure 4.7A, 4.7C), this suggests that A11-reactive species were likely predominant over OC-reactive species for ER, EY, RB, PH and EE at 1x concentration. Alternatively, for EB, the lack of A11 signal and strong OC signal suggest that OC-reactive species were in fact present (Figure 4.7B-D).

Since random coil structure and β -sheet structure are known to correspond with A11-reactive species and OC reactive species, respectively, we applied CD to ER, EY, EB, and RB at 10x concentration to minimize the diversity of secondary structure (Figure 4.8). We found that ER, EY and RB possessed very similar spectra each of which resembled the spectra for random coil secondary structure. On the other hand EB exhibited a spectrum resembling that of β -sheet secondary structure (Figure 4.8). These results support the previous observations while comparing A11 and 4G8 signals suggesting that A11-reactive species were predominant in ER, EY and RB.

4.5 Conclusions

Through this work, we demonstrated that erythrosine B (ER) and eosin Y (EY) had similar modulating activity whereby they eliminated A β -associated toxicity by promoting the formation of non-toxic aggregates and by inhibiting fibrillogenesis. Compared to ER and EY, eosin B (EB) and phloxine B (PH) were less effective, and Rose Bengal (RB) and ethyl eosin (EE) were not significantly effective at modulating A β cytotoxicity. Despite close structural similarity, groups of molecules modulated A β aggregation via unique pathways, and all were

able to inhibit fibril formation. Except for EB, each of the dyes inhibited fibrillar oligomer formation. We also found that RB, PH and EE had similar A β -cytotoxicity modulating activity.

Based on the comparison of structure and modulating activity between ER and EY, and RB, PH and EE, we have shown that a benzoate attached to the xanthene was more effective at modulating A β cytotoxicity than a tetrachlorobenzoate or an ethyl benzoate attached to xanthene. Our results suggest that halogenated xanthene benzoates are a novel family of A β modulators. At the same time this body of work opens the door to exciting new small-molecules with diverse chemistry.

4.6 Literature Cited

1. Kaye R, Head E, Thompson JL, McIntire TM, Milton SC, et al. (2003) Common structure of soluble amyloid oligomers implies common mechanism of pathogenesis. *Science* 300: 486-489.
2. Bucciantini M, Giannoni E, Chiti F, Baroni F, Formigli L, et al. (2002) Inherent toxicity of aggregates implies a common mechanism for protein misfolding diseases. *Nature* 416: 507-511.
3. Hawkes CA, Ng V, McLaurin J (2009) Small Molecule Inhibitors of A beta-Aggregation and Neurotoxicity. *Drug Dev Res* 70: 111-124.
4. Hamaguchi T, Ono K, Yamada M (2006) Anti-amyloidogenic therapies: strategies for prevention and treatment of Alzheimer's disease. *Cell Mol Life Sci* 63: 1538-1552.
5. McLaurin J, Golomb R, Jurewicz A, Antel JP, Fraser PE (2000) Inositol stereoisomers stabilize an oligomeric aggregate of Alzheimer amyloid beta peptide and inhibit A beta-induced toxicity. *J Biol Chem* 275: 18495-18502.
6. McLaurin J, Kierstead ME, Brown ME, Hawkes CA, Lambermon MHL, et al. (2006) Cyclohexanehexol inhibitors of A beta aggregation prevent and reverse Alzheimer phenotype in a mouse model. *Nat Med* 12: 801-808.
7. Ehrnhoefer DE, Bieschke J, Boeddrich A, Herbst M, Masino L, et al. (2008) EGCG redirects amyloidogenic polypeptides into unstructured, off-pathway oligomers. *Nat Struct Mol Biol* 15: 558-566.

8. Feng Y, Wang X-P, Yang S-G, Wang Y-J, Zhang X, et al. (2009) Resveratrol inhibits beta-amyloid oligomeric cytotoxicity but does not prevent oligomer formation. *Neurotoxicology* 30: 986-995.
9. Reinke AA, Gestwicki JE (2007) Structure-activity relationships of amyloid beta-aggregation inhibitors based on curcumin: Influence of linker length and flexibility. *Chemical Biology & Drug Design* 70: 206-215.
10. Yang FS, Lim GP, Begum AN, Ubeda OJ, Simmons MR, et al. (2005) Curcumin inhibits formation of amyloid beta oligomers and fibrils, binds plaques, and reduces amyloid in vivo. *J Biol Chem* 280: 5892-5901.
11. Moss MA, Varvel NH, Nichols MR, Reed DK, Rosenberry TL (2004) Nordihydroguaiaretic Acid Does Not Disaggregate beta-Amyloid(1-40) Protofibrils but Does Inhibit Growth Arising from Direct Protofibril Association. *Molecular Pharmacology* 66: 592-600.
12. Shin HJ, Lee EK, Lee JH, Lee D, Chang CS, et al. (2000) Eosin interaction of alpha-synuclein leading to protein self-oligomerization. *Biochimica Et Biophysica Acta-Protein Structure and Molecular Enzymology* 1481: 139-146.
13. Borzelleca JF, Hallagan JB (1990) Multigeneration study of FD & C Red No. 3 (erythrosine) in Sprague-Dawley rats. *Food Chem Toxicol* 28: 813-819.
14. Gardner DF, Utiger RD, Schwartz SL, Witorsch P, Meyers B, et al. (1987) Effects of oral erythrosine (2',4',5',7'-tetraiodofluorescein) on thyroid-function in normal men. *Toxicology and Applied Pharmacology* 91: 299-304.
15. Hirohashi T, Terasaki T, Shigetoshi M, Sugiyama Y (1997) In vivo and in vitro evidence for nonrestricted transport of 2',7'-bis(2-carboxyethyl)-5(6)-carboxyfluorescein tetraacetoxymethyl ester at the blood-brain barrier. *J Pharmacol Exp Ther* 280: 813-819.
16. Levitan H, Ziylan Z, Smith QR, Takasato Y, Rapoport SI (1984) Brain uptake of a food dye, erythrosine B, prevented by plasma-protein binding. *Brain Research* 322: 131-134.
17. Lee S, Fernandez EJ, Good TA (2007) Role of aggregation conditions in structure, stability, and toxicity of intermediates in the A beta fibril formation pathway. *Protein Science* 16: 723-732.
18. Qi W, Zhang A, Patel D, Lee S, Harrington JL, et al. (2008) Simultaneous monitoring of peptide aggregate distributions, structure, and kinetics using amide hydrogen exchange: Application to A beta(1-40) fibrillogenesis. *Biotechnol Bioeng* 100: 1214-1227.

19. Qi W, Zhang AM, Good TA, Fernandez EJ (2009) Two Disaccharides and Trimethylamine N-Oxide Affect A beta Aggregation Differently, but All Attenuate Oligomer-Induced Membrane Permeability. *Biochemistry* 48: 8908-8919.
20. Chen B, Thurber KR, Shewmaker F, Wickner RB, Tycko R (2009) Measurement of amyloid fibril mass-per-length by tilted-beam transmission electron microscopy. *Proc Natl Acad Sci U S A* 106: 14339-14344.
21. Komatsu H, Feingold-Link E, Sharp KA, Rastogi T, Axelsen PH (2010) Intrinsic Linear Heterogeneity of Amyloid beta Protein Fibrils Revealed by Higher Resolution Mass-per-length Determinations. *J Biol Chem* 285: 41843-41851.
22. Paravastu AK, Leapman RD, Yau WM, Tycko R (2008) Molecular structural basis for polymorphism in Alzheimer's beta-amyloid fibrils. *Proc Natl Acad Sci U S A* 105: 18349-18354.
23. Chimon S, Shaibat MA, Jones CR, Calero DC, Aizezi B, et al. (2007) Evidence of fibril-like beta-sheet structures in a neurotoxic amyloid intermediate of Alzheimer's beta-amyloid. *Nat Struct Mol Biol* 14: 1157-1164.
24. Khurana R, Coleman C, Ionescu-Zanetti C, Carter SA, Krishna V, et al. (2005) Mechanism of thioflavin T binding to amyloid fibrils. *J Struct Biol* 151: 229-238.
25. LeVine H (1999) Quantification of beta-sheet amyloid fibril structures with thioflavin T. *Amyloid, Prions, and Other Protein Aggregates*. pp. 274-284.
26. Wu JW, Breydo L, Isas JM, Lee J, Kuznetsov YG, et al. (2010) Fibrillar oligomers nucleate the oligomerization of monomeric amyloid beta but do not seed fibril formation. *J Biol Chem* 285: 6071-6079.
27. Chen YR, Glabe CG (2006) Distinct early folding and aggregation properties of Alzheimer amyloid-beta peptides A beta 40 and A beta 42 - Stable trimer or tetramer formation by A beta 42. *J Biol Chem* 281: 24414-24422.
28. Kaye R, Head E, Sarsoza F, Saing T, Cotman CW, et al. (2007) Fibril specific, conformation dependent antibodies recognize a generic epitope common to amyloid fibrils and fibrillar oligomers that is absent in prefibrillar oligomers. *Mol Neurodegener* 2: 18.
29. Ladiwala ARA, Lin JC, Bale SS, Marcelino-Cruz AM, Bhattacharya M, et al. (2010) Resveratrol Selectively Remodels Soluble Oligomers and Fibrils of Amyloid A beta into Off-pathway Conformers. *J Biol Chem* 285: 24228-24237.
30. Hu Y, Su BH, Kim CS, Hernandez M, Rostagno A, et al. (2010) A strategy for designing a peptide probe for detection of beta-amyloid oligomers. *ChemBioChem* 11: 2409-2418.

31. Iijima K, Liu HP, Chiang AS, Hearn SA, Konsolaki M, et al. (2004) Dissecting the pathological effects of human A beta 40 and A beta 42 in *Drosophila*: A potential model for Alzheimer's disease. *Proc Natl Acad Sci U S A* 101: 6623-6628.
32. Kimura N, Yanagisawa K, Terao K, Ono F, Sakakibara I, et al. (2005) Age-related changes of intracellular A beta in cynomolgus monkey brains. *Neuropathol Appl Neurobiol* 31: 170-180.
33. Klyubin I, Walsh DM, Lemere CA, Cullen WK, Shankar GM, et al. (2005) Amyloid beta protein immunotherapy neutralizes A beta oligomers that disrupt synaptic plasticity in vivo. *Nat Med* 11: 556-561.
34. Thakker DR, Weatherspoon MR, Harrison J, Keene TE, Lane DS, et al. (2009) Intracerebroventricular amyloid-beta antibodies reduce cerebral amyloid angiopathy and associated micro-hemorrhages in aged Tg2576 mice. *Proc Natl Acad Sci U S A* 106: 4501-4506.
35. Sarroukh R, Cerf E, Derclaye S, Dufrêne Y, Goormaghtigh E, et al. (2010) Transformation of amyloid β (1–40) oligomers into fibrils is characterized by a major change in secondary structure. *Cell Mol Life Sci*: 1-10.
36. Schmidt M, Sachse C, Richter W, Xu C, Fandrich M, et al. (2009) Comparison of Alzheimer A beta(1-40) and A beta(1-42) amyloid fibrils reveals similar protofilament structures. *Proc Natl Acad Sci U S A* 106: 19813-19818.
37. Feng Y, Yang SG, Du XT, Zhang X, Sun XX, et al. (2009) Ellagic acid promotes A beta 42 fibrillization and inhibits A beta 42-induced neurotoxicity. *Biochem Biophys Res Commun* 390: 1250-1254.
38. Pollack SJ, Sadler IIIJ, Hawtin SR, Tailor VJ, Shearman MS (1995) Sulfonated dyes attenuate the toxic effects of beta-amyloid in a structure-specific fashion. *Neuroscience Letters* 197: 211-214.
39. Datki Z, Juhász A, Gálfi M, Soós K, Papp R, et al. (2003) Method for measuring neurotoxicity of aggregating polypeptides with the MTT assay on differentiated neuroblastoma cells. *Brain Res Bull* 62: 223-229.
40. Nishimura S, Murasugi T, Kubo T, Kaneko I, Meguro M, et al. (2003) RS-4252 Inhibits Amyloid β -Induced Cytotoxicity in HeLa Cells. *Pharmacol Toxicol* 93: 29-32.
41. Olivieri G, Otten U, Meier F, Baysang G, Dimitriadis-Schmutz B, et al. (2003) [beta]-amyloid modulates tyrosine kinase B receptor expression in SHSY5Y neuroblastoma cells: influence of the antioxidant melatonin. *Neuroscience* 120: 659-665.

42. Ono K, Yoshiike Y, Takashima A, Hasegawa K, Naiki H, et al. (2003) Potent anti-amyloidogenic and fibril-destabilizing effects of polyphenols in vitro: implications for the prevention and therapeutics of Alzheimer's disease. *J Neurochem* 87: 172-181.
43. Wang SS-S, Rymer DL, Good TA (2001) Reduction in Cholesterol and Sialic Acid Content Protects Cells from the Toxic Effects of β -Amyloid Peptides. *J Biol Chem* 276: 42027-42034.
44. Liu Y, Schubert D (1997) Cytotoxic Amyloid Peptides Inhibit Cellular 3-(4,5-Dimethylthiazol-2-yl)-2,5-Diphenyltetrazolium Bromide (MTT) Reduction by Enhancing MTT Formazan Exocytosis. *J Neurochem* 69: 2285-2293.
45. Abe K, Saito H (1998) Amyloid [beta] protein inhibits cellular MTT reduction not by suppression of mitochondrial succinate dehydrogenase but by acceleration of MTT formazan exocytosis in cultured rat cortical astrocytes. *Neurosci Res* 31: 295-305.
46. Hertel C, Hauser N, Schubnel R, Seilheimer B, Kemp JA (1996) β -Amyloid-Induced Cell Toxicity: Enhancement of 3-(4,5-Dimethylthiazol-2-yl)-2,5-Diphenyltetrazolium Bromide-Dependent Cell Death. *J Neurochem* 67: 272-276.
47. Török B, Sood A, Bag S, Kulkarni A, Borkin D, Lawler E, Dasgupta S, Landge S, Abid M, Zhou W, Foster M, Levine H 3rd, Török M. (2012) Structure-Activity Relationships of Organofluorine Inhibitors of β -Amyloid Self-Assembly. *ChemMedChem (Online)*.
48. Török M, Abid M, Mhadgut SC, Török B. (2006) Organofluorine inhibitors of amyloid fibrillogenesis. *Biochemistry* 45: 5377-5383.
49. Sood A, Abid M, Hailemichael S, Foster M, Török B, Török M. (2009) Effect of chirality of small molecule organofluorine inhibitors of amyloid self-assembly on inhibitor potency. *Bioorg Med Chem Lett.* 19(24): 6931-6934.
50. Ganesan L, Margolles-Clark E, Song Y, Buchwald P. (2011) The food colorant erythrosine is a promiscuous protein-protein interaction inhibitor. *Biochem Pharmacol.* 81(6): 810-818.
51. Gales L, Almeida MR, Arsequell G, Valencia G, Saraiva MJ, Damas AM. (2008) Iodination of salicylic acid improves its binding to transthyretin. *Biochim Biophys Acta.* 1784(3): 512-517.
52. Gazit E. (2002) A possible role for pi-stacking in the self-assembly of amyloid fibrils. *FASEB* 16(1):77-83.
53. Ryan DM, Doran TM, Nilsson BL. (2011) Complementary π - π interactions induce multicomponent coassembly into functional fibrils. *Langmuir* 27(17): 11145-11156.

Chapter 5

Conclusions and Recommendations for Future Work

5.1 Conclusions

Our research has focused on the discovery of small-molecule modulators of A β aggregation and cytotoxicity for the purpose of discovering potential therapies for Alzheimer's disease. At the same time we have also striven to understand their mode of action and to identify certain structural features that confer modulating activity.

For this purpose, two groups of molecules were investigated, BBG and its family of triphenylmethane dyes, and erythrosine B and its family of halogenated xanthene benzoate derivatives. BBG is a close structural analogue of Brilliant Blue FCF, which is a Food and Drug Administration (FDA)-approved food dye. More importantly, BBG is BBB-permeable and neuroprotective. ER is an FDA-approved food dye and has been shown to penetrate the BBB in *in vitro* uptake studies. We determined that a number of molecules from each group modulated A β aggregation and inhibited A β -associated toxicity. Through this research we were able to meet each of the objectives outlined in the Introduction section. The following is a summary of conclusions based on the objectives.

- 1) Evaluate the ability of BBG to modulate A β aggregation and cytotoxicity.

BBG was discovered to completely eliminate A β -associated cytotoxicity at both 1x and 3x concentration (ratio of dye to A β) by inhibiting the formation of toxic aggregates while promoting the formation of non-toxic aggregates. Consequently, BBG inhibited fibril formation. The half-maximal BBG concentration for inhibition of A β cytotoxicity (EC₅₀) was 0.55x.

- 2) Evaluate the ability of BBG analogues to modulate A β aggregation and cytotoxicity.

BBR was also discovered to completely eliminate A β -associated cytotoxicity at 3x concentration, while slightly less effective at 1x. Similar to BBG, BBR inhibited fibril formation, and reduced cytotoxicity by inhibiting the formation of toxic aggregates while promoting the formation of non-toxic A β aggregates. Compared to BBG and BBR, BBF and FGF were less effective in modulating both aggregation and toxicity.

- 3) Compare the efficacy of BBG and its analogues to determine structure-to-activity relationships.

Based on the comparison between the efficacy and structure of the molecules, we also found that the 4-ethoxy aniline group which is unique to BBG and BBR is likely responsible for their ability to strongly modulate A β aggregation and cytotoxicity. A comparison between BBG and BBR also revealed the importance of two additional methyl groups on BBG that allow it to inhibit A β toxicity at lower stoichiometric concentrations.

- 4) Evaluate the ability of ER to modulate A β aggregation and cytotoxicity.

Our results demonstrated that ER eliminates A β -associated toxicity by promoting the formation of non-toxic A β aggregates and inhibiting fibrillogenesis. ER also induced

protofibril formation where the average length is inversely proportional to the concentration of ER.

- 5) Evaluate the ability of ER analogues to modulate A β aggregation and cytotoxicity.

EY also eliminated A β -associated toxicity by promoting the formation of non-toxic A β aggregates. Compared to ER and EY, EB and PH were less effective, and RB and EE were not significantly effective at modulating A β cytotoxicity at 1x concentration. Despite close structural similarity, all of the molecules possessed unique A β aggregation modulating activity, and all were able to inhibit fibril formation.

- 6) Compare the efficacy of ER and its analogues to determine structure-to-activity relationships.

Comparison between structure and modulating activity showed that a benzoate attached to the xanthene was more effective at modulating A β cytotoxicity than a tetrachlorobenzoate or an ethyl benzoate attached to xanthene.

Collectively our results suggest that aromaticity is an important feature towards the modulating activity of each of these molecules. But more importantly, our results suggest that functional groups attached to aryl constituents may be vital for conferring a unique modulating activity to each molecule. How each functional group impacts the electronics of the benzene ring may ultimately dictate the mode of A β -to-compound interaction and the modulation activity.

Most importantly, our endeavors have uncovered a number of potent A β neurotoxicity modulators and demonstrated that triphenylmethane and halogenated xanthene benzoate derivatives are novel families of molecules that show remarkable promise in the search for Alzheimer's disease therapies.

5.2 Recommendations for Future Work

Although our work has identified a pool of promising therapeutic compounds, a number of questions still remain. 1) While we have demonstrated that these molecules can modulate A β aggregation and cytotoxicity, can these compounds be applied to targeting preexisting toxic aggregates? 2) Since aggregation-prone proteins have a similar disease mechanism, can these molecules be employed against a spectrum of aggregation-prone proteins? 3) And finally, how do these molecules directly interact with its intended target protein? To answer these questions we have proposed the following work.

- 1) Our results have shown that a number of compounds possess the potential to slow or stop disease progression by modulating newly synthesized A β . However due to the dynamic nature of protein aggregation, the most effective class of therapies would likely also be required to target preexisting toxic aggregates. Logically the next step in characterizing these molecules is to evaluate whether they can remodel preexisting toxic aggregates, such as fibrils and oligomers into non-toxic conformers or more simply, determine if they can provide neuroprotection against preexisting toxic aggregates.

- 2) Previously, it has been shown that aggregation-prone proteins have a similar disease mechanism that is substantially linked to toxic oligomers, suggesting that a common structure exists in these oligomers (Kayed et al., 2003). Consequently, it has been hypothesized that universal modulators may exist. In fact, erythrosine B has been shown to modulate both amyloid-beta and alpha-synuclein aggregation (Shin et al., 2000). In the case of Alzheimer's disease, a number of A β isoforms and aggregation-prone proteins are present. While our work has demonstrated that each of these molecules is capable of interacting with the A β 40 isoform the next step is to attempt to expand their utility by determining if they can modulate A β 42 as well as other known aggregation-prone proteins.

- 3) Finally, since we have identified structural features that seem to impart modulating activity, next we would like to determine how these molecules directly interact with A β . Interaction modes can be determined through binding studies using well designed overlapping and contiguous A β peptide fragments as well as the application of competitive binding studies between compounds and sequence-specific antibodies.